8-1-1996

Modeling Coupled Transient Transport of Mass, Momentum and Energy in Wellbore/Reservoir Systems

Xiaowei Wang

MODELING COUPLED TRANSIENT TRANSPORT OF MASS, MOMENTUM AND ENERGY IN WELLBORE/RESERVOIR SYSTEMS

by

Xiaowei Wang
Bachelor of Thermal Engineering, Tsinghua University, 1989

A Dissertation
Submitted to the Graduate Faculty
of the
University of North Dakota
in partial fulfillment of the requirements

for the degree of
Doctor of Philosophy

Grand Forks, North Dakota
August
1996

This dissertation, submitted by Xiaowei Wang in partial fulfillment of the requirements for the Degree of Doctor of Philosophy from the University of North Dakota, has been read by the Faculty Advisory Committee under whom the work has been done and is hereby approved.

R. Hosur
(Chairperson)
Thomas C. Owens
John Erjavec
N.S. Grendal
Neil D. Hoosley

This dissertation meets the standards for appearance, conforms to the style and format requirements of the Graduate School of the University of North Dakota, and is hereby approved.

Harvey Knull
Dean of the Graduate School

7-15-96
Date

PERMISSION

Title Modeling Coupled Transient Transport of Mass, Momentum and Energy in Wellbore/Reservoir Systems

Department Energy Engineering

Degree Doctor of Philosophy

In presenting this dissertation in partial fulfillment of the requirements for a graduate degree from the University of North Dakota, I agree that the library of this University shall make it freely available for inspection. I further agree that permission for extensive copying for scholarly purposes may be granted by the professor who supervised my thesis work or, in his absence, by the chairperson of the department or the dean of the Graduate School. It is understood that any copying or publication or other use of this thesis or part thereof for financial gain shall not be allowed without my written permission. It is also understood that due recognition shall be given to me and to the University of North Dakota in any scholarly use which may be made of any material in my dissertation.

Signature Xiaowei Wang

Date 07/12/1996

TABLE OF CONTENTS

LIST OF ILLUSTRATIONS

LIST OF TABLES

ACKNOWLEDGMENTS

My special thanks go to my advisor, Dr. A.R. Hasan, who not only financially supported but also encouraged and helped me throughout this project. His wonderful implementations of the ideas often led to important improvements. Without his guidance and patience, this work would never be fulfilled. My special thanks extend to Shah Kabir of Chevron Petroleum Technology Company, who provided all the field data as well as excellent technical assistance. He was also enormously helpful in suggesting improvements and finding errors in this work.

My thanks also go to Dr. T.C. Owens, who provided many useful insights to this project. His careful reading of the text and suggestions strongly influenced my dissertation. Other people I especially wish to thank are Dr. John Erjavec, Dr. Nanak Grewal, and Dr. Neil Woolsey. They served as my committee members and gave me many insightful comments.

The financial support provided by the Petroleum Research Fund and the American Chemical Society and North Dakota EPSCoR is deeply appreciated. I am very grateful for the people who verified our model and published this work.

Finally, I would like to express my gratitude to my parents and my wife for their love and continuous support.

ABSTRACT

The total reserve of a hydrocarbon bearing formation and its ability to economically produce the fluids determine a reservoir's development potential. Oil companies in the United States and abroad spend millions of dollars a year in well testing to estimate parameters related to these factors. A large fraction of these tests are surface "buildup" tests in which a producing well in the reservoir is "shut-in" either at the wellhead or at the bottom, or "drawdown" tests in which a well initially closed, is suddenly opened at the wellhead. The transient response of the pressure to these changes at the well bottom provides valuable information about formation properties. Shut-in at the bottom is usually very difficult and expensive, especially in the hostile environment of a high temperature/high pressure reservoir.

Fluid flow in the wellbore is complicated by heat transfer between the fluid and the surrounding earth. Earth temperature generally increases with depth. Thus, as the hot fluid from the bottom flows upward, its temperature becomes higher than its surrounding causing heat loss from the wellbore. Conversely, when a well is shut-in at the wellhead, the warm fluid losses heat to the surrounding colder formation more rapidly than it gains it from the decreasing mass influx. Since fluid properties are temperature sensitive, pressure profile computation, which depends on fluid properties, is influenced by the fluid temperature profile in the wellbore. Thus, the transport processes in the wellbore are coupled.

In this work we presented a transient wellbore/reservoir model for testing wells. We

used a hybrid approach to couple the wellbore with the reservoir. The reservoir flow was modeled using the standard analytic approach, including superposition effects. The wellbore model, requiring simultaneous solution of the mass, momentum, and energy balance equations, used a finite difference numerical approach. Two simulators based on our model were developed: the forward simulator allowed us to simulate wellbore fluid temperature, pressure, and other variables at any depth and time for given reservoir parameters and well completion details; the reverse simulator allowed us to convert measured wellhead pressure and temperature to bottomhole pressure for subsequent analysis.

Three field examples were used to demonstrate various applications of these two simulators. The good agreement between field data and predictions showed the quality of our simulators. We also identified the phenomenon of wellbore thermal storage. Wellbore thermal storage is the energy absorbed or released by the tubulars and cement sheaths, which is a significant fraction of the energy exchange between the wellbore and the formation at early time.

A sensitivity study gave us further insights into the effect of various process variables on wellbore pressure and temperature. Thus, our simulators can be very useful in designing well tests as well as to augment conventional well test analysis.

CHAPTER 1

INTRODUCTION

The total energy consumption in the world has increased exponentially over the last few decades. A very large fraction of the energy consumed in the developed nations comes from hydrocarbon reserves buried deep in the earth. Although the energy crisis of the seventies and early eighties is a distant memory, it behooves us to remember that the total hydrocarbon reserve of the world is finite and it is dwindling every day. It is very important that the available reserve be produced efficiently.

Oil and gas bearing *pay zones*, which are porous rock media, occur in 10-ft to 100-ft thick strips in formations that could be 1,000-ft to 25,000-ft below the earth's surface. The fluids are produced through wells drilled to the pay zone. In producing the fluid, engineers have to contend with two major types of energy loss. The fluid loses energy, thus experiencing loss of pressure, in moving through the porous medium to the wellbore. Additional energy loss is encountered to get the fluid to the wellhead from the well bottom (called bottomhole). If the pressure in the reservoir is not high enough for the fluid to flow by itself, artificial lift procedures – such as sucker-rod pumps, gas-lift, etc. – are used.

The total reserve of a hydrocarbon bearing formation and its ability to economically produce the fluids determine a reservoir's development potential. Oil companies in the United States and abroad spend millions of dollars a year in well testing

to estimate parameters related to these factors. The basis of most of these tests is to introduce a perturbation in the flow of fluid in the formation and measure the transient bottomhole pressure response.

The flow perturbation is usually effected by either shutting off a producing well or starting to produce a previously shut-in well. Shutting off a producing well causes its pressure to increase with time, and is known as a *shut-in* or *buildup* test. A *drawdown test* involves producing a previously shut-in well with consequent decrease in wellbore pressure with time. The transient response of the bottomhole pressure with time in either type of test provides valuable information about the formation's flow properties.

The mathematical development of models to describe flow through porous media is considerably simplified if the rate of fluid withdrawal is held constant in a drawdown test or if the flow is suddenly stopped at the sandface (bottomhole). In such cases, the resulting second order differential equations describing flow through the porous medium become amenable to analytical solution for many types of reservoirs. Unfortunately, shutting a well at the bottom results in lost production in addition to being very time-consuming. In deep reservoirs where temperatures and pressures are high, failure of measuring gauges often add to the cost and uncertainty of a test. Thus, many of the buildup tests are conducted by turning the valves off at the wellhead and measuring *wellhead* (instead of bottomhole) pressure with time. Similar reasons cause many operators to measure wellhead data in drawdown tests.

Analysis of wellhead data, however, is plagued by a number of problems. The large volume of many wells, combined with the compressible nature of the wellbore fluid,

causes wellbore transients to last for a long time. Thus, when a producing well is shut off at the wellhead, fluid flow from the formation into the bottom of the well does not cease immediately. In some wells, depending on the well volume, previous production, and formation properties, such gradually diminishing *after-flow* can last for a very long time. Similar transient behavior is observed during a drawdown test.

Thus, a proper analysis of transient wellhead pressure requires incorporating wellbore flow with that in the reservoir. Hydrocarbons produced from a petroleum reservoir consist of many components, some of which remain dissolved at the high pressures typical of most reservoirs. However, as the fluid is moved up the well, its pressure gradually decreases, which may allow dissolved gases to come out of solution. In addition, water is often produced along with oil and gas. Thus, flow of three distinct phases – gas, oil, and water – may occur in the wellbore.

Fluid flow in the wellbore is further complicated by heat transfer between the fluid and the surrounding earth. Earth temperature generally increases with depth. Thus, as the hot fluid from the bottomhole flows upward, its temperature becomes higher than its surrounding causing heat loss from the wellbore. Hence wellbore fluid temperature decreases with time and depth during production. Conversely, when a well is shut-in at the wellhead as in a build-up test, the warm fluid loses heat to the surrounding colder formation more rapidly than it gains it from the decreasing mass influx. Consequently, the wellbore fluid temperature decreases with time during a shut-in period. Because fluid properties are temperature sensitive, pressure profile computation, which depend on fluid properties, are influenced by the fluid temperature profile in the wellbore. Thus, the

transport processes in the wellbore are coupled.

In this work we have undertaken the task of developing a model for the transient transport processes in a wellbore/formation systems. We use a hybrid approach to couple the wellbore with the reservoir. For flow through the porous reservoir medium, we use the available analytical solution for an infinite acting cylindrical reservoir. The wellbore model, requiring simultaneous solution of the mass, momentum, and energy balance equations, uses a finite difference numerical approach.

In the next chapter, we discuss the available literature on wellbore fluid flow and energy transport. In the first part of that chapter our emphasis is on the recent flow pattern based approach to modeling multiphase flow. In the second part of Chapter 2, we present a survey of literature on heat transfer between the wellbore fluid and the surrounding earth.

In Chapter 3, we show how we model transient, coupled transport processes in a wellbore, basing our approach on the earlier works discussed in Chapter 2. We first develop a model for single-phase gas flow. The model for multiphase flow is presented after that. In Chapter 4, we present results of computations from our model and compare these with field data supplied by Chevron Petroleum Technology Company. In Chapter 5, we present a sensitivity analysis that points out the influence of various production and reservoir parameters on the wellbore pressure and temperature response. Conclusions and recommendations are given in Chapter 6.

CHAPTER 2

LITERATURE SURVEY

In this chapter we discuss the previous work done in the area of fluid flow and heat transfer in wellbores. In the first part of this chapter we present the relevant literature on wellbore fluid flow. This is followed by an examination of recent research on heat transfer between the wellbore fluid and the surrounding earth.

2.1 Multiphase Flow in Wellbores

Fluid flow in wellbores is complicated by the fact that often two or three phases flow simultaneously through the same well competing for the available area in the channel. Even when the well bottom receives single-phase oil from the reservoir, decompression of the fluid in moving upward often results in gas coming out of solution. Such gases include, methane, ethane, nitrogen, carbon dioxide, etc. Wells intended for single-phase gas flow often also produce condensates.

The importance of multiphase flow in vertical and inclined wells has led to the development of several models to estimate in-situ phase fraction and pressure gradient. The basis for all these models is the mechanical momentum balance equation,

$$\frac{dp}{dz} = -\left(\rho_m \frac{\partial v_m}{\partial t} + \rho_m v_m \frac{\partial v_m}{\partial z} + \rho_m g \sin\theta + \frac{2 \rho_m f_m v_m^2}{d} \right) \qquad (2.1)$$

The first right hand term accounts for the energy loss due to a velocity transient while the last three terms on the right hand side of Eq. 2.1 represent the kinetic energy loss, the static head loss, and the friction loss, respectively. Hence we may write the total pressure gradient, dp/dz, during multiphase flow as the sum of the transient head, $(dp/dz)_t$; the kinetic head, $(dp/dz)_A$; the static head, $(dp/dz)_H$; and the frictional head, $(dp/dz)_F$,

$$\frac{dp}{dz} = \left(\frac{dp}{dz}\right)_t + \left(\frac{dp}{dz}\right)_A + \left(\frac{dp}{dz}\right)_H + \left(\frac{dp}{dz}\right)_F \qquad (2.2)$$

One problem in modeling multiphase flow is finding appropriate expressions for the mixture density, ρ_m , and the friction factor, f_m. Usually the static head is the major contributor to the total pressure drop in vertical and near-vertical wells, often accounting for more than 95% of the total gradient. Therefore, accurately estimating the mixture density is essential for computing pressure gradient.

The density of a flowing fluid mixture depends directly on the in-situ volume fraction of the phases. For example, in the case of gas-liquid two-phase flow, the mixture density can be related to the in-situ gas volume fraction (also known as gas void fraction), E_g, as follows,

$$\rho_m = E_g \rho_g + (1 - E_g)\rho_l \qquad (2.3)$$

Unfortunately, the in-situ fraction of a phase is generally different from its input fraction (the fraction that can be calculated from a material balance) because of the differences in individual phase densities and the resulting effect of buoyancy. Thus, a major effort in modeling multiphase flow is directed towards accurately estimating the in-situ volume fractions occupied by each phase.

In the next few pages we discuss the methods used to estimate in-situ fractions of the phases. We present our discussion in terms of gas-liquid two-phase flow but point out that the methods are generally applicable to immiscible oil-water flow as well. In the case of three-phase gas-oil-water flow, treating the two liquid phases as one effectively reduces the system to a two-phase flow situation and has been generally found to yield acceptable predictive accuracy.

Homogeneous Models. One simple way to estimate mixture density is to assume that the phases are well mixed and that the phase velocities are identical. With this *no-slip*(v_g-v_l=0) assumption the in-situ fractions become the same as the input fractions, allowing easy computation of the mixture properties. A number of researchers taking this approach have reported satisfactory agreement of predicted pressure gradient with data in horizontal systems.

However, for vertical or near-vertical systems the no-slip assumption may lead to large errors. The primary difficulty with the homogeneous model is that the density difference between gases and liquids and the tendency of the gases to channel through the center of the conduit make the assumption of equal in-situ phase velocities unrealistic. The higher in-situ velocity of the gas phase compared to that ascribed by the homogeneous model causes the model estimated void fraction to be higher and the estimated density to be lower for upwardly inclined systems. A number of empirical approaches (Poettmann and Carpenter, 1952; Tek and Chan, 1959; Baxendell and Thomas, 1961; Fancher and Brown, 1963) proposed two-phase friction factor correlations that compensated for the lower estimated static head caused by the underestimated mixture density. However the basic

theoretical shortcoming of the homogeneous model makes this approach unreliable for vertical and near-vertical systems.

Separated Flow Model. The separated flow model makes the more realistic assumption that the two phases are segregated and flow with different velocities. If the difference between the in-situ velocities of the phases – termed slip (v_g-v_l) – is estimated, void fraction and pressure drop can also be estimated.

Lockhart and Martinelli (1945) and Lockhart, Martinelli and Nelson (1949) proposed a correlation to estimate slip in gas-liquid two-phase flow. Since then, many modifications to the Lockhart-Martinelli-Nelson correlation have been proposed (Sher and Green, 1959; Muscettola, 1963; Hasan and Rhodes, 1983). These correlations have generally performed better than the homogeneous model. However, like the homogeneous model, the separated flow model does not take differences in flow patterns into account. Ignoring the influence of such an important parameter as the flow regimes has often been cited as the cause for inaccurate predictions where using the separated flow model. Collier (1981) pointed out that the model leads to a theoretically incorrect relationship in annular two-phase flow.

The correlation proposed by Duns and Ros (1963) attempted to incorporate flow regimes into the separated flow model. Duns and Ross (1963), as well as others (Beggs and Brill, 1972; Orkiszewiski, 1967) prescribe individual slip correlations for different flow patterns. However, the exclusive reliance of these correlations on empiricism for predicting both flow pattern and pressure gradient has often led to unsatisfactory results.

Flow Pattern Based Mechanistic Models. During two-phase flow, the phases take

up a number of distinct configurations, called flow patterns. Recent attempts to model two-phase flow has been aided by recognizing the hydrodynamic conditions that lead to the various patterns of flow and proposing individual models for each flow regime. Generally, four major flow patterns – bubbly, slug, churn, and annular – are recognized in vertical and near-vertical systems, as shown in Figure 1. In this work we have adopted this flow pattern based approach to modeling two-phase flow.

Bubbly Flow. At low gas velocities the gas phase flows as small, nearly spherical bubbles through a continuous liquid medium. The in-situ gas velocity, v_g, is influenced by the tendency of the bubbles to move through the central portion of the channel where the mixture velocity is higher than the cross-sectional average velocity, v_m. In addition, buoyancy resulting from the density difference between the liquid and the gas phase adds a velocity equal to the terminal rise velocity, v_∞, to the lighter phase. Thus,

$$v_g = C_o v_m + v_\infty \qquad (2.4)$$

where the flow parameter, C_o, is related to the bubble concentration and velocity profiles. Noting that in-situ velocity is related to the superficial velocity (phase flow rate/ total cross-sectional area) by $v_g = v_{sg}/E_g$, we arrive at the following expression for the void fraction,

$$E_g = \frac{v_{sg}}{C_0 v_m + v_\infty} \qquad (2.5)$$

For turbulent flow, when the channel center velocity is 1.2 times the cross-sectional average mixture velocity, the value of C_o may be taken as 1.2. This flow parameter value

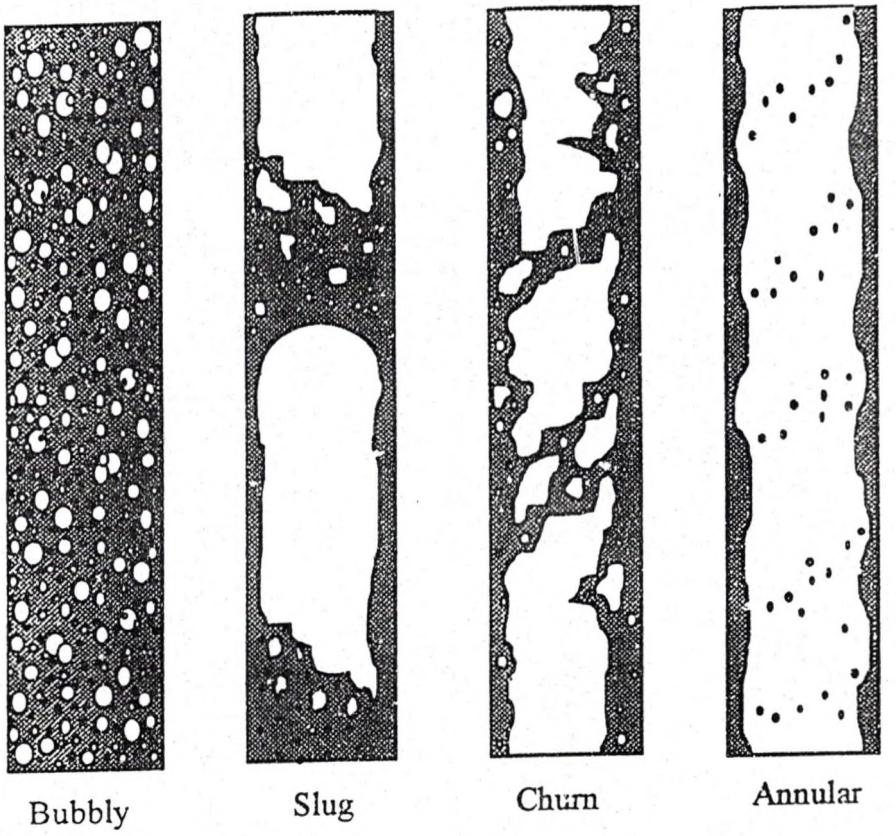

Figure 1. Four Major Flow Patterns

has been proposed by Hasan and Kabir (1992) and others (Aziz et al., 1972). A higher value of 2.0 for C_o has been suggested by many (Zahrdnik, 1979; Haug, 1976; Hasan and Kabir, 1988) for bubbly flow through stagnant liquid columns in large diameter pipes.

For estimating bubble terminal rise velocity, the Harmathy (1960) correlation (Eq. 2.6), is used because of its simplicity and accuracy,

$$v_{sg} = 1.53\left[\frac{g\,\sigma_s\,(\rho_l-\rho_g)}{\rho_l^2}\right]^{1/4} \qquad (2.6)$$

where σ_s is the surface tension.

Transition from Bubbly Flow to Slug Flow. As gas velocity increases, bubbles begin to collide with each other forming larger bubbles. Bubble coalescence and agglomeration may lead to the formation of large bubbles that occupy almost the entire pipe cross-section. Such large bubbles are known as Taylor bubbles and the resulting flow type is termed slug flow because of the typical liquid slugs between Taylor bubbles. The rate of collision between bubbles increases sharply when the gas void fraction exceeds 0.25. Hasan (1988) and others (Griffith and Snyder 1964, Hasan and Kabir 1988a, Ansari 1990) have experimentally confirmed $E_g = 0.25$ as the criterion for transition from bubbly to slug flow. Hasan and Kabir (1988a) have expressed this transition criterion in terms of superficial velocities of the phases assuming that Eq. 2.5 applies at the transition. The resulting expression for transition to slug flow,

$$v_{sg} > \left(0.429\,v_{sl} + 0.357\,v_{\infty}\right) \qquad (2.7)$$

is found to agree well with data from several sources. For flow through inclined channels, when bubbles preferentially flow along the upper wall of the pipe, Hasan and Kabir (1988b) proposed the following modification to Eq. 2.7,

$$v_{sg} > \left(0.429\, v_{sl} + 0.357\, v_{\infty}\right) \sin\theta \qquad (2.8)$$

where θ is the channel inclination to the horizontal. The rise velocity of Taylor bubbles, which depends on channel diameter (discussed later under slug flow), could be smaller than the small bubble rise velocity (given by Eq. 2.4) for narrow pipes. In such cases, Shoham et al. (1982) maintains that bubbly flow is unstable, and slug flow occurs at extremely low gas velocities. Another exception to the transition criterion proposed by Shoham et al. (1982) was pointed out for high velocity systems when turbulence could break up the larger bubbles and maintain bubbly flow even when the void fraction exceeds 0.25. He proposed that when the mixture velocity exceeds that given by Eq. 2.9,

$$v_m^{1.12} = 4.68\, d^{0.48} (\sigma/\rho_l)^{0.6} \left[(\rho_l - \rho_g)\, g/\sigma\right]^{1/2} (\rho_l/\mu_l)^{0.08} \qquad (2.9)$$

bubbly flow persists up to a void fraction of 0.52. Bubbly flow, caused by such dispersion of bubbles at high velocities, is termed dispersed bubbly flow.

Slug Flow. In slug flow, large Taylor bubbles, separated by slugs of liquids, flow through the channel. The liquid slugs generally contain small gas bubbles. The analysis of this flow regime is thus complicated by the presence of two different types of bubbles which have different rise velocities. Fernandes et al. (1983) considered a cell of length, L, consisting of a typical Taylor bubble of length, L_T, and a liquid slug of length, L_s, to analyze

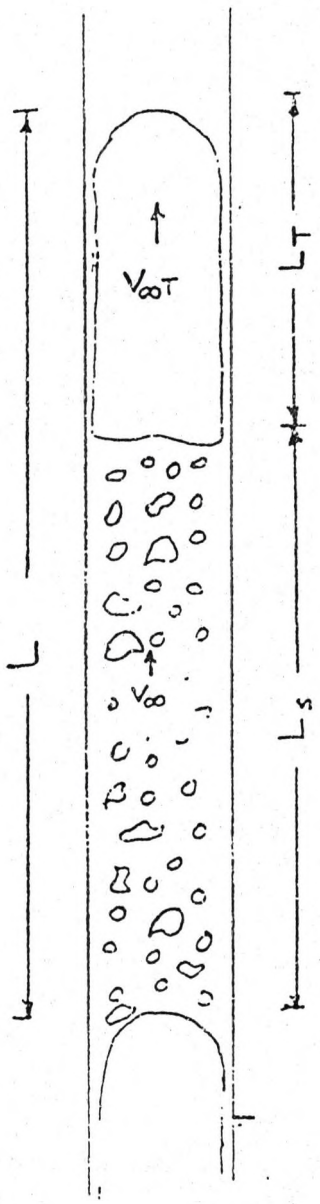

Figure 2. Slug Flow in Vertical Channels

slug flow in vertical channels (Fig. 2).

Later, Hasan and Kabir (1992) simplified the cellular approach and extended it to deviated wells as well as to flow through annuli. The void fraction in slug flow is expressed as the sum of the contribution of the Taylor bubble ($E_{gT}L_T/L$) and the bubbles in the liquid slug ($E_{gs}L_s/L$). Data gathered by Akagawa and Sagaguchi (1966) were used to express the void contribution of the liquid slug, and the void fraction during slug flow can be estimated by using

$$E_g = \left(\frac{L_T}{L}\right) E_{gT} + 0.1 \qquad for \quad v_{sg} > 0.4 \ m/s$$
$$E_g = \left(\frac{L_T}{L}\right) E_{gT} + 0.25\, v_{sg} \qquad for \quad v_{sg} \le 0.4 \ m/s \qquad (2.10)$$

where the second term on the right side of Eq. 2.10 represents the contribution of the liquid slug. Analogous to the approach taken in bubbly flow, Hasan and Kabir (1992) used the following expression for E_{gT}, using $v_{\infty T}$ for the rise velocity of a Taylor bubble,

$$E_{gT} = \frac{v_{sg}}{C_o v_m + v_{\infty T}} \qquad (2.11)$$

Hasan and Kabir (1992) used Akagawa and Sagaguchi (1966) data to arrive at the following expression for L_s/L (=1- L_T/L),

$$\frac{L_s}{L} = 0.1\left(\frac{C_o v_m + v_\infty}{v_{sg}}\right) \qquad for \quad v_{sg} > 0.4\, m/s \qquad (2.12)$$

$$\frac{L_s}{L} = 0.25\,(C_o v_m + v_\infty) \qquad for \quad v_{sg} < 0.4\,m/s \tag{2.13}$$

The value of the flow parameter, C_o, remains 1.2 in slug flow. For the rise velocity of a Taylor bubble, Hasan and Kabir gave the following expression based on their data and the work of others (Nicklin, 1972; Wallis, 1969),

$$v_{\infty T} = \left(0.345 + \frac{0.1 d_t}{d_c}\right)\sqrt{\sin\theta}\,(1+\cos\theta)^{1.2}\sqrt{\frac{g d_c (\rho_l - \rho_g)}{\rho_l}} \tag{2.14}$$

Eq. 2.14 is an unified expression for Taylor bubble rise velocity in channels of any inclination angle as well as for flow through an annulus having an inner diameter of d_t and an outer diameter of d_c. Using a value of $d_t = 0$ and $\theta = 90$ degrees, reduces Eq. 2.14 to the Taylor bubble rise velocity expression proposed by Nicklin et al. (1962) for vertical circular channels.

Transition from Slug to Churn Flow. Brauner and Barnea (1986) viewed the cause of the transition from slug to churn flow to be the inability of the liquid slug to maintain its identity. When the mixture velocity is high enough for dispersed bubbly flow to exist (Eq. 2.9) and the void fraction is higher than 52%, Brauner and Barnea (1986) postulated that transition to slug flow becomes unstable. We may use 0.52 for E_{gT} in Eq. 2.11 and arrive at one of the conditions for the onset churn flow.

$$v_{sg} > 1.66\, v_{sl} + 2.66\, v_\infty \tag{2.15}$$

Eq. 2.9 forms the other condition.

Another view of the cause for transition from slug flow is the breakdown of the Taylor bubble. The thin liquid film between a Taylor bubble and the pipe wall generates drag on the Taylor bubble which, at high velocities, may cause the bubble to break. For channels that are deviated from vertical, the Taylor bubbles ride the upper portion of the pipe, allowing the liquid to flow along the lower portion. The reduction in drag on the Taylor bubble in deviated wells makes transition to churn flow less likely. Brauner and Barnea (1986) note that churn flow never occurs in pipes that are less than 70 degrees inclined with the horizontal (i.e. more than 20 degrees deviated from vertical)

Churn Flow. Modeling the churn flow regime is difficult because of its chaotic nature. Hasan and Kabir (1992) proposed using the correlations for slug flow (Eqs. 2.11. - 2.13), but, they suggest using a value of 1.15 for the flow parameter, C_o (instead of 1.2).

For transition from churn (or slug) flow to annular flow, we follow the analysis presented by Taitel et al. (1980). During annular flow, the gas velocity is high enough for it to flow through the core of the channel, pushing the liquid phase to the wall. The liquid phase flows as a thin film through the "annulus" formed by the gas core and the pipe wall. The gas core carries a significant amount of liquid as droplets. Analyzing the drag force necessary to keep the entrained liquid droplets in suspension, Taitel et al. (1980) arrived at the following equation for transition to annular flow,

$$v_{sg} > 3.1\left[\frac{g\,\sigma_s(\rho_l-\rho_g)}{\rho_g^2}\right]^{1/4} \qquad (2.16)$$

Annular Flow. In this flow regime, the system can be considered as the single phase flow of gas through a channel formed by the liquid film. The complicating factors are the amount of liquid droplets that influence the gas core density and the "roughness" of the liquid film that determines friction. The pressure gradient can be calculated using Eq. 2.1 with ρ_c for the gas core mixture density, and f_f for the film friction factor.

Core Density, ρ_c. We define liquid entrainment as the fraction, E_e, of the input liquid that is entrained in the vapor core. Wallis and Steen (1969) found that entrainment is an unique function of the critical vapor velocity, $(v_{sg})_c$ defined as,

$$(v_{sg})_c = \frac{v_{sg}\,\mu_g\sqrt{\rho_g/\rho_l}}{\sigma} \tag{2.17}$$

Their correlation for entrainment in terms of critical vapor velocity may be represented by the following equations (Hasan and Kabir, 1988a),

$$\begin{aligned} E_e &= 0.0055\left[10^4\,(v_{sg})_c\right]^{2.86} \qquad \text{if } 10^4\,(v_{sg})_c<4 \\ E_e &= 0.857\log_{10}\left[10^4\,(v_{sg})_c\right] - 0.20 \quad \text{if } 10^4\,(v_{sg})_C>4 \end{aligned} \tag{2.18}$$

with an upper limit of $E_e = 1.0$. The gas core density is calculated from,

$$\rho_c = E_{gc}\,\rho_g + (1 - E_{gc})\,\rho_l \tag{2.19}$$

where gas void fraction for the core fluid (not the entire pipe), E_{gc}, is given by

$$E_{gc} = \frac{v_{sg}}{v_{sg} + E_e\,v_{sl}} \tag{2.20}$$

Film Friction Factor, f_f. A number of correlations are available to predicte the film friction factor, f_f. We recommend the simplest one, which was proposed by Wallis (1969),

$$f_f = f_g\left[1 + 75\,(1 - E_g)\right] \qquad (2.21)$$

Computation Algorithm. The procedure used in this work is to use the transition criteria discussed above to determine the flow regime for a particular condition of flow. For example, if the superficial gas velocity satisfies the inequality given by Eq. 2.16, the flow is taken as annular. If v_{sg} is less than required by Eq. 2.16 but the mixture velocity is higher than that needed to satisfy Eq. 2.9, then the flow regime is either (dispersed) bubbly or churn depending on whether void fraction is less or more than 0.52 (Eq. 2.15). Mixture velocity less than that calculated using Eq. 2.9 indicates slug flow (if Eq. 2.8 is satisfied) or bubbly flow.

After determining the flow pattern, we estimated the mixture density using Eq. 2.19 for annular flow and Eq. 2.3 for all other flow regimes. To estimate the void fraction, we used Eq. 2.5 for bubbly flow, and Eqs. 2.10, 2.11, and 2.12 for slug and churn flows. In these expressions, a value of 1.2 is used for C_o if the pattern is slug flow, but $C_o = 1.15$ for churn flow. After estimating mixture density, pressure gradient is estimated using Eq. 2.1.

2.2 Heat Transfer Between Wellbore Fluid and Surrounding

Producing of gas and oil often involves significant heat transfer between the wellbore fluid and the formation. The temperature of the fluid in the wellbore is generally higher than the surrounding earth temperature, causing heat loss from the fluid. The extent of heat

exchange between the wellbore and the surrounding is a function of time as well as the position in the wellbore. Because fluid properties depend on temperature, accurate estimation of temperature profile in the wellbore becomes essential. In addition, accelerated corrosion potential at certain temperature ranges makes accurate fluid temperature estimation important for proper choice of materials for the facilities and for equipment design.

As early as 1937, Schlumberger et al. pointed out the usefulness of measuring wellbore fluid temperature. Later Lesem et al. (1957) and Moss and White (1957) suggested procedures for predicting wellbore fluid temperature. The first theoretical model to estimate fluid temperature as a function of well depth and production time was proposed by Ramey (1963) and Edwardson et al. (1963). Since then many researchers, such as Willhite (1967), Farouq Ali (1970), Pacheco and Farouq Ali (1972), Herrera et al. (1978), Hong and Griston (1986), and Griston and Willhite (1987), have used Ramey's model in various applications.

The models proposed by Ramey and Edwardson et al. neglect kinetic and frictional energy losses and are limited to the flow of single-phase fluids. In addition, these models assume a well of negligible radius, which causes significant inaccuracy at early times. In recent years, several improvements have been suggested (Shiu and Beggs, 1980; Sagar et al., 1989; Hasan and Kabir, 1994). In this section we closely follow the work of Hasan and Kabir.

The basis of Hasan and Kabir's (1994) analysis is that the steady state heat flow from the tubing fluid to the wellbore/formation interface equals the heat flow from this interface to the formation. The flow of heat through the various layers facilitated by referring to the schematic shown in Fig. 3. The heat flow from the tubing fluid to the wellbore/formation

interface may be expressed in terms of an overall heat transfer coefficient and the appropriate temperature difference. The flow of heat in the formation in presence of a heat source can be modeled with a few simplifying assumptions. In the following, we first discuss formation temperature distribution. The wellbore resistances to heat flow are examined after that.

Formation Temperature Distribution. We neglect heat diffusion in the vertical direction because the vertical temperature gradient is small. Assuming symmetry around the well reduces the system to a one-dimensional diffusion problem described by the following equation,

$$\frac{\partial^2 T_e}{\partial r^2} + \frac{1}{r}\frac{\partial T_e}{\partial r} = \frac{c_e \rho_e}{k_e}\frac{\partial T_e}{\partial t} \qquad (2.22)$$

In Eq. 2.22 T_e is the temperature of earth at time, t, and distance, r, measured from the center of the wellbore. In addition, c_e, k_e, and, ρ_e represent the heat capacity, thermal conductivity, and density of the formation, respectively. Three boundary conditions are needed to solve this second order partial differential equation. The initial (t = 0) formation temperature at particular depth is constant; this provides the first of these conditions. We also assume that at the outer boundary ($r = \infty$), the formation temperature does not change with radial position. Finally, we assume that the heat flow rate at the wellbore/formation interface, governed by Fourier's law of heat conduction, is assumed constant. The effect of changing heat flow at the interface and methods to account for it are discussed in Chapter 3. The three boundary conditions then are,

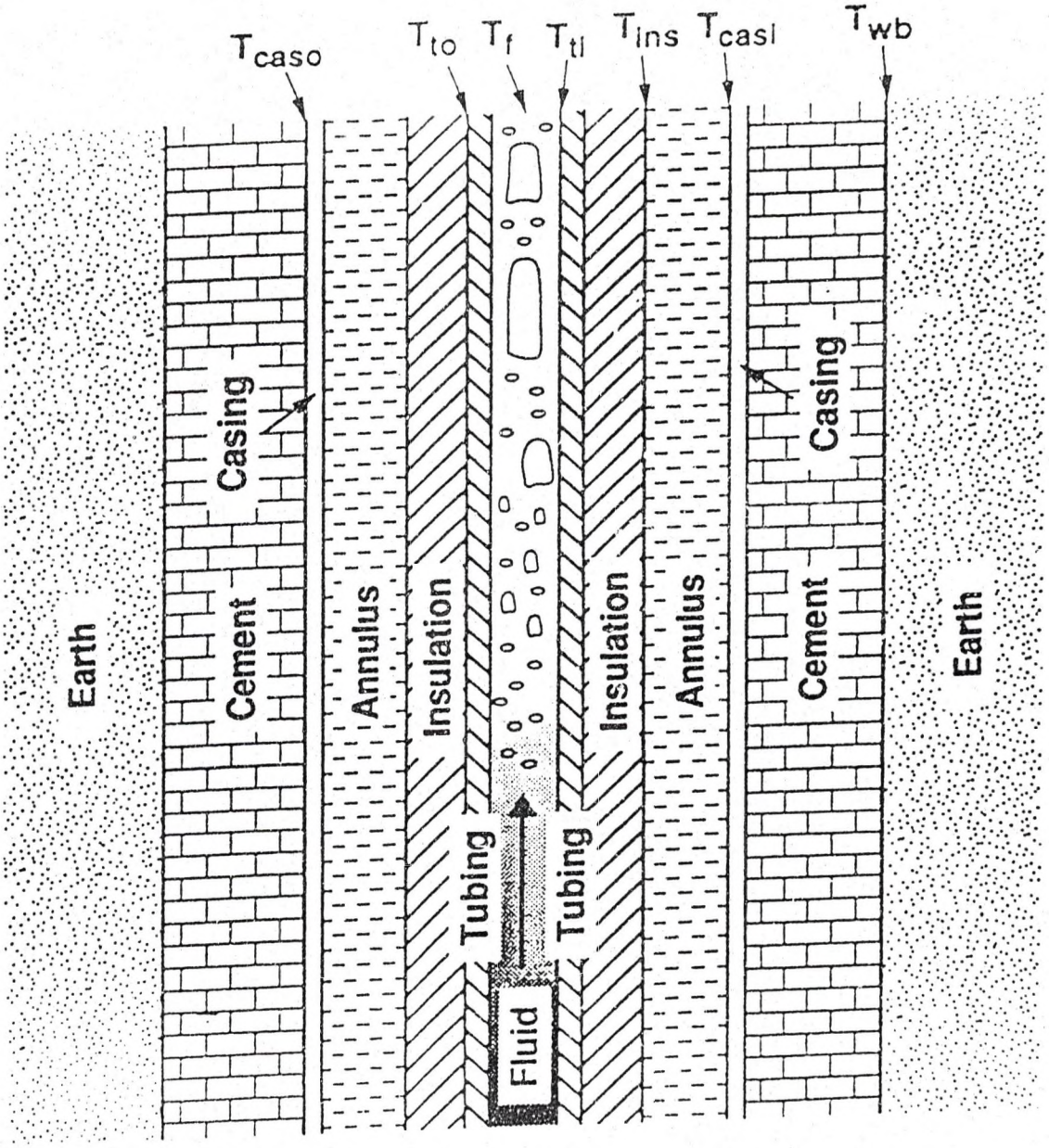

Figure 3. A General Well Configuration Involving Variety of Elements

$$\lim_{t \to 0} T_e = T_{ei} \tag{2.23}$$

$$\lim_{r \to \infty} \frac{\partial T_e}{\partial r} = 0 \tag{2.24}$$

$$\overline{Q} = -2\pi k_e \frac{r \partial T_e}{\partial r} \Big|_{r = r_{wb}} \tag{2.25}$$

In these equations, $\overline{Q}$ is the heat exchange rate per unit length and r_{wb} is the outer radius of the wellbore. Eq. 2.22 can be solved using Laplace transform (Lok, 1991) (see appendix B). The result gives the formation temperature as a function of radial distance and dimensionless time, t_D ($=\alpha t/r_{wb}^2$ where, $\alpha = k_e/\rho_e c_e$, is the thermal diffusivity),

$$T(r_D, t_D) = T_{ei} + \frac{\overline{Q}}{w \pi^2 k_e} I' \tag{2.26}$$

where

$$I' = \int_0^\infty \frac{1 - e^{-u^2 t_D}}{u^2} \frac{Y_1(u) J_0(u r_D) - J_1(u) Y_0(u r_D)}{J_1^2(u) + Y_1^2(u)} du \tag{2.27}$$

By setting r_D ($=r/r_{wb}$) equal to 1, the wellbore temperature as a function of time is obtained,

$$T_{wb} = T_{ei} + \frac{\overline{Q}}{\pi^2 k_e} I \tag{2.28}$$

where

$$I = \int_0^{\infty} \frac{1-e^{-u^2 t_D}}{u^2} \frac{Y_1(u)J_0(u) - J_1(u)Y_0(u)}{J_1^2(u) + Y_1^2(u)} du \qquad (2.29)$$

We can define a dimensionless temperature, T_D, in terms of the temperature difference between the earth and the earth/wellbore interface,

$$T_D \equiv -\frac{2\pi k_e}{\overline{Q}}\left(T_{wb} - T_{ei}\right) \qquad (2.30)$$

Thus, $T_D = -2I/\pi$. Eq. 2.30 provides a means of relating T_{wb} to T_{ei} if the dimensionless temperature, T_D, can be evaluated. However, Eqs. 2.28 and 2.29 require evaluation of an integral involving modified Bessel functions of zero and first orders over the limits of zero and infinity. Hasan and Kabir (1994) found the following algebraic expressions in terms of the dimensionless time, $t_D = \alpha t/r_w^2$, to represent the solutions quite accurately

$$\begin{aligned} T_D &= 1.1281\sqrt{t_D}\left[1 - 0.3\sqrt{t_D}\right] \qquad \text{if } t_D \le 1.5 \\ &= \left[0.4063 + 0.5\ln(t_D)\right]\left(1 + \frac{0.6}{t_d}\right) \qquad \text{if } t_D > 1.5 \end{aligned} \qquad (2.31)$$

Eq. 2.31 reduces to the log-linear approximation used by Ramey at large producing times. Unfortunately, T_D given by Eq. 2.31 is discontinuous at $t_D = 1.5$. To avoid the discontinuity and to improve accuracy, Hasan (1994) suggested the following expression which is adopted in this work.

$$T_D = \ln\left[e^{-0.2t_D} + \left(1.5 - 0.3719e^{-t_D}\right)\sqrt{t_D}\right] \qquad (2.32)$$

Wellbore Heat Flow. Estimating the rate of heat flow from the wellbore to the earth/wellbore interface requires consideration of heat transport through the well configuration shown in Fig. 3. The tubing, which produces the fluid, is surrounded by a concentric casing. Although both the tubing and casing are very conductive, their thickness requires that the resistances offered by them are properly considered. The annular space between the tubing and the casing may contain either a liquid (mud) or a gas (air) which allows transport of heat via conduction as well as convection. Surrounding the well casing are layers of cement that can convey heat by conduction. The radial heat transfer between the wellbore fluid and the surrounding may be expressed in terms of an overall heat transfer coefficient. At steady state, the rate of heat flow through a wellbore per unit length of the well, $\overline{Q}$, can be expressed as

$$\overline{Q} = 2 \pi r_{to} U_{to} (T_f - T_{wb}) \tag{2.33}$$

where U_{to} is the overall heat-transfer coefficient based on tubing outside area.

Overall Heat-Transfer Coefficient for Wellbores. An expression for overall heat transfer coefficient for heat transmission through a series of resistances can be found in any standard text on heat transfer. We reproduce below the one used by Hasan and Kabir (1991), and by Willhite (1967),

$$\frac{1}{U_{to}} = \frac{r_{to}}{r_{ti}\, h_{to}} + \frac{r_{to} \ln\left(r_{to}/r_{ti}\right)}{k_t} + \frac{r_{to} \ln\left(r_{ins}/r_{to}\right)}{k_{ins}} + \frac{r_{to}}{r_{ins}\, h_c} + \frac{r_{to} \ln\left(r_{co}/r_{ci}\right)}{k_{cas}} + \frac{r_{to} \ln\left(r_{wb}/r_{co}\right)}{k_{cem}} \tag{2.34}$$

The last six terms on the right hand side of Eq. 2.34 represent the resistances offered by the tubing fluid, tubing wall, tubing insulation, the fluid in the tubing-casing annulus, the casing wall, and the cement, respectively (see Fig. 3).

Most of the terms in Eq. 2.37 are easily computed. However, the resistance to heat flow offered by the annulus, represented by the fourth term, poses some challenge. The fluid in the annulus (air or a mud) may cause natural convection cells to set up allowing heat transfer to take place by conduction and convection. Very little work is found in the literature for convection in long annular spaces. Willhite (1967) and Hasan and Kabir adopted the following correlation proposed by Dropkin and Sommerscales (1965) for the heat-transfer coefficient for natural convection in fluids between two vertical plates,

$$h_c = \frac{0.049\ (Gr\ Pr)^{0.333}\ Pr^{0.074}\ k_a}{r_{ins}\ \ln\left(r_{cl}/r_{ins}\right)} \qquad (2.35)$$

Where Grashof number, Gr, and Prandtl number, Pr, are defined as,

$$Gr = \frac{(r_{cl} - r_{ins})^3\ g\ \rho_a^2\ \beta\ (T_{ins} - T_{cl})}{\mu_a^2} \qquad (2.36)$$

$$Pr = \frac{c_p\ \mu_a}{k_a} \qquad (2.37)$$

Effect of Production Through a Sea-bed. Production from an offshore environment is very common. In these cases, the wellbore fluid temperature can be significantly affected

by the extent of the exposure of the well to the sea water and the seawater temperature. For production through seawater (for a well exposed to air), a tubing/casing configuration without any cement is assume The overall heat-transfer coefficient in such a case can be represented by the following equation,

$$\frac{1}{U_{to}} = \frac{r_{to}}{r_{ti}\, h_{to}} + \frac{r_{to}\, \ln\left(r_{to}/r_{ti}\right)}{k_t} + \frac{r_{to}\, \ln\left(r_{ins}/r_{to}\right)}{k_{ins}} + \frac{r_{to}}{r_{ins}\, h_c} + \frac{r_{to}\, \ln\left(r_{co}/r_{ci}\right)}{k_{cas}} + \frac{r_{to}}{r_{co}\, h_{sea}} \tag{2.38}$$

where h_{sea} is given by Fishenden and Saunders (1950) to account for the forced convection.

2.3 Well Testing

Well-testing, in which a producing well is "shut-in" (buildup test) or a previously shut-in well is "drawn down" (drawdown test) and the transient pressure response at the well bottom measured, provides valuable information about the reservoir. Modeling the process of buildup is very similar to modeling drawdown. In the following, we briefly outline the analysis of a buildup test.

Initially the increase in the bottomhole pressure (BHP, p_{ws}) with time is caused entirely by static head of the fluid influx. The unsteady-state material balance for early times is given by

$$(\textit{mass rate in} - \textit{mass rate out})\, dt = V_{wb}\, d\rho \tag{2.39}$$

where V_{wb}, is the wellbore volume. In terms of volumetric flow rates and fluid sandface

density

$$(q_{sf} - q_{wh})\rho_{sf} = \left(\frac{V_{wb}}{B}\right)\frac{d\rho}{dp_s}\frac{dp_{ws}}{dt} \qquad (2.40)$$

where q_{sf} is the sandface (bottomhole) influx rate, q_{wh} is the exit rate, and B is the formation volume factor which accounts for the effect of pressure on reservoir fluid volume. Using $c_{wb} = (1/\rho)(d\rho/dp)$ as fluid compressibility, Eq. 2.40 is generally written as,

$$q_{sf} = q_{wh} + \left(\frac{V_{wb}}{B}\right) c_{wb}\frac{dp_{ws}}{dt} \qquad (2.41)$$

Note that for oil wells, c_{wb} is a constant because there is negligible change in liquid density with pressure. Even for real gases at high pressures, if the compressibility factor, Z_c, does not change much with pressure, density becomes linear with pressure and c_{wb} may be assumed constant.

During a surface shut-in, q_{wh} is zero. Eq. 2.41 shows that during this initial period, called the storage affected period, pressure increases linearly with time if c_{wb} remains constant. Hence a cartesian plot of pressure increase ($= p_{ws} - p_{wf}$) (or pressure) versus time is linear. A log-log plot of these variables is also linear with a slope of unity.

Eventually the fluid influx into the wellbore becomes negligible. However, the pressure gradient established in the formation due to earlier production through the well, causes formation fluid to flow towards the wellbore which results in a gradual increase in BHP with time. The differential equation governing fluid flow through the porous medium is very similar to the declining flow of heat described in Section 2.2. Indeed, the same

diffusivity equation in terms of temperature (the driving force for heat flow) that applies for heat flow applies in terms of pressure to fluid flow. The applicable boundary conditions for a cylindrical reservoir of radius r_e, producing through a wellbore of dimensionless radius, r_D, ($= r_w/r_e$), are also similar to those given by Eqs. 2.23-2.25. The details are decribed in the book "Pressure Transient Analysis" (J.F. Stanislav/C.S. Kabir, 1990). The solution to the flow equation in this case is,

$$p_i - p_{ws} = m_g^* \log\left[\frac{t_p + \Delta t}{\Delta t}\right] \qquad (2.42)$$

Or

$$\Delta p = m_g^* \log t' \qquad (2.43)$$

$$m_g^* = 162.6 \frac{qB\mu}{kh} \qquad (2.44)$$

where t_p is the time the well has been producing at the constant rate of q prior to shut-in, Δt is the shut-in time, μ is the fluid viscosity, k is the reservoir permeability, h is the pay zone thickness and $t' = (t_p+\Delta t)/\Delta t$.

Eq.2.43 shows that a plot of Δp (or p_{ws}) versus log (t') is linear and the slope of this line can be used to estimate the permeability-thickness parameter kh. In addition, differentiating Δp with respect to log t' we obtain,

$$d\Delta p = m_g^* \, d\log t' \qquad (2.45)$$

Thus, plot of $d(\Delta p)$ versus $d(\log t')$ gives m_g^*.

In a drawdown test, the change in bottomhole pressure with time can be represented

by similar expressions during both the storage dominated period and the infinite acting period. Quite often, these relationships are expressed in terms of dimensionless variables. Thus, for the storage dominated period,

$$\frac{dp_{wD}}{dt_D} = \frac{1}{C_D}\left(1 - \frac{q_{sf}}{q}\right) \tag{2.46}$$

where q is any reference flow rate. The dimensionless pressure, dimensionless time and the dimensionless wellbore storage coefficient are defined respectively as,

$$p_{wD} = 0.00708\,\frac{kh\left(p_{ws} - p_{wf}\right)}{q_{wf} B\,\mu}$$

$$t_D = 0.00264\,\frac{k\,t}{\phi\,\mu\,c_t\,r_w^2} \tag{2.47}$$

$$C_D = \frac{0.894\,C_s}{h\,\phi\,c_t\,r_w^2}$$

where p_{wf} and q_{wf} are the bottomhole pressure and the flow rate, respectively, at the time of shut-in. The wellbore storage coefficient C_s is defined as the product of gas formation volume and the gas compressibility. During the infinite-acting period

$$p_{wD} = \frac{1}{2}\ln\left(t_D / r_D^2 + 0.809\right) \tag{2.48}$$

Communication between a well and the reservoir is established by perforating the well at selected points in the pay zone. Often the perforations are less than ideal because of short penetration, partial plugging due to fines, etc. The obstructions to flow in the vicinity of the

wellbore are usually represented as an addition to pressure drop, s. Thus,

$$p_{wD} = \frac{1}{2}\ln\left(t_D / r_D^2 + 0.809\right) + s \qquad \textbf{(2.49)}$$

At "very late" times (pseudosteady-state period) dp_{wD}/dt_D is affected by the reservoir boundary, which allows estimates of reservoir size.

CHAPTER 3

THEORY

3.1 Introduction to Transient Flow of Mass, Momentum and Energy

Many petroleum production operations involve frequent shutting and restarting. Transient flow of mass, momentum, and energy occurs whenever the coupled wellbore/reservoir system is perturbed. The large storage capacities of many wells result in long duration of the transients initiated by the flow perturbation. When production occurs from high temperature reservoirs, considerable heat exchange takes place between the wellbore fluid and its surroundings. The flow condition becomes even more complicated in an offshore producing environment when a portion of the wellbore is exposed to the colder seawater. Modeling such systems is further exacerbated if we have to contend with unsteady flow. Yet, the classical approach to modeling these flow processes has been to ignore, or at best minimize, the effects of these transients. For "well testing", in which formation transport properties are estimated from transient pressure response in a well, ignoring the effect of transient heat transfer could lead to serious errors.

Oil companies conduct millions of dollars worth of well tests to gain information about a hydrocarbon reservoir's production potential. A large fraction of these well tests are buildup tests in which a producing well in the reservoir is "shut-in" at the well

bottom (bottomhole or sandface) or at the surface (wellhead) and the transient pressure response at the well bottom is measured. Some of the tests are "drawdown tests" in which a previously shut well is produced at a constant rate. The change in bottomhole pressure (BHP) with time in such tests provides valuable information about formation (reservoir) properties. However, conducting shut-in or drawdown tests is very expensive and time consuming. This is particularly true in the hostile environment of a high temperature/high pressure reservoir where corrosion and other problems may cause equipment failure. A fully transient wellbore/reservoir simulator is very useful in such circumstances.

A simulator can be used to estimate surface and bottomhole pressures and temperatures when these data are impractical to gather or can be gathered only infrequently because of equipment malfunction or cost considerations. In addition, even when running well tests is cost effective and easy, such a simulator would be very convenient in designing these tests. Transient simulations are also very helpful for designing and maintaining pipelines, equipment, and facilities, particularly in an offshore environment. Other applications, such as performing transient nodal analysis, designing or interpreting temperature logs, etc. emphasize the importance of such a simulator.

Only a few simulators have been reported in the literature. For example, Miller (1980) presented a coupled wellbore/reservoir numeric simulator for geothermal reservoirs. Baker and Price (1990) discussed the results of a finite-element model, while Mitchell and Wedelich (1989) presented some computational results from a finite-difference simulator. In both these studies, the energy equation was solved but the details of the model

formulation were not shown. A fully implicit three-dimensional wellbore/reservoir simulator was reported by Stone et al.(1989) for thermal recovery processes. Models were also presented by Winterfeld (1989) and Alhmehaideb et al. (1989) for simulating gas-oil systems without solving the energy equation. However, these models only work well for near-isothermal well testing problems.

In this chapter, we develop a hybrid approach to couple the wellbore with the reservoir. For flow through the porous reservoir medium, we use the available analytical solution for an infinite acting cylindrical reservoir. The wellbore model, requiring simultaneous solution of the mass, momentum, and energy balance equations, uses a numerical approach. We begin with model development for single-phase flow of gas in the wellbore. The general case of two-phase flow in the well is considered after that. A limiting case of the two-phase flow model is the production of single-phase oil. The agreement between simulation results and field data will be shown in Chapter 4.

3.2 Modeling Transport Processes in a Gas Well

Mass, momentum, and energy balances, along with the equation of state relation for the gas, are used to generate the constitutive equations. Figure 4 sketches the basis for these balances for a control volume of unit length within the wellbore.

Material Balance. The amount of gas in a given control volume is the product of the volume and the density. The volume is given by the product of the area (or average area, when the area varies with the length) and the length of the element. The change in the mass of gas in this control volume per unit time is the mass rate of fluid leaving the system minus

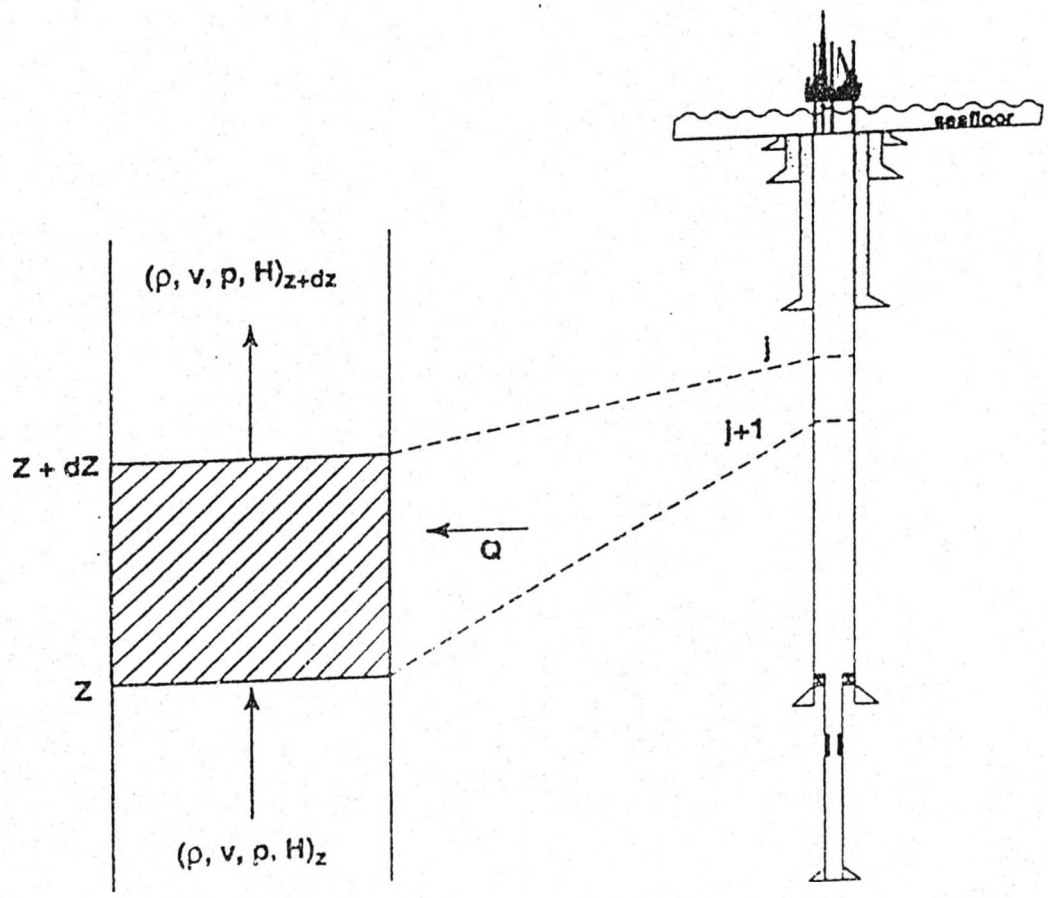

Figure 4. Transient Mass, Momentum and Energy Balance in a Gas Wellbore

that entering. Thus, the mass balance equation for a differential length, dz, of the well in terms of wellbore gas density, ρ, and gas velocity, v, is written as

$$\frac{\partial \rho}{\partial t} + \frac{\partial (\rho v)}{\partial z} = 0 \qquad (3.1)$$

Momentum Balance. For a steady flow system, the pressure gradient, dp/dz, is balanced by the static head, ρgsinθ, the friction head, $2\rho f v^2/d$, and the kinetic head, (ρv)(dv/dz). For transient flow, the additional term, ρdv/dt, is needed. Hence, the momentum balance equation becomes,

$$\frac{\partial v}{\partial t} + v\frac{\partial v}{\partial z} = -\frac{1}{\rho}\frac{\partial p}{\partial z} - g\sin\theta - \frac{2fv^2}{d} \qquad (3.2)$$

Equation of State. The pressure-volume-temperature relationship for real gases may be described by the law of corresponding state,

$$p = Z_c \rho R T_f \qquad (3.3)$$

where Z_c is the compressibility factor. The compressibility factor for gases depends on the reduced pressure ($p_r = p/p_c$) and reduced temperature ($T_r = T_f/T_c$). We used the expression proposed by Gopal (1977) to estimate Z_c.

Energy Balance. During production, the temperature of the fluid entering the wellbore at the bottom is usually the same as the formation temperature at this depth. Formation temperature generally increases, often linearly, with depth. Thus, as this fluid moves up the well, it loses heat to the surrounding earth. In Chapter 2, we discussed the estimation procedure for heat transfer through the well configuration. Here we note that

during the initial phase of production (or shut-in) when the system is transient, we need to account for the temperature change (heat accumulation or storage) of the tubing/casing/cement configuration as well as the change in fluid temperature with time.

Thus, the energy balance includes the conductive heat loss to (or gain from) the formation, $\overline{Q}$, as well as the convective energy transport into and out of a control volume of unit length. The term involving convective energy transport is written as changes in the enthalpy of the gas, plus its kinetic energy and potential energy changes. Energy accumulation in the control volume is responsible for the change in the internal energy (hence temperature) of the gas as well as the change in the internal energy of the tubing/casing/cement material.

Thus, in terms of the internal energy of the gas, E, its enthalpy, H, its flow rate, w, mass in the control volume, m, and the internal energy and the mass of the wellbore system (the tubing, casings, and cement sheaths combined), $(m'E)_w$, the energy balance equation, is given by

$$\overline{Q} = \frac{d(mE)_{cv}}{\Delta z\, dt} + \frac{d(m'E)_w}{\Delta z\, dt} + \frac{d}{dz}\left[w\left(H + \frac{1}{2}v^2 + gz\right)\right] \qquad (3.4)$$

Expressing internal energy in terms enthalpy, and enthalpy variation in terms of temperature and pressure, we obtain,

$$E = H - \frac{p}{\rho} \qquad (3.5)$$

$$dH = \left(\frac{\partial H}{\partial p}\right)_{Tf} dp + \left(\frac{\partial H}{\partial T_f}\right)_p dT_f \qquad (3.6)$$

$$= -C_J C_p dp + C_p dT_f$$

The heat capacity, C_p, is a function of temperature and can be calculated using the following correlation,

$$C_p = \left(c_1 + c_2 T + c_3 T^2 + c_4 T^{-2}\right) \times 1.986 \qquad (3.7)$$

Values of the parameters, c_i (I= 1, 2, 3, 4) can be found in Handbook of Chemistry and Physics. For a mixture of gases, the values of c_i are the weighted average values of all the components. For example, if the mixture contains four components, say CO_2, H_2S, N_2 and CH_4, c_i is calculated using

$$c_i = c_{iCO_2} CO_2\% + c_{iH_2S} H_2S\% + c_{iN_2} N_2\% + c_{iCH_4} CH_4\% \qquad (3.8)$$

Joule-Thompson coefficient. The change in enthalpy per unit change in pressure is termed the Joule-Thompson effect and the related coefficient is called the Joule-Thompson coefficient, $C_J = -\partial p/\partial z$. For a single phase gas, the coefficient can be calculated from changes in the compressibility factor, Z_c. For a multiphase system, one may use the empirical approach used by Sagar et al. (1991). However, we prefer the theoretical approach developed by Alves et al. (1991) which leads to the following expression for the coefficient, C_J,

$$C_J = -\frac{1}{C_p}\left[\frac{x}{\rho_g}\left(\frac{-T}{Z_c}\left(\frac{\partial Z_c}{\partial T}\right)_p\right) + \frac{(1-x)}{\rho_l}\right] \tag{3.9}$$

where x is the mass fraction of gas in the mixture. For a single phase, x is 1 for gas and zero for liquid.

Variable Wellbore Cross-sectional Area. Tubings of differing sizes are often used at various depths in a well. For a flowing fluid, cross-sectional area change causes additional momentum loss. In addition, the discretization of the differential equation across such a change needs to be done carefully. We use the average cross-section area, A, for the control volume to account for variation of the cross-section area. The first left term d(mE)/(Δz dt) in Eq. 3.4 can be expanded as,

$$\begin{aligned}
\frac{\partial (m E)_{cv}}{\Delta z\, \partial t} &= A \frac{\partial (\rho E)_{cv}}{\partial t} \\
&= A\left[\rho \frac{\partial (H - p/\rho)}{\partial t} + \left(H - \frac{p}{\rho}\right)\frac{\partial \rho}{\partial t}\right] \\
&= A\left[\rho \frac{\partial H}{\partial t} - \rho \frac{\partial (p/\rho)}{\partial t} + \left(H - \frac{p}{\rho}\right)\frac{\partial \rho}{\partial t}\right] \\
&= A\left[\rho \frac{\partial H}{\partial t} - \rho R \frac{\partial (Z_c T_f)}{\partial t} + \left(H - \frac{p}{\rho}\right)\frac{\partial \rho}{\partial t}\right]
\end{aligned} \tag{3.10}$$

Energy Absorbed (or Released) by the Tubulars and Cement Sheaths. The second term on the right side of Eq. 3.4, d(mE')/(Δz dt), represents the energy absorbed (or released) by the tubulars and cement sheaths in the wellbore. Omitting this term, as done by Miller (1980), could lead to serious error because it accounts for a significant fraction of the total

energy exchange between the wellbore and the formation. Analogous to the first term in Eq. 3.4, we set this term equal to $Ad(\rho' c' T_f)/(dt)$ where c' represents weighted-average specific heat of the wellbore cement/tubular material. It may be prohibitively complicated to account for the individual heat capacity and transient temperature of each element of the wellbore. Instead, one may use a weighted-average temperature of the cement/tubular material and assume that at any time, the temperature rise of this composite material is a fraction of the rise in the gas temperature. This approach simplifies the mathematical foundation and saves computation time without significantly affecting prediction accuracy.

Heat Exchange With Formation. Eq. 2.30 represents the heat lost (or gained) by the wellbore fluid to the formation, $\bar{Q}$, in terms of wellbore/earth interface temperature and formation temperature,

$$\bar{Q} = -\frac{2\pi k_e}{T_D}(T_{wb} - T_{ei}) \qquad \textbf{(2.30)}$$

Eq. 2.33, reproduced below, relates $\bar{Q}$ to the overall heat transfer coefficient and the fluid temperature,

$$\bar{Q} = 2\pi r_{to} U_{to}(T_f - T_{wb}) \qquad \textbf{(2.33)}$$

Combining these two equations to eliminate the T_{wb}, we obtain

$$\bar{Q} = w c_p L_R (T_{ei} - T_f) \qquad \textbf{(3.11)}$$

where

$$L_R = \frac{2\pi}{w\, c_p}\left(\frac{r_{to} U_{to} K_e}{K_e + r_{to} U_{to} T_D}\right) \tag{3.12}$$

Variable Heat Flux at the Wellbore/formation Interface. In deriving Eq. 2.30 for formation temperature distribution, we assumed that the heat transfer across the interface does not change with time. At the beginning of a temperature transient this constancy of $\bar{Q}$ may not be accurate. As the wellbore gas loses heat, the surrounding formation temperature will rise, slowing the heat exchange. The superposition principle can be adapted to account for changes in both the heat and mass flow rates with time.

To estimate fluid temperature at any time t, first, we divide the total time into n periods-$(t_1-t_0),(t_2-t_1).....(t_n-t_{n-1})$. In each of these time period, we assume that the heat flow is constant. Thus, at the first time period,

$$T_{ei} - T_{wb1} = \frac{1}{2\pi k_e}\bar{Q}\, T_D(t_D) \tag{3.13}$$

During the second time period, t_2-t_1, the heat flow rate, $\bar{Q}_2$ is equal to adding another constant heat flow rate whose magnitude is $(\bar{Q}_2-\bar{Q}_1)$, hence,

$$T_{ei} - T_{wb2} = \frac{1}{2\pi k_e}\left[\bar{Q}_1 T_D(t_D) + (\bar{Q}_2-\bar{Q}_1) T_D(t_D-t_{D1})\right] \tag{3.14}$$

Similarly the third time period can be represented by three sources of heat resulting in,

$$T_{ei} - T_{wb3} = \frac{1}{2\pi k_e}[\bar{Q}_1 T_D(t_D) + (\bar{Q}_2-\bar{Q}_1) T_D(t_D-t_{D1}) + (\bar{Q}_3-\bar{Q}_2) T_D(t_D-t_{D2})] \tag{3.15}$$

By setting $\ddot{Q}_0=0$. the heat flow rate, $\bar{Q}_n$, during the n^{th} time period, can be simply expressed as,

$$T_{ei} - T_{wbn} = \frac{1}{2\pi k_e}\sum_{i=1}^{n} (\overline{Q_i}-\overline{Q_{i-1}})\, T_D\,(t_D - t_{D_{i-1}}) \qquad \textbf{(3.16)}$$

Rearranging Eq. 2.33 for T_{wbn}, we get,

$$T_{wbn} = T_{fn} + \frac{\overline{Q_n}}{2\pi r_{to} U_{to}} \qquad \textbf{(3.17)}$$

Substituting this expression for T_{wbn} into equation Eq. 3.16,

$$\begin{aligned} T_{ei} - T_{fn} &= \frac{\overline{Q}}{2\pi r_{to} U_{to}} + \frac{1}{2\pi k_e}(\overline{Q_n}-\overline{Q_{n-1}})\, T_D(t_D - t_{D_{n-1}}) \\ &\quad + \frac{1}{2\pi k_e}\sum_{i=1}^{n-1} (\overline{Q_i}-\overline{Q_{i-1}})\, T_D(t_D - t_{D_{i-1}}) \\ &= \frac{\overline{Q_n}}{2\pi}\left[\frac{1}{r_{to}u_{to}} + \frac{T_D(t_D - t_{D_{n-1}})}{k_e}\right] - \frac{1}{2\pi k_e}\overline{Q_{n-1}}\, T_D(t_D - t_{D_{n-1}}) \\ &\quad + \frac{1}{2\pi k_e}\sum_{i=1}^{n-1} (\overline{Q_i}-\overline{Q_{i-1}})\, T_D(t_D - t_{D_{i-1}}) \end{aligned} \qquad \textbf{(3.18)}$$

If we let the superscript denote the value of the variables at the timestep, the heat flow at time step l+1, $\bar{Q}^{l+1}$, can be obtained from Eq. 3.18,

$$\overline{Q^{l+1}} = w^{l+1} C_p L_R^{l+1} (T_{ei} - T_f^{l+1}) + \sigma^l \qquad \textbf{(3.19)}$$

where

$$\sigma^l = \frac{\overline{Q}^l c_p w^{l+1} L_R^{l+1} T_D(t_D - t_D^l)}{2\pi k_e} - \frac{c_p w^{l+1} L_R^{l+1} \sum_{i=1}^{l} (\overline{Q_i} - \overline{Q_{i-1}}) T_D(t_D - t_D^{i-1})}{2\pi k_e} \tag{3.20}$$

In many situations, the differences in predictions when using Eq. 3.11 and Eq. 3.19 are not large. Thus, while less accurate, using Eq. 3.11 instead of Eq. 3.19, for the sake of simplicity and saving computation time, may be acceptable.

Wellbore Fluid Temperature. An equivalent form of the energy equation can be obtained by dividing Eq. 3.4 throughout by the average cross-sectional area, A,

$$\frac{\overline{Q}}{A} = \rho \frac{\partial H}{\partial t} - \rho R \frac{\partial (Z_c T_f)}{\partial t} + \left(H - \frac{p}{\rho}\right) \frac{\partial \rho}{\partial t} + \frac{d(\rho' c' T_f)}{dt} + \frac{(\rho v)_{out}}{\Delta z} \left(H_2 + \frac{1}{2} v_2^2 + g z_2\right)_{out} - \frac{(\rho v)_{in}}{\Delta z} \left(H_1 + \frac{1}{2} v_1^2 + g z_1\right)_{in} \tag{3.21}$$

Substituting Eq. 3.19, one can obtain following finite differential energy equation,

$$\frac{(\overline{Q})_j^{l+1}}{A} = \rho_j^l \frac{\Delta H}{\Delta t} - \rho_j^l R \frac{\Delta\left[Z_c(T_f)\right]}{\Delta t} + \left(H_j^l - \frac{p_j^l}{\rho_j^l}\right) \frac{(\rho_j^{l+1} - \rho_j^l)}{\Delta t}$$

$$+ \frac{\rho' c' (T_f^{l+1} - T_f^l)}{\Delta t} + \frac{(\rho v)_{j+1}^l}{\Delta z}\left(H^l + \frac{1}{2}(v^l)^2 + g z\right)_{j+1} \qquad (3.22)$$

$$- \frac{(\rho v)_j^l}{\Delta z}\left(H^l + \frac{1}{2}(v^l)^2 + g z\right)_j$$

$$= G_j^{l+1} c_{p_j}^{l+1} (T_{el_j} T_{f_j}^{l+1}) L_{R_j}^{l+1} + \frac{\sigma_j^l}{A}$$

where

$$G_j^{l+1} = \rho_j^{l+1} v_j^{l+1} \qquad (3.23)$$

$$\Delta H = - C_{Jj}^l C_{pj}^l \left(p_j^{l+1} - p_j^l\right) + C_{pj}^l \left[(T_f)_j^{l+1} - (T_f)_j^l\right] \qquad (3.24)$$

$$\Delta\left(Z_c T_f\right) = Z_{c_j}^{l+1} T_{f_j}^{l+1} - Z_{c_j}^l T_{f_j}^l \qquad (3.25)$$

and

$$\sigma_j^l = \frac{\overline{Q^l} c_{p_j}^l L_{R_j}^{l+1} T_D(t_D - t_D^l)}{2\pi k_e}$$

$$- \frac{w_j^{l+1} c_{p_j}^l L_{R_j}^{l+1} \sum_{i=1}^{l} (\overline{Q^i} - \overline{Q^{i-1}}) T_D(t_D - t_D^{i-1})}{2\pi k_e} \qquad (3.26)$$

Rearranging Eq.3.22, we get an explicit expression for wellbore fluid temperature at any

time and any depth, T_{fj}^{l+1},

$$(T_f)_j^{l+1} = \frac{G_j^{l+1} T_{ei_j} c_p^{l+1} (L_R)_j^{l+1} + \sigma_j^l/A - \psi_j^l + \xi_j^l (T_f)_j^l + \omega_j^l}{G_j^{l+1} (L_R)_j^{l+1} + \xi_j^l - \lambda_j^l} \tag{3.27}$$

where expressions for various terms, ψ_j^l, ξ_j^l, λ_j^l, ω_j^l, are

$$\psi_j^l = (H_j^l - \frac{p_j^l}{\rho_j^l J}) \frac{(\rho_j^{l+1} - \rho_j^l)}{\Delta t}$$

$$+ \frac{(\rho v)_{j+1}^l}{\Delta z} \left(H^l + \frac{1}{2} (v^l)^2 + g z \right)_{j+1} \tag{3.28}$$

$$- \frac{(\rho v)_j^l}{\Delta z} \left(H^l + \frac{1}{2} (v^l)^2 + g z \right)_j$$

$$\xi_j^l = \frac{C_p^l \rho_j^l}{\Delta t} + \frac{\rho^l c^l}{\Delta t} \tag{3.29}$$

$$\lambda_j^l = \frac{R \rho_j^l Z_{c_j}^{l+1}}{\Delta t} \left(1 + C_J C_p^l \rho_j^{l+1} \right) \tag{3.30}$$

$$\omega_j^l = -\frac{R C_{Jj}^l C_p^l \rho_j^l}{\Delta t} \left(Z_{c_j}^l \rho_j^l T_{f_j}^l \right) - \frac{R \rho_j^l}{\Delta t} \left(Z_{cj}^l T_{f_j}^l \right) \tag{3.31}$$

3.3 Computational Algorithm

As discussed in Chapter 2 and the beginning of Chapter 3, the total pressure gradient is the sum of the transient head, the kinetic head, the static head and the frictional head (Eq. 3.2). For a single gas phase, the density can be easily calculated using an equation of state given gas pressure and temperature. For computing friction factor, we use the correlation proposed by Chen (1979).

$$f = \frac{1}{\left[-4\log_{10}\left(\frac{\varepsilon/d}{3.7065} - \frac{5.0452}{Re}\log_{10}\Lambda\right)\right]^2} \tag{3.32}$$

where ε is pipe roughness with length unit, and the dimensionless parameter, Λ, is given by

$$\Lambda = \frac{(\varepsilon/d)^{1.1098}}{2.8257} + \left(\frac{7.149}{Re}\right)^{0.8981} \tag{3.33}$$

As usual, Reynolds number, Re, is defined as,

$$Re = \frac{d v \rho}{\mu} \tag{3.34}$$

We use a finite difference technique to solve the governing differential equations using "j" to designate the spatial coordinate (starting at the well head) and "l" for the time coordinate.

Fluid Pressure. Fluid pressure at any depth and any time step, p_j^l, is calculated from the total pressure gradient using the following finite difference equation,

$$p_j^l = p_{j+1}^l - \Delta Z \left(\frac{dp}{dz}\right)_{j+1/2}^l \tag{3.35}$$

where pressure gradient at the mid point between two nodes, $(dp/dz)_{j+1/2}^{l}$, is calculated by,

$$-\frac{dp^{l}}{dz}_{j+1/2} = \rho^{l}_{j+1/2}\frac{v^{l+1}_{j+1/2}-v^{l}_{j+1/2}}{dt} + \rho^{l}_{j+1/2}v^{l}_{j+1/2}\frac{v^{l}_{j+1}-v^{l}_{j}}{z_{j+1}-z_{j}} + \rho^{l}_{j+1/2}g + \frac{2\rho^{l}_{j+1/2}f^{l}_{j+1/2}v^{l}_{j+1/2}{}^{2}}{d} \quad (3.36)$$

Wellbore Mass and Velocity Distribution. Fluid pressure and temperature depend on the fluid velocity, thus, we need an accurate estimate of fluid velocity as a function of well depth and time. When a previously shut well is suddenly opened, most of the produced gas is provided by the wellbore with very little fluid coming from the formation into the well. In addition, the upper parts of the well provide a higher fraction of the produced gas than the lower parts. In other words, mass flow rate and velocity varies with well depth. A similar phenomenon occurs during the initial period of a shut-in.

To obtain the mass and velocity distribution in the well, we multiply the material balance equation (Eq. 3.1) by v,

$$v\frac{\partial\rho}{\partial t} + v\frac{\partial(\rho v)}{\partial z} = 0 \quad (3.37)$$

and combine it with the momentum balance equation, Eq. 3.2 to obtain,

$$\rho\frac{\partial v}{\partial t} + v\frac{\partial\rho}{\partial t} + \rho v\frac{\partial v}{\partial z} + v\frac{\partial(\rho v)}{\partial z} = -\frac{\partial p}{\partial z} - \rho g - \frac{2\rho f v^{2}}{d} \quad (3.38)$$

or,

$$\frac{\partial(\rho v)}{\partial t} + \frac{\partial(\rho v^{2})}{\partial z} = -\frac{\partial p}{\partial z} - \rho g - \frac{2\rho f v^{2}}{d} \quad (3.39)$$

Eq. 3.39 allows us to write mid point $(\rho v)_{j+1/2}^{l}$ value as

$$(\rho v)_{j+1/2}^{l+1} = (\rho v)_{j+1/2}^{l} - \Delta t\, \beta_v\, \Phi_j^{l} - \Delta t\,(1-\beta_v)\, \Phi_j^{l+1} \qquad (3.40)$$

where Φ_j^{l} represents previous timestep variables,

$$\Phi_j^{l} = \frac{(\rho v^2)_{j+1}^{l} - (\rho v^2)_j^{l}}{z_{j+1} - z_j} + \frac{p_{j+1}^{l} - p_j^{l}}{z_{j+1} - z_j} + \rho_{j+1/2}^{l} g + \frac{2\,\rho_{j+1/2}^{l} f_{j+1/2}^{l} v_{j+1/2}^{l\,2}}{d} \qquad (3.41)$$

and Φ_j^{l+1} stands for present timestep values,

$$\Phi_j^{l+1} = \frac{(\rho v^2)_{j+1}^{l+1} - (\rho v^2)_j^{l+1}}{z_{j+1} - z_j} + \frac{p_{j+1}^{l+1} - p_j^{l+1}}{z_{j+1} - z_j} + \rho_{j+1/2}^{l+1} g + \frac{2\,\rho_{j+1/2}^{l+1} f_{j+1/2}^{l} v_{j+1/2}^{l+1\,2}}{d} \qquad (3.42)$$

In Eq. 3.40, β_v is the relaxation factor whose value lies between 0 and 1 ($0 \le \beta_v \le 1$). Note that the solution of Eq. 3.42 for the next time-step value of the mass flux $(\rho v)^{l+1}$ requires values of various properties at the next ($l+1$) time-step. Thus an iterative solution procedure is required.

We use b_n (n = 1, 2, 3, ...) to denote the spatial mid-point mass flux, $(\rho v)_{j+1/2}^{l+1}$, and a_n for node-point values, $(\rho v)_{j+1}^{l+1}$. Further, we assume the following relationships among the nodes,

$$\begin{aligned} a_2 &= \frac{1}{4}(a_1 + b_1 + b_2 + a_3) \\ a_3 &= \frac{1}{4}(a_2 + b_2 + b_3 + a_4) \\ &\cdots \\ a_n &= \frac{1}{4}(a_{n-1} + b_{n-1} + b_n + a_{n+1}) \end{aligned} \qquad (3.43)$$

Separating a_n and b_n and manipulating, we get

$$\begin{aligned} -4a_2 + a_3 &= -b_1 - b_2 - a_1 \\ a_2 - 4a_3 + a_4 &= -b_2 - b_3 \\ &\cdots \\ a_{n-1} - 4a_n &= -b_{n-1} - b_n - a_{n+1} \end{aligned} \tag{3.44}$$

During a well test, a known constant surface flow rate is maintained. We also assume that the fluid flow into the wellbore during the very first time-step is zero. The bottomhole flow rates during subsequent time-steps are calculated from the computed bottomhole pressure at the earlier time-steps and equations that are discussed in the next section. Thus, mass flow rates are known at the top and the bottom of the system, i.e., a_1 and a_{n+1} are known. In matrix form, we rewrite Eq. 3.44 as,

$$A.\vec{x} = C \tag{3.45}$$

where

$$A = \begin{bmatrix} -4 & 1 & 0 & 0 & 0 & 0 & . & . \\ 1 & -4 & 1 & 0 & 0 & 0 & . & . \\ 0 & 1 & -4 & 1 & 0 & 0 & . & . \\ 0 & 0 & 1 & -4 & 1 & 0 & . & . \\ . & . & . & . & . & . & . & . \\ . & . & . & . & . & . & . & . \\ 0 & 0 & 0 & 0 & . & . & 1 & -4 \end{bmatrix} \tag{3.46}$$

$$\vec{x} = \begin{bmatrix} a_2 \\ a_3 \\ a_4 \\ . \\ . \\ a_n \end{bmatrix} \tag{3.47}$$

$$C = \begin{bmatrix} -b_1 - b_2 - a_1 \\ -b_2 - b_3 \\ -b_3 - b_4 \\ .. \\ .. \\ -b_{n-1} - b_n - a_{n+1} \end{bmatrix} \tag{3.48}$$

The matrix A is tridiagonal, therefore, three vectors can be used to store the nonzero elements. The notation can be arranged as follows,

$$\begin{bmatrix} d_1 & e_1 & 0 & 0 & 0 & . & . & 0 \\ f_1 & d_2 & e_2 & 0 & 0 & . & . & 0 \\ 0 & f_2 & d_3 & c_3 & 0 & . & . & 0 \\ . & . & . & . & . & . & . & . \\ 0 & 0 & 0 & 0 & . & . & f_{n-1} & d_n \end{bmatrix} \begin{bmatrix} a_1 \\ a_2 \\ . \\ . \\ a_n \end{bmatrix} = \begin{bmatrix} g_1 \\ g_2 \\ . \\ . \\ g_n \end{bmatrix} \tag{3.49}$$

Two-step simple Gaussian elimination can be used to solve the equations. Step 1, forward elimination, involves a multiple row 1 be subtracted from row 2 to produce a zero where f_1 stood originally. The appropriate multiple is f_1/d_1,

$$d_2 \leftarrow d_2 - (f_1/d_1)\, e_1$$
$$g_2 \leftarrow g_2 - (f_1/d_1)\, g_1$$

All the remaining calculations in the forward elimination phase are similar to the first step. Step 2 is backward elimination,

$$a_n \leftarrow g_n/d_n$$
$$a_{n-1} \leftarrow (g_{n-1} - e_{n-1} x_n)/d_{n-1} \qquad (3.51)$$

Sandface Flow Rate. The solution procedure outlined above requires knowledge of the flow rate from the formation into the wellbore at the well bottom (known as the sandface). Fluid flow through the porous medium of the formation is modeled exactly the same way as heat flow, which was discussed in Chapter 2. Indeed, the diffusivity equation for flow of a single phase fluid in a homogeneous reservoir in terms of the pressure differential driving force, given by

$$\frac{\partial p_{pn}}{\partial t} = \frac{k}{\phi \mu c} \frac{1}{r} \frac{\partial}{\partial r}\left(r \frac{\partial p_{pn}}{\partial r} \right) \qquad (3.52)$$

is similar to Eq. 2.22 for heat flow in terms of temperature. Applying boundary conditions identical to these used for Eq. 2.22 (i.e. 2.23, 2,24, 2,25) we arrive at the following solution,

$$p_i - p_w = m^* q \left[p_D(t_D) + s \right] \qquad (3.53)$$

where P_i is the reservoir pressure (analogous to T_{ei}). Compared to Eq. 2.42, Eq. 3.53 has an extra term, s, called skin. Skin represents the additional pressure drop often experienced by a flowing fluid near the wellbore/formation interface. This additional resistance to flow occurs because of incomplete perforation to establish the communication between the

wellbore and the formation, sand infiltration in the perforation during the drilling process, etc. In some cases when exceptionally good communication between the well and the reservoir occurs, the value of the skin factor, s, may be negative.

Here m^* represents the flow properties of the reservoir involving its permeability, k, thickness of the pay zone, h, and viscosity of the fluid, μ_g,

$$m^* = \frac{141.2\,\mu_g}{kh} \tag{3.54}$$

The dimensionless time, t_D, is given by,

$$t_D = \frac{4\alpha t}{(2r_w)^2} = \frac{t}{r_w^2}\frac{0.0002637\,k}{\phi\,\mu_g C_t} \tag{3.55}$$

while dimensionless pressure, P_D, is given by

$$P_D = \ln\left[e^{(-0.2t_D)} + \left(1.5 - 0.3719e^{-t_D}\right)\sqrt{t_D}\right] \tag{3.56}$$

Fluid influx into the wellbore changes rapidly at early times during either a buildup or a draw down. The superposition in time is used to account for the variation in influx rate, q, with time. Analogous to the case of heat flux, we divide the total time t into n periods $(t_1-t_0),(t_2-t_1)$ $\ldots\ldots(t_n-t_{n-1})$ and assume that during each period the bottomhole flow rate is constant. During the first time period,

$$p_i - p_{wf} = m^* q_1 (P_D(t_D)+S) \tag{3.57}$$

At the second time period, flow rate q_2 can be obtained by adding another influx source,

$$\begin{aligned}\Delta P_2 &= P_i - P_{w2} \\ &= m^* \left\{ q_1 \left[P_D(t_D) + S \right] + (q_2 - q_1) \left[P_D(t_D - t_1) + S \right] \right\}\end{aligned} \tag{3.58}$$

Similarly at the n^{th} time period, the flow rate is

$$\begin{aligned}\Delta p_n &= P_i - P_{wn} \\ &= m^* \left\{ q_1 \left[P_D(t_D) + S \right] + (q_2 - q_1) \left[P_D(t_D - t_1) + S \right] \right\} \\ &+ \ldots + m^* \left\{ (q_n - q_{n-1}) \left[P_D(t_D - t_{n-1}) + S \right] \right\}\end{aligned} \tag{3.59}$$

or

$$\begin{aligned}q_n &= q_{n-1} + \frac{\Delta p_n}{m^* \left[P_D(t_D - t_{n-1}) + s \right]} \\ &- \frac{\sum_{i=1}^{n-1} (q_i - q_{i-1}) \left[P_D(t_D - t_{i-1}) + s \right]}{P_D(t_D - t_{n-1}) + s}\end{aligned} \tag{3.60}$$

Eq. 3.60 simplifies if the flow becomes steady. Assume at timestep k the bottomhole flow rate becomes the same as that in the wellhead, Eq. (3.60) can be rewritten in following equivalent form,

$$\begin{aligned}\Delta p_n &= P_i - P_{wn} \\ &= m^*\{q_1[P_D(t_D)+s] + (q_2-q_1)[P_D(t_D-t_1)+s]\} \\ &+ \ldots m^*\{(q_k-q_{k-1})[P_D(t_D-t_{k-1})+s]\} \\ &+ m^*\{(q_{k+1}-q_k)[P_D(t_D-t_k)+s]\} \\ &+ \ldots + m^*\{(q_n-q_{n-1})[P_D(t_D-t_{n-1})+S]\}\end{aligned} \tag{3.61}$$

After timestep k, the flow rate is constant, therefore,

$$q_n - q_{n_1} = \ldots = q_{k+1} - q_k = 0 \tag{3.62}$$

Eq. 3.62 allows us to express the bottomhole pressure as follows,

$$\begin{aligned}P_{wn} = p_i &- m^*\{q_1[P_D(t_D)+s] - (q_2-q_1)[P_D(t_D-t_1)+s]\} \\ &- \ldots\ m^*\{(q_k-q_{k-1})[P_D(t_D-t_{k-1})+s]\}\end{aligned} \tag{3.63}$$

A similar expression for pressure, Δp_j, during buildup may be written when buildup begins at timestep n+1,

$$\begin{aligned}\Delta p_j &= P_i - P_{wj} \\ &= m^*\{q_1[P_D(t_D)+S] + (q_2-q_1)[P_D(t_D-t_1)+S]\} \\ &+ \ldots m^*\{(q_k-q_{k-1})[P_D(t_D-t_{k-1})+S]\} \\ &+ m^*\{(q_{n+1}-q_n)[P_D(t_D-t_n)+S]\} \\ &+ \ldots + m^*\{(q_j-q_{j-1})[P_D(t_D-t_{j-1})+S]\}\end{aligned} \tag{3.64}$$

Further, if the flow rate becomes 0 at timestep m, the total pressure difference between P_i and

bottomhole pressure at any timestep n greater than m is,

$$\begin{aligned}\Delta p_n &= P_i - P_{wn} \\ &= m^*\{q_1[P_D(t_D)+S] + (q_2-q_1)[P_D(t_D-t_1)+S]\} \\ &+ \ldots m^*\{(q_k-q_{k-1})[P_D(t_D-t_{k-1})+S]\} \\ &+ m^*\{(q_{n+1}-q_n)[P_D(t_D-t_n)+S]\} \\ &+ \ldots + m^*\{(q_m-q_{m-1})[P_D(t_D-t_{m-1})+S]\}\end{aligned} \tag{3.65}$$

Inspection of Eq. 3.65 shows that there are two unknowns, q_n and P_{wn}. Knowing one would allow calculating the other. At the first time-step of a drawdown, bottomhole flow rate, q, is assumed to be negligibly small. The solution of Eq. 3.45 then gives bottomhole pressure at the end of the first time-step. This is used in Eq. 3.65 to calculate flow at the beginning of the second time-step. The procedure is repeated until flow becomes steady. After flow has become steady, we use Eq. 3.65 to calculate bottomhole pressure at each time-step.

One important thing, which should be pointed out, is that the pressure transient theory of gas well testing is preferably described using the pseudopressure as a dependent variable because of the compressibility of the gas. The definition of the pseudopressure can be found in many basic petroleum books, such as "Petroleum Production Systems" (Michael J. Economides, A. Daniel Hill and Christine Ehlig-Economides, 1994). Translations from normal pressure to pseudopressure or from pseudopressure to normal pressure is accomplished by the computer program kindly provided by the Chevron.

3.4 Modeling Transient Two-phase Flow in Wellbores

Modeling transient two-phase transport processes is analogous to that for single-phase gas flow described earlier in this chapter. The same three basic conservation equations for mass, momentum, and energy are used to generate the constitutive equations.

Momentum Balance. The momentum balance equation (3.2) is complicated in this case due to the simultaneous flow of two phases. During the drawdown process we use the model proposed by Hasan and Kabir (1992) to estimate void fraction and pressure drop during two-phase flow in the wellbore. For a buildup process, a different procedure is used. After the well is shut-in at the surface, fluid continues to flow into the wellbore for some time. However, the rate of such after-flow diminishes quickly making the application of continuous flow models for estimating void fraction difficult. Hence, our approach for a surface shut-in situation is to model migration of bubbles within the wellbore and calculate void fraction based on this information. Such a bubble migration model for near-stagnant liquid columns has been proposed by Hasan and Kabir (1995). We adopt that model for this work and describe the outline of the model below.

Bubble Migration Model. For the purpose of calculating fluid movement, we divided the wellbore into N cells, as shown in Figure 4. The basis for estimating gas void fraction in each cell at any time is to add to the gas volume calculated from prior time step, the net (in - out) gas movement into the cell.

During any timestep t_{i-1} to t_i, cell, j, receives gas from the cell below (j+1) and loses gas to the cell above. Hasan and Kabir (1995) estimate the volume of gas received by noting that the volume of gas in the lower cell at the previous time period is the total volume of that

cell times the void fraction of the cell, i.e. $(Vol)_{j+1}(E_g)_{j+1}$. The portion of this gas that would move up to the jth cell would depend on the in-situ velocity of this gas (given by Eq. 2.4, $v_g = C_o v_m + v_\infty$) and the length of the cell l_{j+1}. Of course, in moving from a lower cell to the upper one, the gas volume would change due to pressure and temperature changes. Thus, the volume of gas received is,

$$(Vol)_{j+1}\,(E_g)_{j+1}\,\frac{v_g\,(t_l - t_{l-1})}{l_{j+1}}\,\frac{p_l}{p_{l+1}}\,\frac{T_{l+1}}{T_l}\,\frac{Z_{l+1}}{Z_l} \qquad (3.66)$$

The volume of gas lost by the cell j can be similarly estimated allowing us to calculate the gas left in the cell at the end of the time period t_l. The void fraction at this time then is simply the gas volume divided by the total cell volume.

Energy Balance. For two-phase flow, the energy balance equation is better written if the energy contents of the two phases are separately accounted for. Eq.3.9 represents the general expression for the Joule-thompson coefficient, C_J. For the case of single phase liquid flow, x is 0. Therefore C_{Jl} becomes,

$$C_{Jl} = -\frac{1}{C_p \rho_l} \qquad (3.67)$$

Eq. 3.67 allows us to write the expression for ΔH_l as,

$$\Delta H_l = -C_{Jl} C_{pl} \Delta p + C_{pl} \Delta T \qquad (3.68)$$

The mixture enthalpy can be expressed as,

$$H = x H_g + (1-x) H_l \qquad (3.69)$$

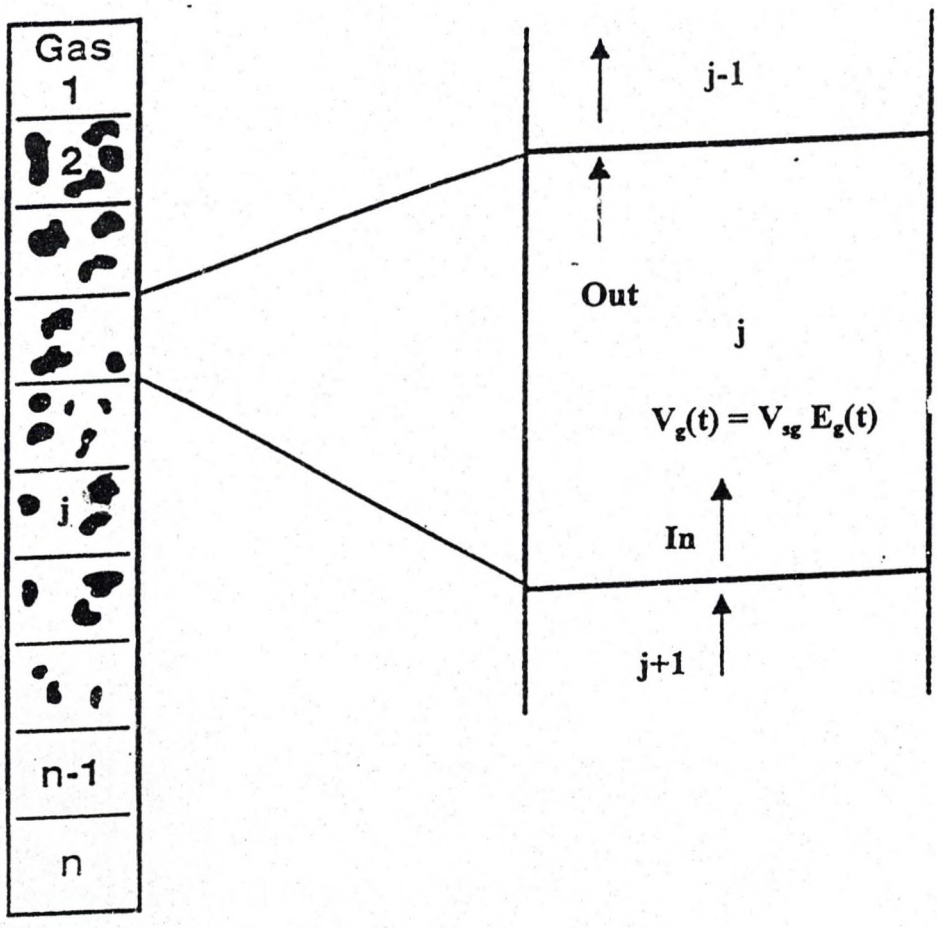

Figure 5. Wellbore Cells for Bubble Migration Model

The internal energy term, d(mE)/(∆zdt), can be further expanded as,

$$\frac{\partial(m\,E)_{cv}}{\Delta z\,\partial t} = \frac{A\,\partial(\rho\,E)_{cv}}{\partial t} = A\left[\rho\,\frac{\partial\,(H-(p/\rho))}{\partial t} + (H-(p/\rho))\,\frac{\partial\,\rho}{\partial t}\right]$$

$$= A\left[\rho\,\frac{\partial H}{\partial t} - \rho\,\frac{\partial(p/\rho)}{\partial t} + (H-(p/\rho))\,\frac{\partial\,\rho}{\partial t}\right]$$

$$= A\left[\rho\,\frac{\partial\,(x\,H_g + (1-x)\,H_l)}{\partial t} - \rho\,\frac{\partial\,(p/\rho)}{\partial t} + \left(H - \frac{p}{\rho}\right)\frac{\partial\,\rho}{\partial t}\right] \qquad (3.70)$$

$$= A\left[\rho\,(H_g-H_l)\,\frac{\partial x}{\partial t} + \rho\,x\,\frac{\partial H_g}{\partial t} + \rho\,(1-x)\,\frac{\partial H_l}{\partial t} - \rho\,\frac{\partial(p/\rho)}{\partial t} + (H-\frac{P}{\rho})\,\frac{\partial\rho}{\partial t}\right]$$

Substituting this (Eq. 3.70) expression for d(mE)/(∆zdt) into energy equation 3.4 gives,

$$\frac{\overline{Q}}{A} = \rho\,(H_g-H_l)\,\frac{\partial x}{\partial t} + \rho\,x\,\frac{\partial H_g}{\partial t} + \rho\,(1-x)\,\frac{\partial H_l}{\partial t} - \rho\,\frac{\partial(\frac{P}{\rho})}{\partial t} + (h-\frac{P}{\rho})\,\frac{\partial\rho}{\partial t}$$

$$+ \frac{\partial(\rho'\,c'\,T_f)}{\partial t} + \frac{(\rho\,v)_{out}}{\Delta z}\left(H + \frac{1}{2}v^2 + g\,z\right)_{out} - \frac{(\rho\,v)_{in}}{\Delta z}\left(H + \frac{1}{2}v^2 + g\,z\right)_{in} \qquad (3.71)$$

In terms of finite differences, Eq. 3.71 becomes,

$$\frac{(\bar{Q})_j^{l+1}}{A} = \rho_j^l (H_{gj}^l - H_{lj}^l)\frac{x_j^{l+1}-x_j^l}{\Delta t} + \rho_j^l x_j^l \frac{\Delta H_g}{\Delta t} + \rho_j^l (1-x_j^l)\frac{\Delta H_l}{\Delta t}$$

$$- \rho_j^l \frac{\left(\frac{P}{\rho}\right)_j^{l+1} - \left(\frac{P}{\rho}\right)_j^l}{\Delta t} + \left(H_j^l - \frac{P_j^l}{\rho_j^l}\right)\frac{\rho_j^{l+1}-\rho_j^l}{\Delta t} + \frac{\rho' c' (T_f^{l+1}-T_f^l)}{\Delta t} \qquad (3.72)$$

$$+ \frac{(\rho v)_{j+1}^l}{\Delta z}\left(H^l + \frac{1}{2}v^{2l} + gz\right)_{j+1} - \frac{(\rho v)_j^l}{\Delta z}\left(H^l + \frac{1}{2}v^{2l} + gz\right)_j$$

$$= G_j^{l+1} c_{pj}^{l+1} (T_{eij} - T_{fj}^{l+1}) L_{Rj}^{l+1} + \sigma_j^l / A$$

where

$$\begin{aligned} \Delta H_g &= -C_{Jgj}^l C_{pgj}^l (P_j^{l+1} - p_j^l) + C_{pgj}^l (T_{fj}^{l+1} - T_{fj}^l) \\ \Delta H_l &= -C_{Jlj}^l C_{plj}^l (p_j^{l+1} - p_j^l) + C_{plj}^l (T_{fj}^{l+1} - T_{fj}^l) \end{aligned} \qquad (3.73)$$

The final expression for fluid temperature, T_j^{l+1}, is obtained by rearranging Eq. 3.73,

$$T_{fj}^{l+1} = \frac{G_j^{l+1} T_{eij} c_{pj}^{l+1} L_{Rj}^{l+1} + \sigma_j^l / A - \psi_j^l + \varphi_j^l T_{fj}^l + \Gamma_j^l - \eta_j^l + \gamma_j^l c_{pgj}^l T_{fj}^l}{G_j^{l+1} c_{pj}^{l+1} L_{Rj}^{l+1} + \varphi_j^l + \gamma_j^l c_{pgj}^l} \qquad (3.74)$$

where σ_j^l and ψ_j^l are defined by Eq.3.26 and Eq.3.28, respectively. Other parameters are defined as follows,

$$\varphi_j^l = \rho_j^l (1-x_j^l)\frac{c_{plj}^l}{\Delta t} + \frac{\rho' \bar{c}}{\Delta t} \qquad (3.75)$$

$$\gamma_j^l = \frac{\rho_j^l x_j^l}{\Delta t} \tag{3.76}$$

$$\eta_j^l = \rho_j^l (H_{gj}^l - H_{lj}^l) \frac{x_j^{l+1} - x_j^l}{\Delta t} \tag{3.77}$$

$$\Gamma_j^l = \frac{\rho_j^l \left[1 - x_j^l c_{pgj}^l c_{Jgj}^l - (1 - x_j^l) c_{plj}^l c_{Jlj}^l\right](p_j^{l+1} - p_j^l)}{\Delta t} \tag{3.78}$$

For single liquid flow,

$$\gamma_j^l = 0 \quad \eta_j^l = 0 \tag{3.79}$$

Therefore, expression for temperature during single phase liquid flow becomes,

$$T_{fj}^{l+1} = \frac{G_j^{l+1} T_{wj} c_{pj}^{l+1} L_{Rj}^{l+1} + \sigma_j^l / A - \psi_j^l + \varphi_j^l T_{fj}^l + \Gamma_j^l}{G_j^{l+1} c_{pj}^{l+1} L_{Rj}^{l+1} + \varphi_j^l} \tag{3.80}$$

3.5 Aspects of Simulator Development

The conservation equations presented above help us simulate wellbore pressure and temperature given the reservoir parameters, fluid properties, and well configuration. The results of such forward simulation is useful in matching field data as well as in designing well tests. Of course, when well test data, i.e. wellhead pressure and temperature, are

available we would like to estimate the formation properties by first estimating the bottomhole transient pressure from the wellhead data. Such a translation of the wellhead data to obtain bottomhole data is known as reverse simulation. Thus, based on our transient wellbore/reservoir model, we have developed both forward and reverse (translating) simulators. The forward simulator allows us to simulate wellbore fluid temperature, pressure, density, velocity and other variables at any depth and any time for given reservoir parameters and well completion details. The reverse (or translating) simulator allows us to convert measured wellhead pressure and temperature to bottomhole pressure for subsequent analysis making use of conventional methods discussed in Section 3 of Chapter 2. Key aspects of these simulators are discussed in the following sections.

3.5.1 Gas simulators

Forward Simulation. The complexity of the governing equations requires solution of the equations presented above using a numerical approach. We divide the wellbore into a number of cells not necessarily of equal length (see figure 4).

The initial conditions assigned in drawdown computation are as follows: the program takes the geothermal temperature profile for the wellbore fluid. If the initial wellhead fluid temperature is different from the formation surface temperature, the difference is proportionally added along the well depth. Bottomhole fluid pressure equals the reservoir pressure creating the no-flow condition. Fluid pressure at various depth in the wellbore is then estimated based on this no-flow initial condition. In buildup simulation, by contrast, the program uses the last temperature and pressure profiles calculated in the

previous drawdown simulation.

We use an explicit approach with successive iterations to solve the differential equations involved. To begin simulation, a small Δp is assigned to bottomhole pressure in the first timestep, allowing computation of the bottomhole mass flow rate from Eq. (3.60). The wellhead flow rate is maintained constant and we assume linear mass flow rate distribution along the wellbore as a first approximation. To account for the finite time required to attain the production rate, the program also allows users to specify the time required to open the wellhead valves. We assume the bottomhole temperature remains constant, thus, all variables at the bottomhole are known.

The iterative computation procedure starts with an assumed pressure at the upper node j. This assumed pressure along with the previous (initial) timestep temperature allows us to compute the compressibility factor and fluid density at node j using an equation of state. Velocity at node j now can be obtained by noting the relationship between mass flow rate and density. Applying Eq. (3.35) gives the new pressure at node j. We then compute improved values of gas compressibility, gas velocity, and other parameters at node j again. This procedure is repeated until pressure difference between two iterations is less than the allowable tolerance. The procedure is then repeated for the subsequent nodes.

The next step is to calculate fluid temperature using Eq. (3.27). At this point we need to calculate the actual mass flow rate distribution in the wellbore. The approach presented in Section 3.2, involving a Gaussian elimination technique of the tridiagonal matrix, is used. If the difference between the new and previous mass flow rates is within the allowable tolerance, the calculation is terminated for this timestep. In most cases, about 15 iteration

steps are needed to achieve appropriate accuracy during the flow transient period. The correct mass flow rate gives the density in the next timestep,

$$\rho_j^{l+1} = \rho_j^l + \frac{\Delta t (w_j^{l+1} - w_{j+1}^{l+1})}{\Delta z A} \tag{3.81}$$

The bottomhole pressure at the next timestep can be obtained from the knowledge of fluid density and an equation of state, which allows us to continue the procedure. This iteration for mass flow rate distribution is no longer necessary once the flow becomes steady (full flow in drawdown and no-flow in buildup). Under that condition, mass flow rate is constant along the wellbore, and the bottomhole pressure can be obtained from Eq. (3.65) by substituting mass flow rate in drawdown or 0 in buildup into this equation. The program will stop if the simulation time is greater than the time inputted by users.

Several important factors should be pointed out. The most important is that our choice of an explicit solution approach means that a relatively large time interval could cause the program to be unstable. We use a $\Delta t = 0.0005$ hr initially, raising it by one percent at each time step. The maximum value of Δt is set at 0.01 hr.

Another important consideration is the gas compressibility factor, Z_c which influences fluid density and hence static pressure loss. Even a small percentage error in estimating Z_c translates into a significant difference in calculated pressure because the wells are usually very deep (often > 20,000-ft). Our initial attempt with the Beggs-Brill correlation that curve-fitted the Standing-Katz Z_c-factor chart, yielded unsatisfactory solutions when the reservoir temperature exceeded 405°F. Gopal's (1977) algorithm,

however, seems to fit for the high-temperature, high-pressure condition often encountered in the field.

Another important factor is the overall heat-transfer coefficient, U_{to}, which is the key parameter in fluid temperature calculation. Eq. (2.34) is used in our simulation. The resistance to heat transfer offered by the annulus, which is somewhat difficult to calculate, is computed by using the Dropkin-Sommerscales correlation (Eq. 2.35). This correlation for natural convection requires the temperature difference across the annulus fluid, i.e. between the tube outside surface and the casing inside surface (Eq. 2.36). Thus, an iterative solution procedure is involved. We first assign an arbitrary value for this difference, say , $\Delta T = T_{ins} - T_{ci} = 5°F$. This allows us to compute the new wellbore fluid temperature T_f^{l+1}. Then heat flux is calculated using

$$\overline{Q_j^{l+1}} = C_{pm_j} w_j^{l+1} L_{Rj}^{l+1} (T_{el} - T_{fj}^{l+1}) \qquad \textbf{(3.82)}$$

and the temperature difference can be obtained by solving the following equation,

$$\Delta T_1 = \overline{Q_j^{l+1}} R_j \qquad \textbf{(3.83)}$$

where the resistance between tubing and annulus fluids, R_j, is defined as,

$$R_j = \frac{1}{2\pi r_{ti} h_{to}} + \frac{\ln(r_{to}/r_{ti})}{2\pi k_t} + \frac{1}{2\pi r_{to} h_c} \qquad \textbf{(3.84)}$$

The iteration procedure continues by replacing ΔT by ΔT_1 until the difference between two successive calculated temperature differences is within the allowable tolerance. Users have

the option to turn off this convection heat transfer coefficient calculation to get the rough wellbore fluid temperature.

In an offshore environment, wells have a portion of their production string exposed to the cooling effects of seawater and air. In such situations, we need to calculate the heat transfer due to natural convection in the annulus and forced convection for that portion of the well exposed to air and sea. The procedure is similar to the one discussed above. For the outside forced convective heat transfer coefficient for air and water, we adopted the Fishenden and Saunders (1950) correlation. The air and water temperatures and velocities, in addition to water salinity, are needed to estimate properties such as density, viscosity, conductivity, and specific heat of the water, which are needed to calculate heat-transfer coefficients for these fluids.

Reverse (Translating) Simulation. In new wells, the parameters for the reservoir are usually unknown. In this case, we need to estimate these parameters first. The translating simulator has been developed to convert wellhead pressure and temperature measurements into bottomhole pressure. Wellbore fluid temperature profile can be obtained by assuming the flow in steady-state condition. Details are discussed below.

For steady-state flow condition, the energy equation (3.4) becomes,

$$\overline{Q} = \frac{d}{dz}\left[w\left(H + \frac{1}{2}v^2 + gz\right)\right] \tag{3.85}$$

Substituting Eq. (3.11) into above equation, we get,

$$w\,c_p L_R (T_{ei} - T_f) = w\frac{d}{dz}\left[\left(H + \frac{1}{2}v^2 + gz\right)\right] \tag{3.86}$$

The mass flow rate, w, is constant in the steady state, therefore it can be canceled out. Substituting Eq. (3.6), we obtain,

$$c_p L_R (T_{ei} - T_f) = -c_J c_p \frac{dp}{dz} + c_p \frac{dT_f}{dz} + v \frac{dv}{dz} + g \qquad (3.87)$$

Rearranging the above equation, one obtains the following first order differential equation,

$$\frac{dT_f}{dz} + L_R T_f = L_R T_{ei} - \frac{v}{c_p}\frac{dv}{dz} - \frac{g}{c_p} + c_J \frac{dp}{dz} \qquad (3.88)$$

The formation temperature T_{ei} is linear with depth,

$$T_{ei} = T_{eibh} - g_T z \qquad (3.89)$$

therefore, the final differential equation for the fluid temperature at steady-state becomes,

$$\frac{dT_f}{dz} + L_R T_f = -L_R g_T z + L_R T_{eibh} - \frac{v}{c_p}\frac{dv}{dz} - \frac{g}{c_p} + c_J \frac{dp}{dz} \qquad (3.90)$$

If we assume the sum of the last four terms on the right side to be independent of depth, the above equation has the general solution,

$$T_f = \frac{\varrho + g_T}{L_R} - g_T z + C e^{-L_R z} \qquad (3.91)$$

where the parameter ϱ is,

$$\varrho = L_R T_{eibh} - \frac{v}{c_p}\frac{dv}{dz} - \frac{g}{c_p} + c_J \frac{dp}{dz} \tag{3.92}$$

At the wellhead (z=L), the fluid temperature is known as measured T_{wh}, which can be used to obtain the constant C,

$$C = e^{L_R L}\left(T_{wh} - \frac{\varrho + g_T}{L_R} + g_T L \right) \tag{3.93}$$

The final expression for T_f is,

$$T_f = \frac{\varrho + g_T}{L_R} - g_T z + e^{L_R (L-z)}\left(T_{wh} - \frac{\varrho + g_T}{L_R} + g_T L \right) \tag{3.94}$$

Since this equation should also be true for the bottomhole fluid, this extra boundary condition allows us to calculate the unknown parameter ϱ. Substituting z=0 and T_f=T_{eibh}, we get

$$T_{eibh} = \frac{\varrho + g_T}{L_R} + e^{L_R L}\left(T_{wh} - \frac{\varrho + g_T}{L_R} + g_T L \right) \tag{3.95}$$

which is equivalent to,

$$\varrho = \frac{e^{L_R L}(L_R T_{wh} - g_T + g_T L L_R) + g_T - T_{eibh} L_R}{e^{L_R L} - 1} \tag{3.96}$$

This equation is only valid for the steady-state flow condition and a constant geogradient.

We extended this equation to unsteady flow situations by evaluating the relaxation distance L_R at each timestep from the measured wellhead temperature and known bottomhole temperature. Synthetic and field data have verified this contention. Once we get the temperature, we can calculate approximate bottomhole pressures as a function of time by using the steady-state flow condition, full flow rate in a drawdown test and 0 in a buildup test. These approximate bottomhole pressures are then used for a semilog analysis for the appropriate data range to estimate reservoir transmissivity. This transmissivity value, in turn, gives a good starting point for calculating the sandface rate in the absence of formation property values. Thereafter, a simplified version of the forward simulation is coupled to obtain better estimates of bottomhole pressure as a function of time. This procedure is repeated until the bottomhole values are within a given tolerance.

The key factors affecting the outputs are the time range chosen by the users for the semilog analysis and the quality of wellhead pressure and temperature measurements. The latter simulation time range, to our knowledge, is always better than the early time range because full flow rate more likely happens in the latter testing time. Therefore, we strongly recommend choosing late time range to get more appropriate results.

3.5.2 Two-Phase Flow Simulators

Formulation of the two-phase flow is analogous to the single-phase gas model described earlier. However, adding an extra phase makes flow in the wellbore more complicated because two phases compete for the available area in the channel. The in-situ gas fraction, known as the gas void fraction, becomes the most important variable

and needs to be accurately estimated. Since the void fraction is generally different from its inlet fraction, our major effort is to directly estimate the in-situ volume fractions occupied by each phase.

During the drawdown simulation, the procedure is similar to that of our gas simulators. After we determine the existing flow regime, the gas void fraction is decided as follows: we use Eq. 2.5 for bubbly flow, and Eqs. 2.10, 2.11, and 2.12 for slug and churn flow. The parameter, C_o, is 1.2 except for churn flow where C_o is 1.15. The mixture density is calculated using Eq. 2.19 in annular flow and Eq. 2.3 in all other flow regimes.

For buildup simulation, the flow into the wellbore diminishes quickly after the well is shut-in at the surface. This makes the application of continuous flow models very difficult. Hence, we use the bubble migration model proposed by Hasan and Kabir (1995) discussed in Section 3.4 to estimate void fraction.

CHAPTER 4

MODEL VERIFICATION WITH FIELD DATA

In this chapter, we will describe the application of the simulators to field examples which can help us gain considerable insight into the mechanics of transient flow in the wellbore. As mentioned earlier, two types of simulators have been developed based on the transient wellbore/ reservoir model. The forward simulators allow us to simulate wellhead pressure (WHP), wellhead temperature (WHT) and bottomhole pressure (BHP) as functions of time for given reservoir parameters and well completion details. The translating (reverse) simulators allow us to translate measured WHP and WHT to BHP for subsequent analysis.

Three examples, one gas field example, obtained from a Gulf Coast gas field, one oil field example, and one two-phase field example, are used to illustrate the capabilities of the simulators.

4.1 Field Example for A Gas Well

The schematic representation of this well is shown in Figure 6. Pressures and temperatures were measured both at bottomhole and wellhead during a multipoint test. The test was comprised of four drawdowns at increasingly higher flow rates (5.8MMscf/D, 10MMscf/D, 13.9MMscf/D and 15.8 MMscf/D). Each drawdown was for about six hours and each was followed by a buildup of equal duration. We interpreted the transients in a series of steps.

First, using conventional methods, we analyzed BHPs to obtain reservoir parameters of permeability, static and non-Darcy skin, and average reservoir pressure. Second, we used these reservoir parameters and well completion details to compute the BHP, WHP, and WHT in a forward mode and compared them with measured values. Third, we used measured WHPs and WHTs to compute BHPs in a reverse mode and compared the results with the measured values.

The forward simulator was used to calculate WHP, WHT, and BHP by assigning formation parameters of permeability, thickness, skin, etc., derived from the well test interpretation. The flow rates and shut-in schedules were part of the input data. Thus, no resetting of the initial conditions were performed in between each set of drawdown and buildup. In other words, one simulation with varying rate schedules was run for the 45 hour of the test.

Forward simulation at different flow rates show that trends of WHT, WHP, and BHP are captured in all cases. Figures 7, 8, and 9 show the quality of match obtained. As we expected, the WHTs increase with increasing flow rates, the WHPs decrease with increasing flow rates. In general, BHPs are reproduced faithfully. In contrast to the BHP computation, the WHP calculations are subject to greater uncertainty because of the changing fluid temperature at the wellhead. Despite this potential problem, the simulation captures the overall signature fairly well. We note that the underestimation occurs during buildups and also during two drawdown periods. This can be explained by the temperature profiles.

In the low-flow-rate case, we underestimate the WHTs. However, for the high-flow-rate cases, WHTs are reproduced very well as Figure 7 shows. We point out that the WHT

data were gathered by wrapping a temperature probe around the pipe, which did not measure the required core fluid temperature. Clearly, the core fluid temperature is somewhat higher than those measured. This measurement problem becomes more acute for the high-flow-rate cases when the higher fluid temperature causes a higher temperature difference across the probe wrap. Because WHTs are underestimated at higher rates in actuality, pressures are underestimated accordingly.

Two other issues contribute to this mismatch. First, although this was a well controlled test, sparse rate measurements show that the rates were declining somewhat during all flow periods. Simulations presupposed constant rates, however. Second, a significant change in the ambient temperature occurred as the test progressed through a day-and-night time cycle during a winter month. Because the ambient temperature was not measured continuously, we could not capture this important variable for wellhead heat loss calculations for each transient.

Figure 10 shows the effect of thermal storage on wellhead temperature prediction for the 13.9 MMscf/D production rate case. In the development of the model we pointed out that the net convective energy transport into the control volume caused change in the fluid temperature as well as that of the tubing/casing/cement material. Neglecting the tubular heat absorption or the thermal storage effect, as was done by Miller (1980), would cause the unusually sharp rise in simulated wellhead temperature during drawdown and equally precipitous decline during buildup as shown by the solid line curve in Figure 10. The heavier dashed curve in Figure 10, which includes thermal storage effects, matches the field data well and points out clearly the importance of accounting for the heat capacity of the

tubular and cement sheath.

For reverse simulators, we verified the capability of the simulator to compute the BHPs from wellhead measurements. Figure 11 compares the computed BHP values with those measured. We note the good overall agreement during both drawdowns and buildups. This agreement provides an indirect proof of the goodness of the BHP calculations.

4.2 Field Example for An Oil Well

This test was run in an offshore producing environment. The water depth was about 31 ft and the wellhead was located 72 ft above the air/water interface. Because of mechanical restrictions downhole, the pressure and temperature sensors were located about 400 ft higher than the mid point of the producing (MPP) interval. To minimize storage, a downhole shut-in tool was used. Wellhead measurements of pressure were made with a deadweight tester and that of temperature by strapping a thermometer onto the flowline, a few feet downstream from the Christmas tree.

Forward Simulation. The reservoir parameters obtained from the conventional analyses, completion details, and the wellbore test hardware configuration allowed us to define the wellbore/reservoir system. Standard black-oil correlation were used to obtain the oil PVT properties: bubble-point pressure and formation volume factor were evaluated using the Standing's correlations and the Beggs-Robinson correlation yielded the oil viscosity. We attempted to reproduce pressure and temperature transients measured both at the wellhead and downhole.

Figures 12 and 13 show the good agreement between the field WHP and BHP

measurements and the simulation WHP and BHP results, respectively.

A vexing problem often arises when one attempts to compare the computed WHT with those measured in the field. The problem originates from the WHT measurement. If one merely straps a thermometer around a section of the wellhead instead of inserting a thermocouple into the tubing fluid, the required core fluid temperature is not measured. Estimates of temperature from an indirect thermometry may be obtained in the following manner

$$T_{Th} = T_f - \frac{\overline{Q}}{h_{Th}} \qquad (4.1)$$

where the heat transfer coefficient h_{Th} is lower than the overall coefficient, U_{to} which is given in Chapter 3, owing to the additional resistance between the wellbore and the thermometer. The goodness of contact between the thermometer and the wellhead metal in addition to the material used for strapping the thermometer present a challenge for estimating h_{Th}. In our simulations, we used a value of h_{Th} that best fits the available data. Thus, when temperature data are collected under less-than-satisfactory conditions, this procedure requires us to consider one additional parameter. Figure 14 shows the quality of the match obtained for each measured entity during drawdown by using this approach. However, we did not attempt to fine tune the pressure match at either end because we simulated a constant-rate behavior when subtle rate variations actually occurred.

Simulations also showed a good agreement with temperature transients measured downhole, during both drawdown and buildup, as shown in Figure 15. Predictably, the measured temperature transients show a trend very similar to that observed at the

wellhead. Close proximity of the measurement point to MPP causes the temperature excursion to be very modest. Thus, matching both pressure and temperature transients at the surface and downhole gives confidence in our modeling approach.

Translating Simulation. Figure 16 shows the quality of match obtained for the flow period data. Because of use of the downhole shut-in tool, no wellhead measurements are available for the buildup test.

4.3 Field Example for A Two-Phase Well

The well depth is 12420 ft and bottomhole temperature is 230°F. Because of mechanical restrictions downhole, the pressure and temperature sensors were placed about 200 ft higher than the mid point of the producing (MPP) interval. Like the oil example, we tried to reproduce pressure and temperature transients both at the wellhead and downhole.

Given the reservoir parameters and well completion data, we are able to run the forward simulators to simulate WHT, WHP, BHT, and BHP. Figure 17 shows the quality of the gauge pressure match between field and simulation data during both drawdown and buildup tests. However, the gauge temperature, as shown in Figure 18, is one degree lower than the measurements during the drawdown test. The problem may lie in the following fact: we assume the temperature at the mid point of the producing interval is constant when actual higher temperature fluid may occur in the wellbore. This can be examined by checking the period when the gauge temperatures exceeded 230°F.

Figures 19 and 20 show fairly good agreements of WHT and WHP between

measurements and simulations. This again shows the qualities of out simulators.

Translating Simulation. We use our model to translate the WHT-WHP measurements to gauge pressure. Again, a good agreement was obtained as shown in Figure 21. In this example, no wellhead measurements are available for the buildup test.

4.4 Discussion

During forward simulations, some degree of uncertainty in predicting a well's performance exists because a few elements of the heat-transfer calculations require reasonable inputs of fluid and rock thermal properties. While most of these properties are well known, computing heat transfer due to natural convection in the annulus and forced convection in the seawater and air can be demanding. Thus, we recommend fine tuning some of the convective heat-transfer parameters with measured BHPs along with WHPs and WHTs in a given area. In addition, real-time measurements of both the core fluid and the ambient temperatures are essential ingredients for proper forward simulations.

We recognize that because we are translating wellhead measurements to BHPs using a wellbore model, regardless of the degree of rigor, the computed values can only approach those measured. Nonetheless, the model and the computational approach as discussed here can complement the downhole measurements in favorable situations and replace them in hostile environments where economic stakes are high.

Besides being a useful tool for aiding well-test design and interpretation, the simulator can answer many questions associated with production operations. For example, fluid temperature at the seafloor for a well completed subsea is critical for pipeline design

when corrosion considerations are important. Similarly, the knowledge of fluid temperature, which is a function of flow rate, is also very important for surface equipment and facilities design when handling fluids from high-temperature reservoirs. For an offshore field, the simulator provides the necessary input for calculations of transient transport of mutiphase fluids in pipelines.

The purposes of this development are twofold. First, the simulator allows forward simulation so that the measured BHP, WHP, and WHT may be matched for a buildup or a drawdown test, given the wellbore/reservoir system parameters. In this way, the early-time data can be modeled using a rigorous approach. Second, given the transient WHP and WHT, we can obtain BHP for conventional transient analysis.

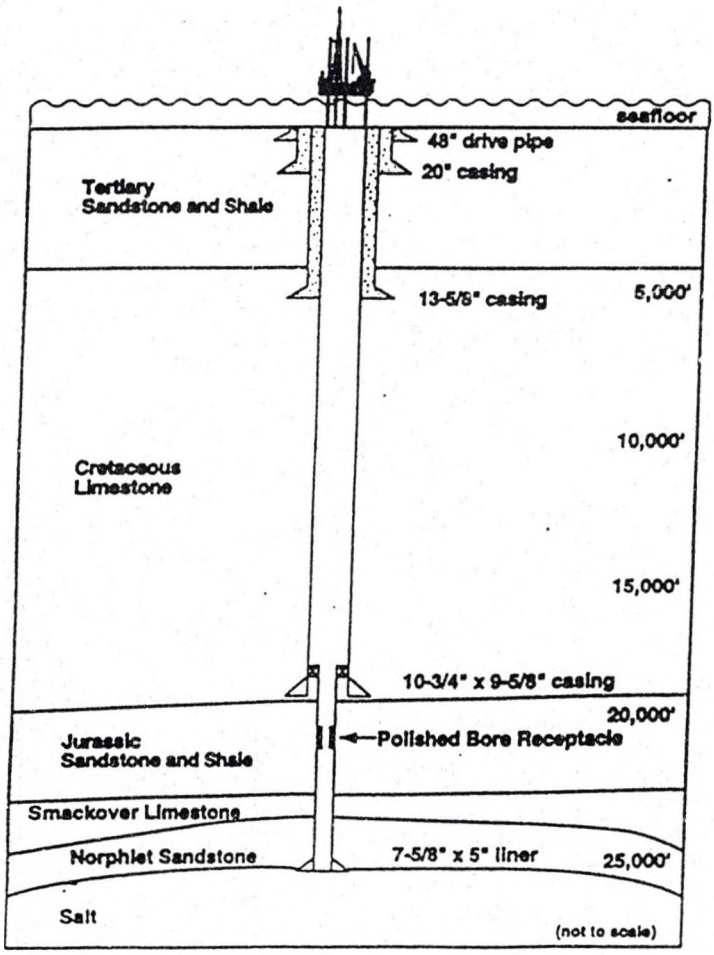

Figure 6. Schematic Representation of a Typical Drilling Program For a Norphlet Well

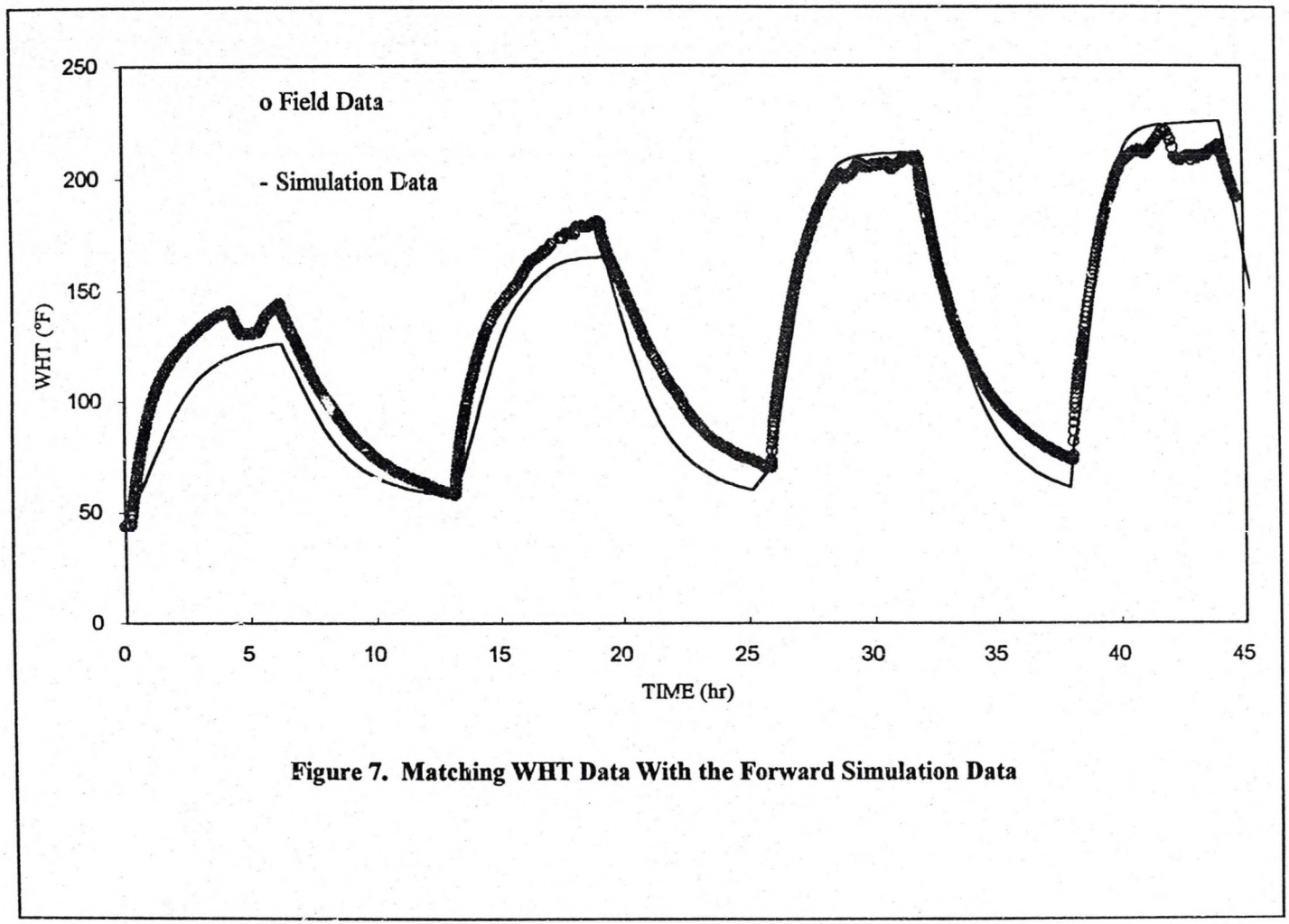

Figure 7. Matching WHT Data With the Forward Simulation Data

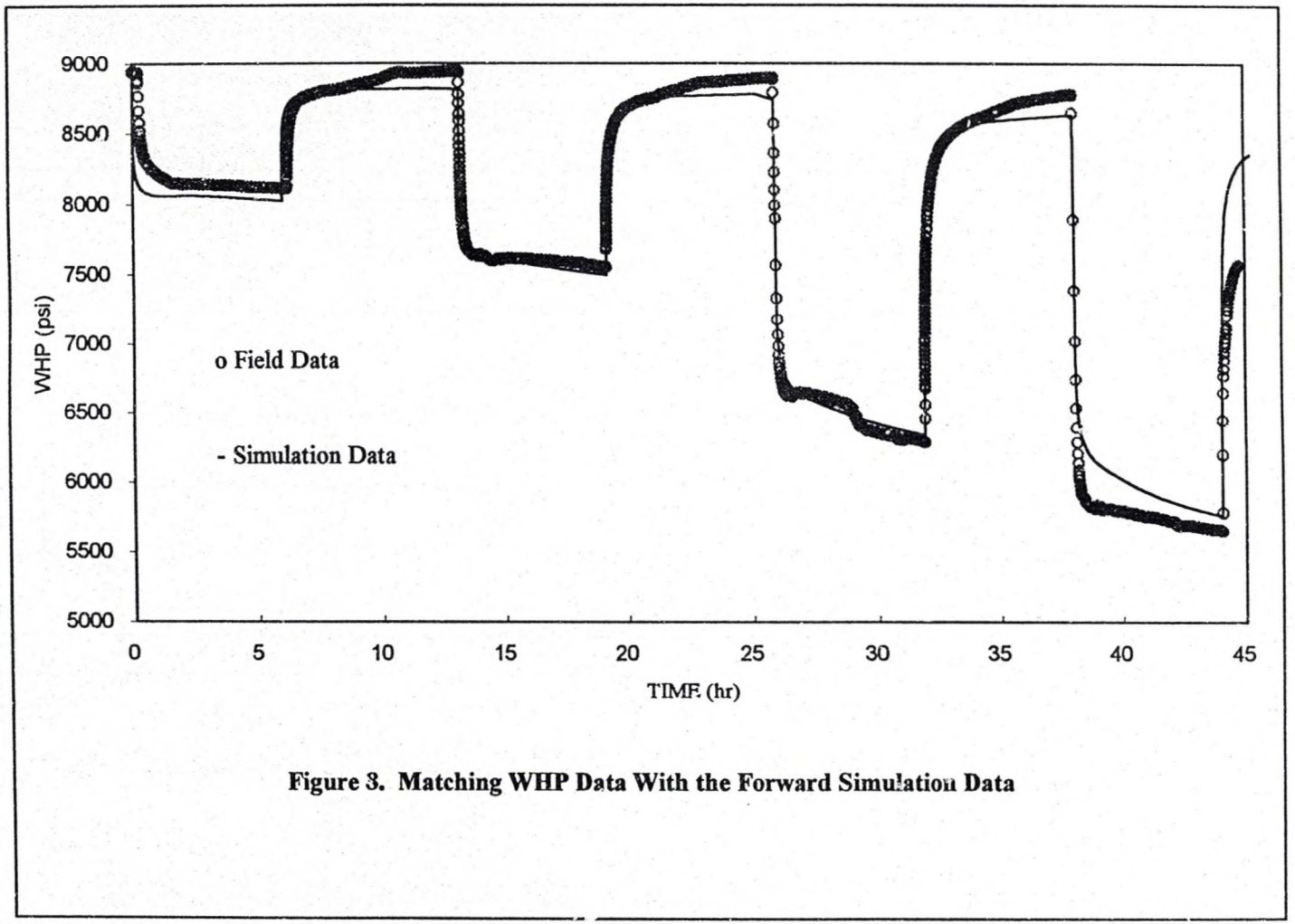

Figure 3. Matching WHP Data With the Forward Simulation Data

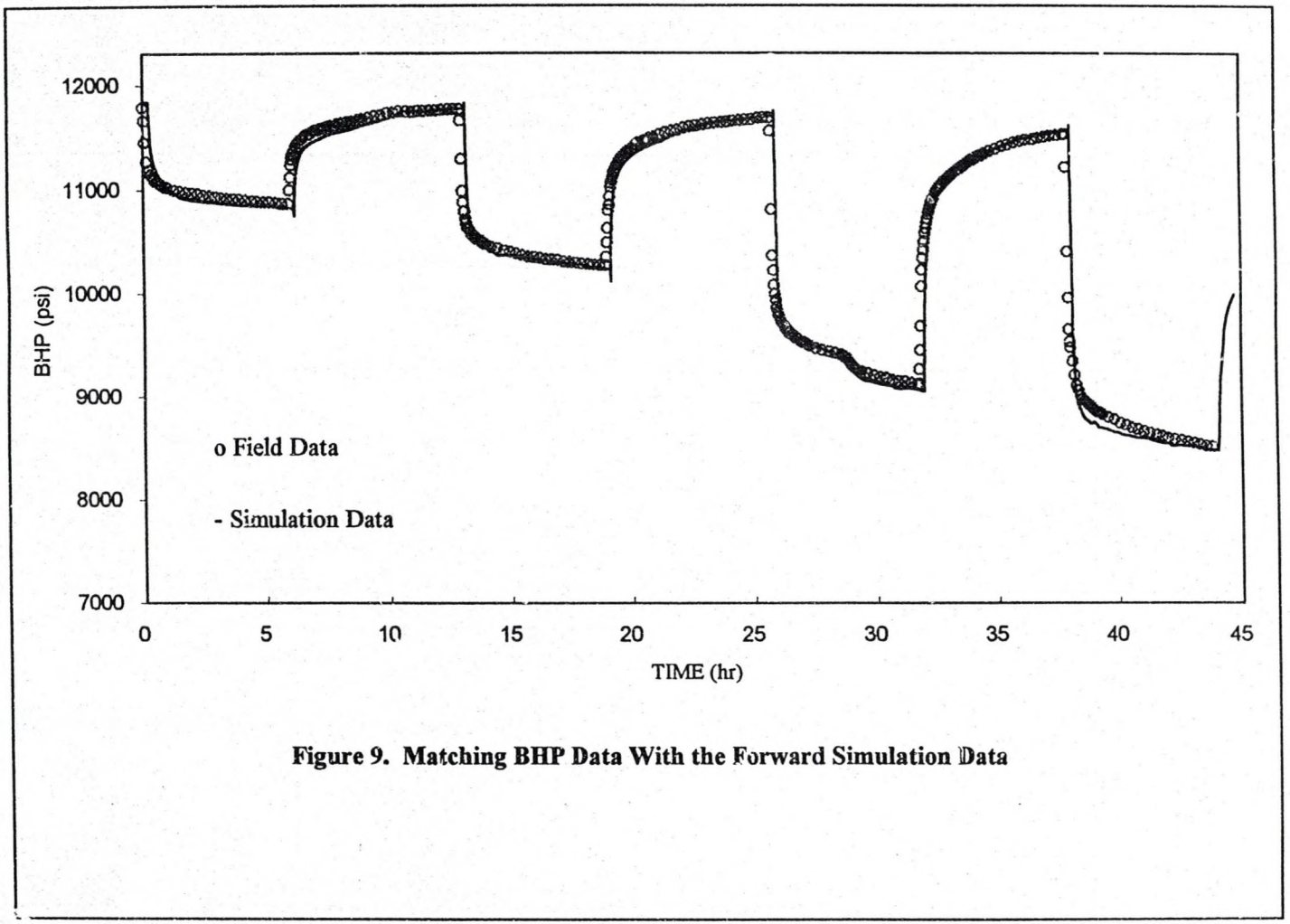

Figure 9. Matching BHP Data With the Forward Simulation Data

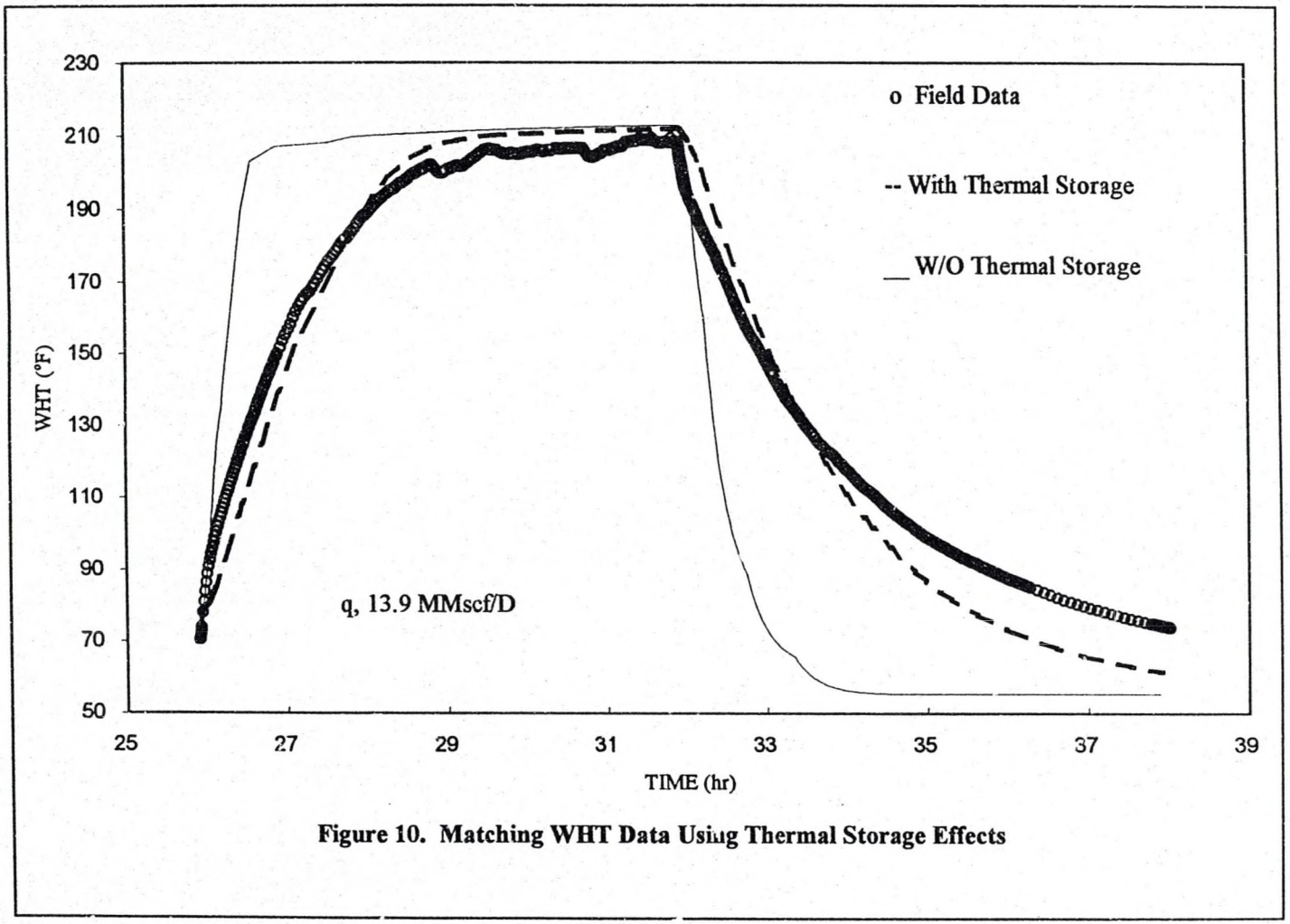

Figure 10. Matching WHT Data Using Thermal Storage Effects

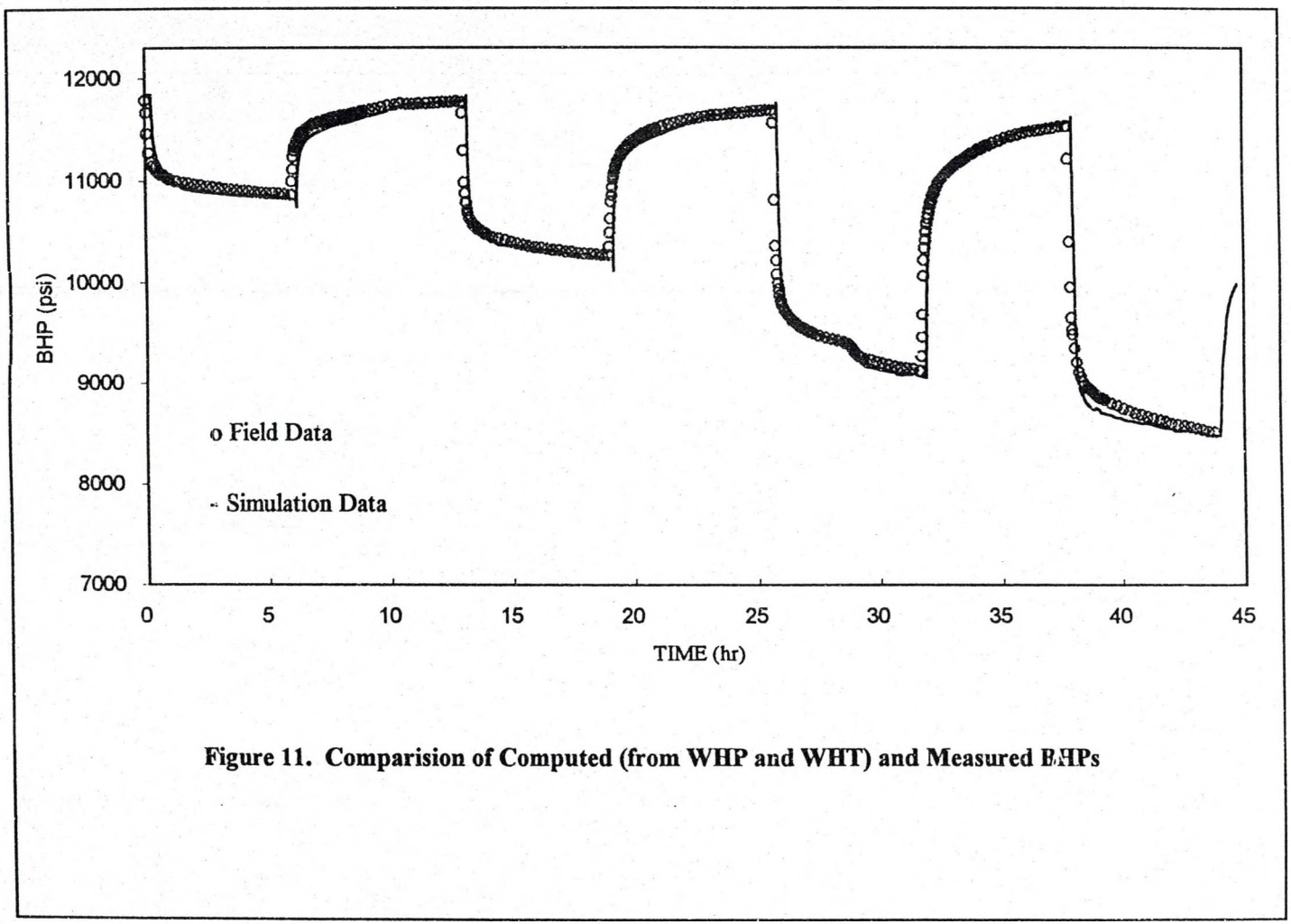

Figure 11. Comparision of Computed (from WHP and WHT) and Measured BHPs

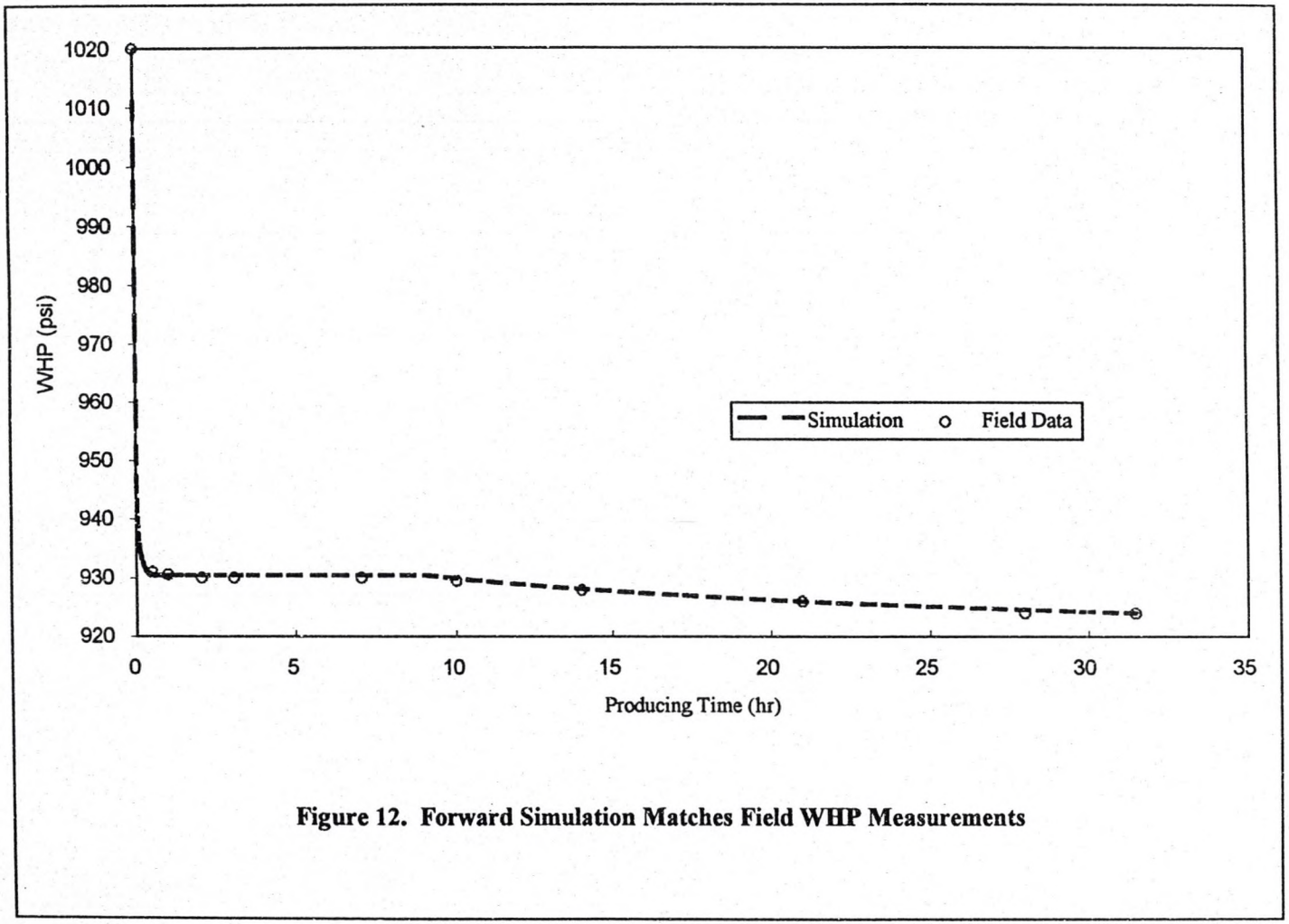

Figure 12. Forward Simulation Matches Field WHP Measurements

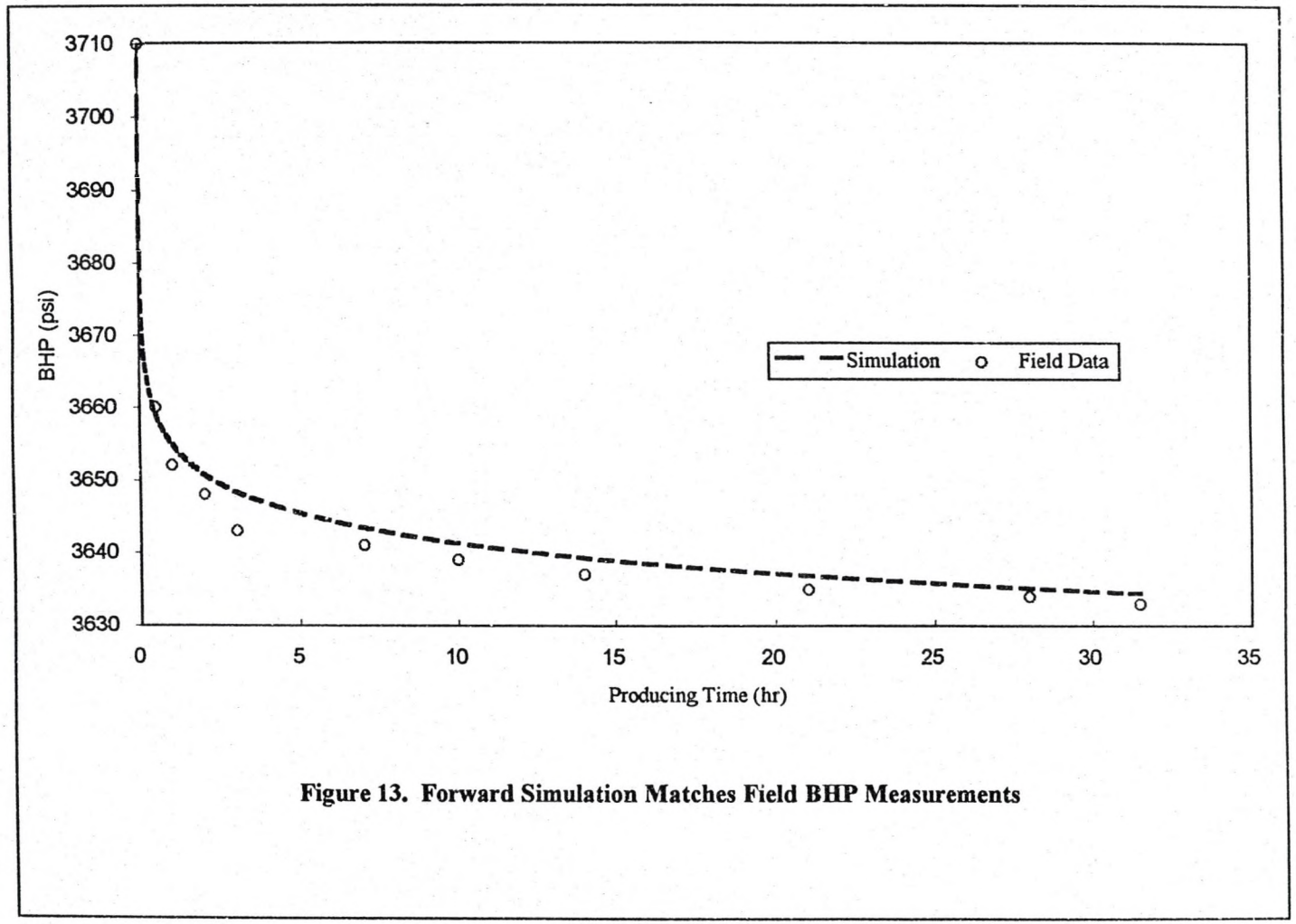

Figure 13. Forward Simulation Matches Field BHP Measurements

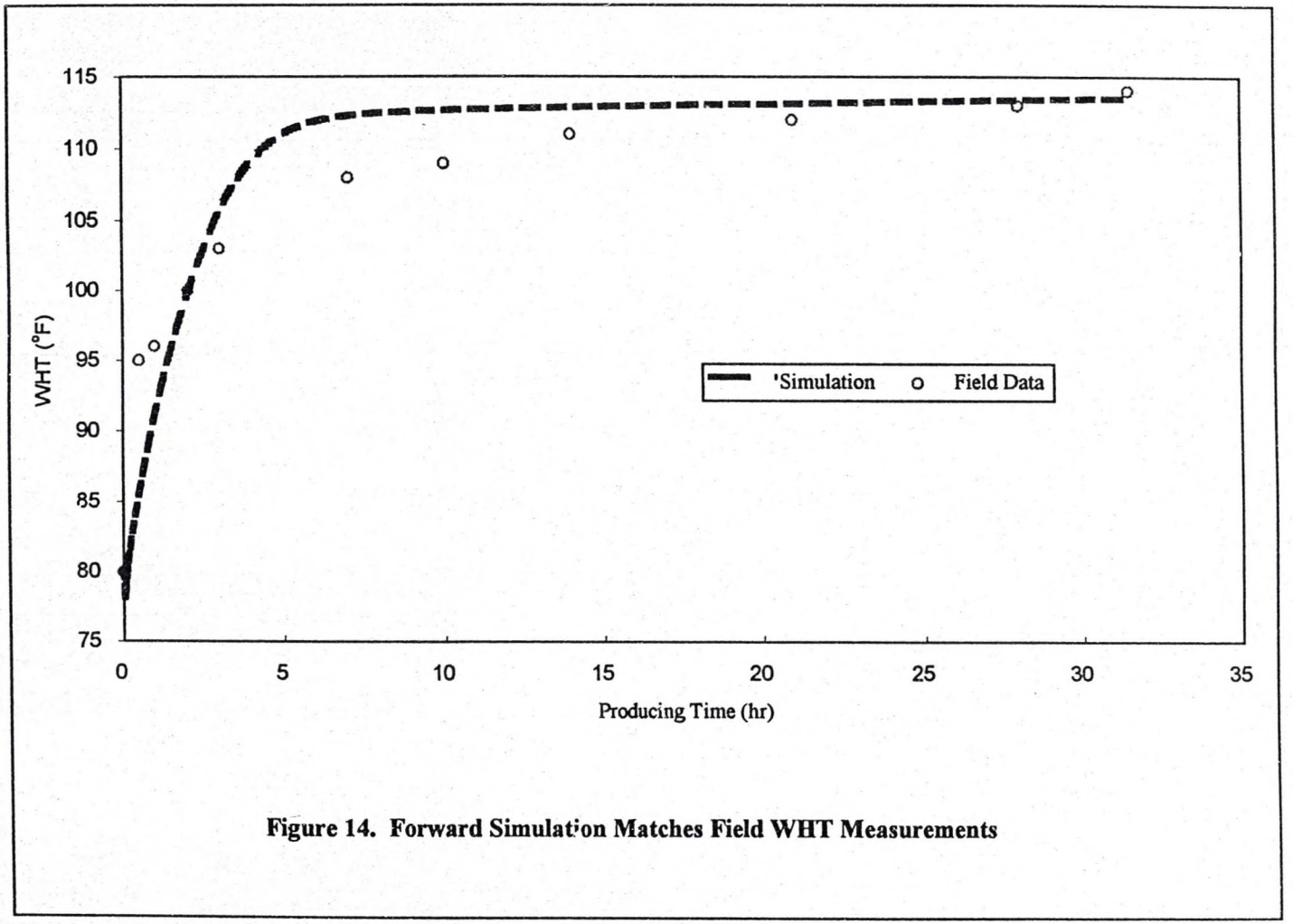

Figure 14. Forward Simulation Matches Field WHT Measurements

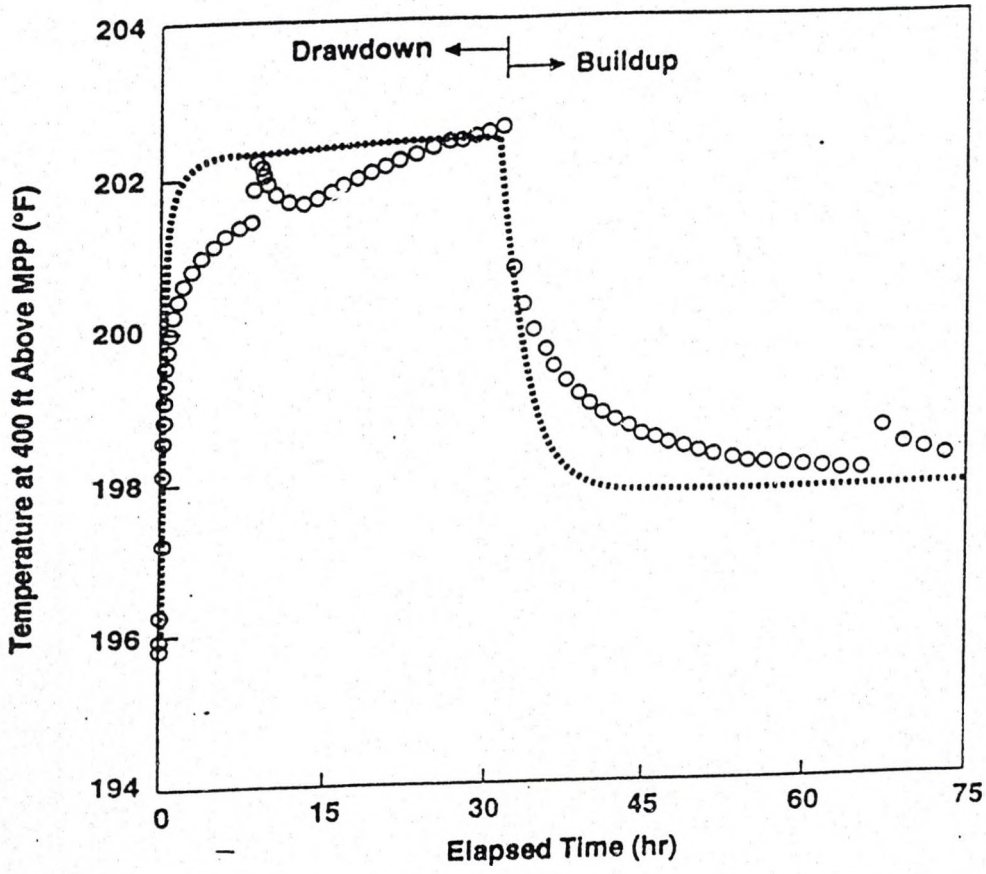

Figure 15. Matching Downhole Temperature Transients by Forward Simulation

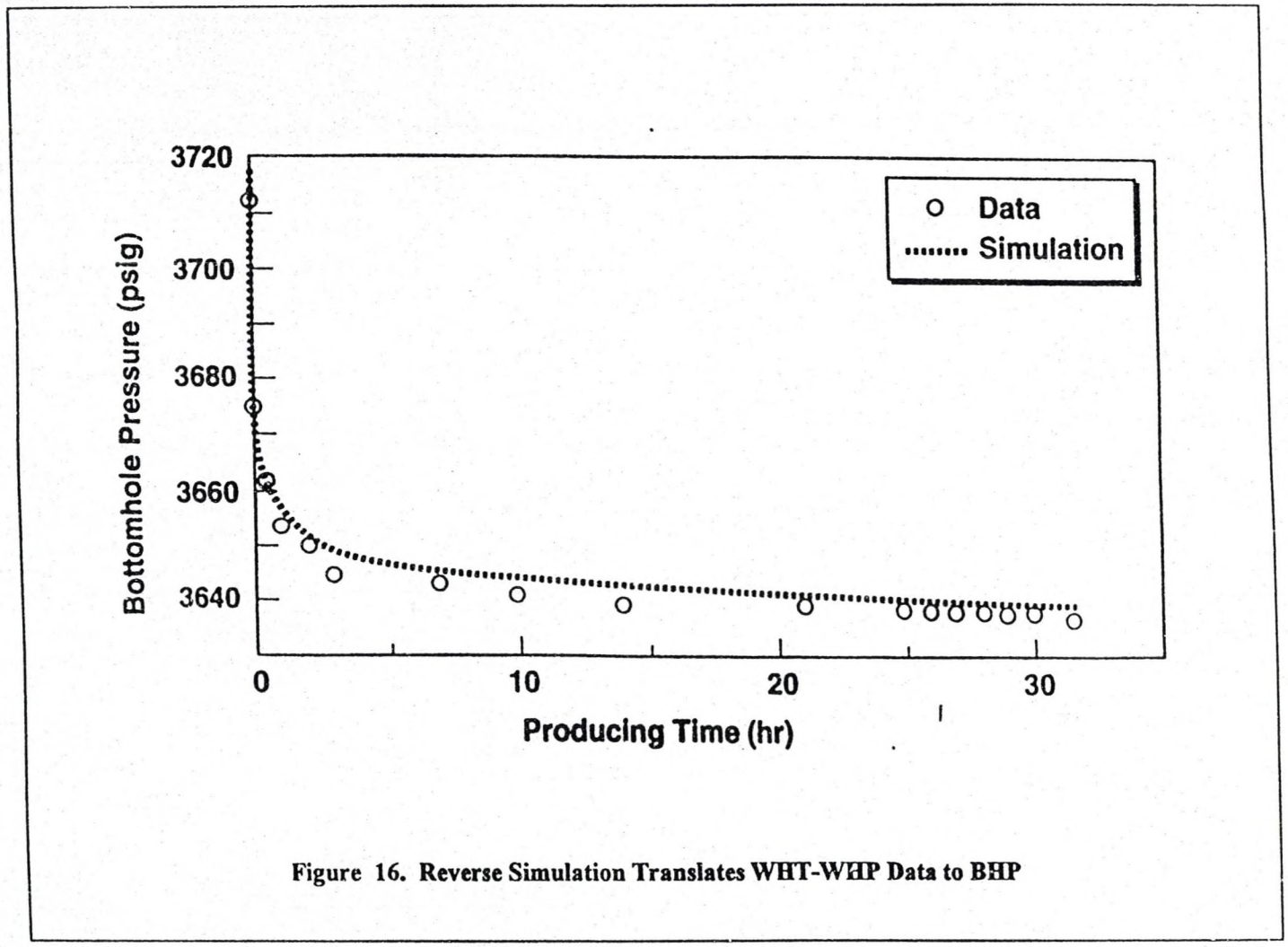

Figure 16. Reverse Simulation Translates WHT-WHP Data to BHP

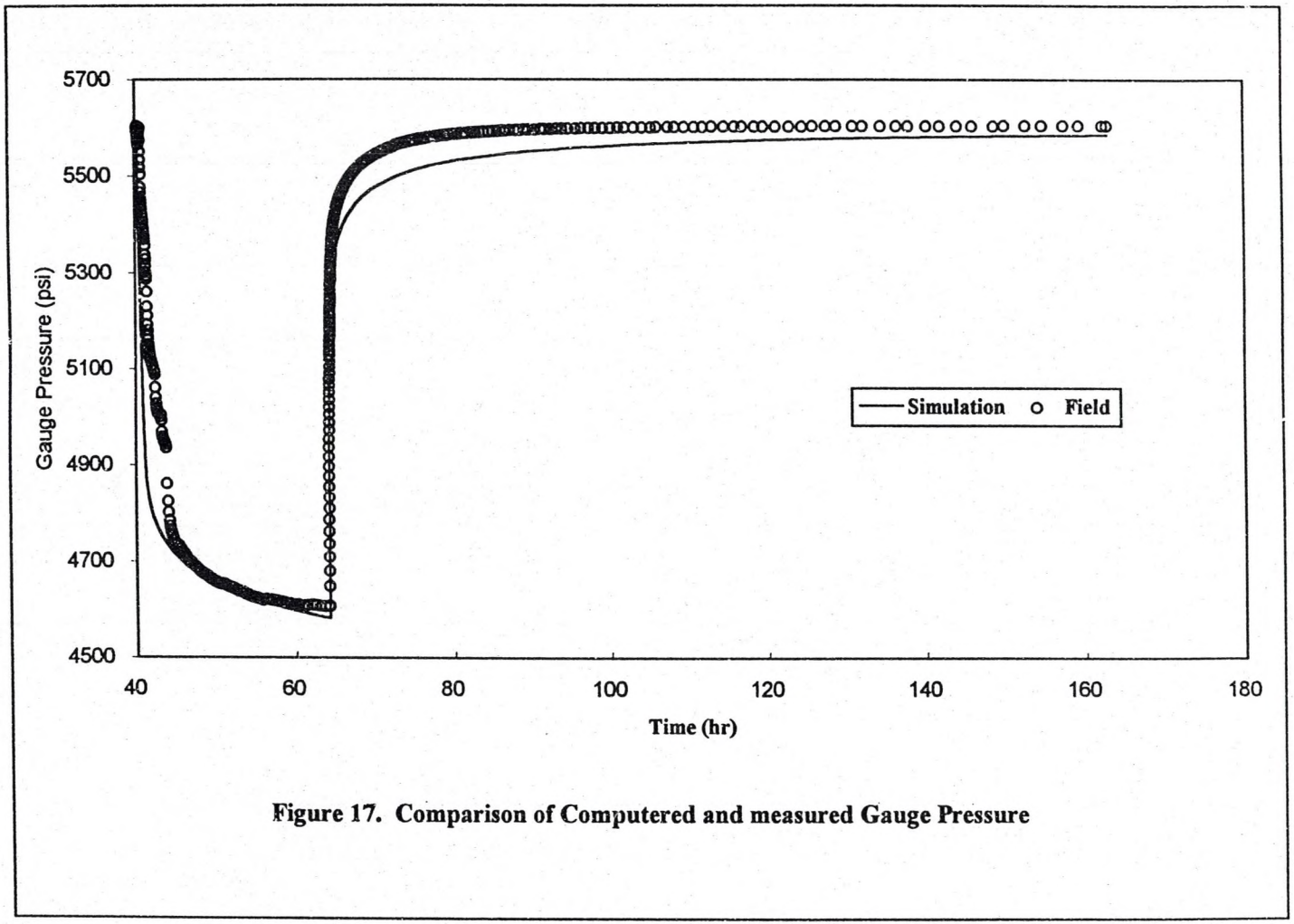

Figure 17. Comparison of Computered and measured Gauge Pressure

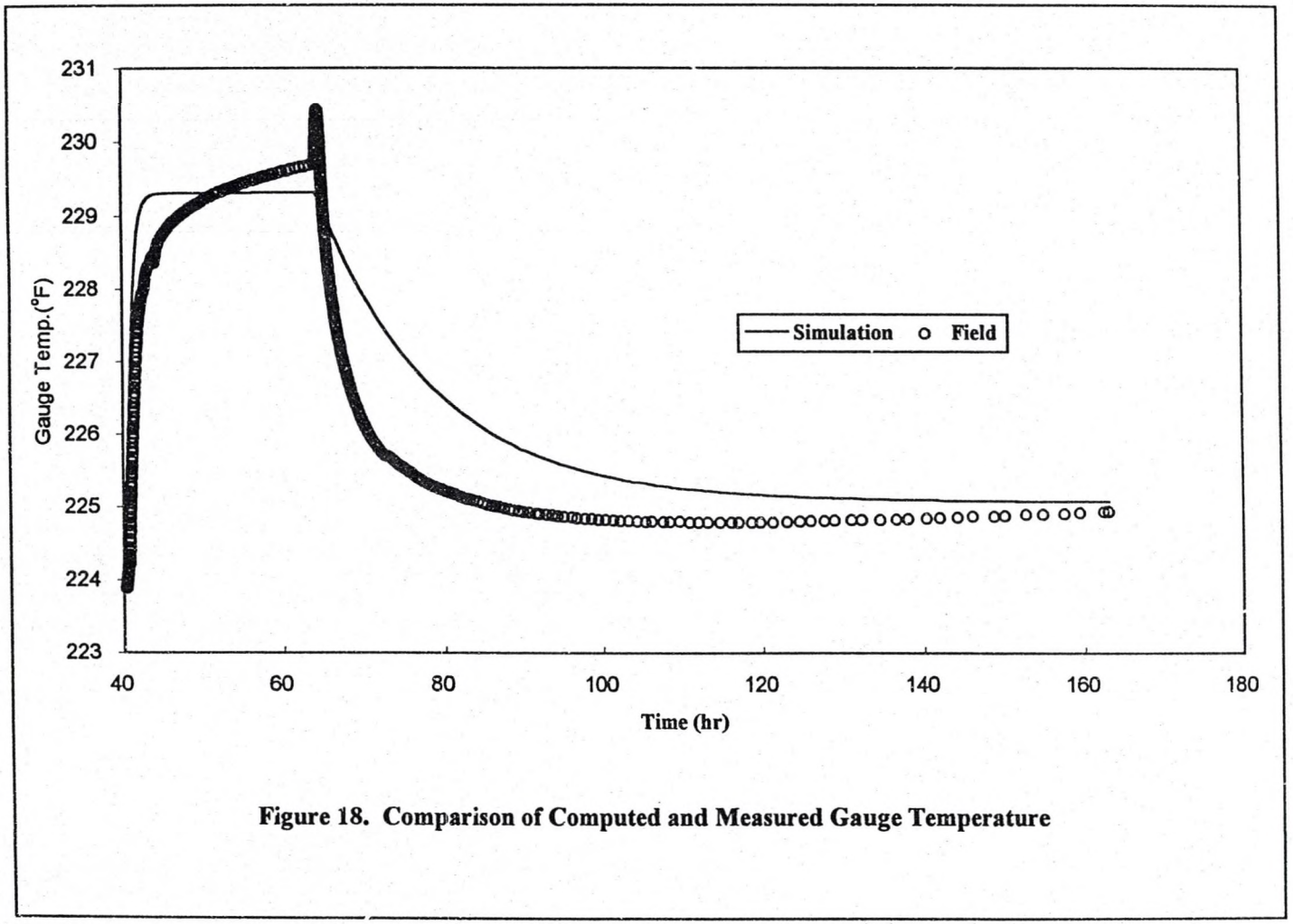

Figure 18. Comparison of Computed and Measured Gauge Temperature

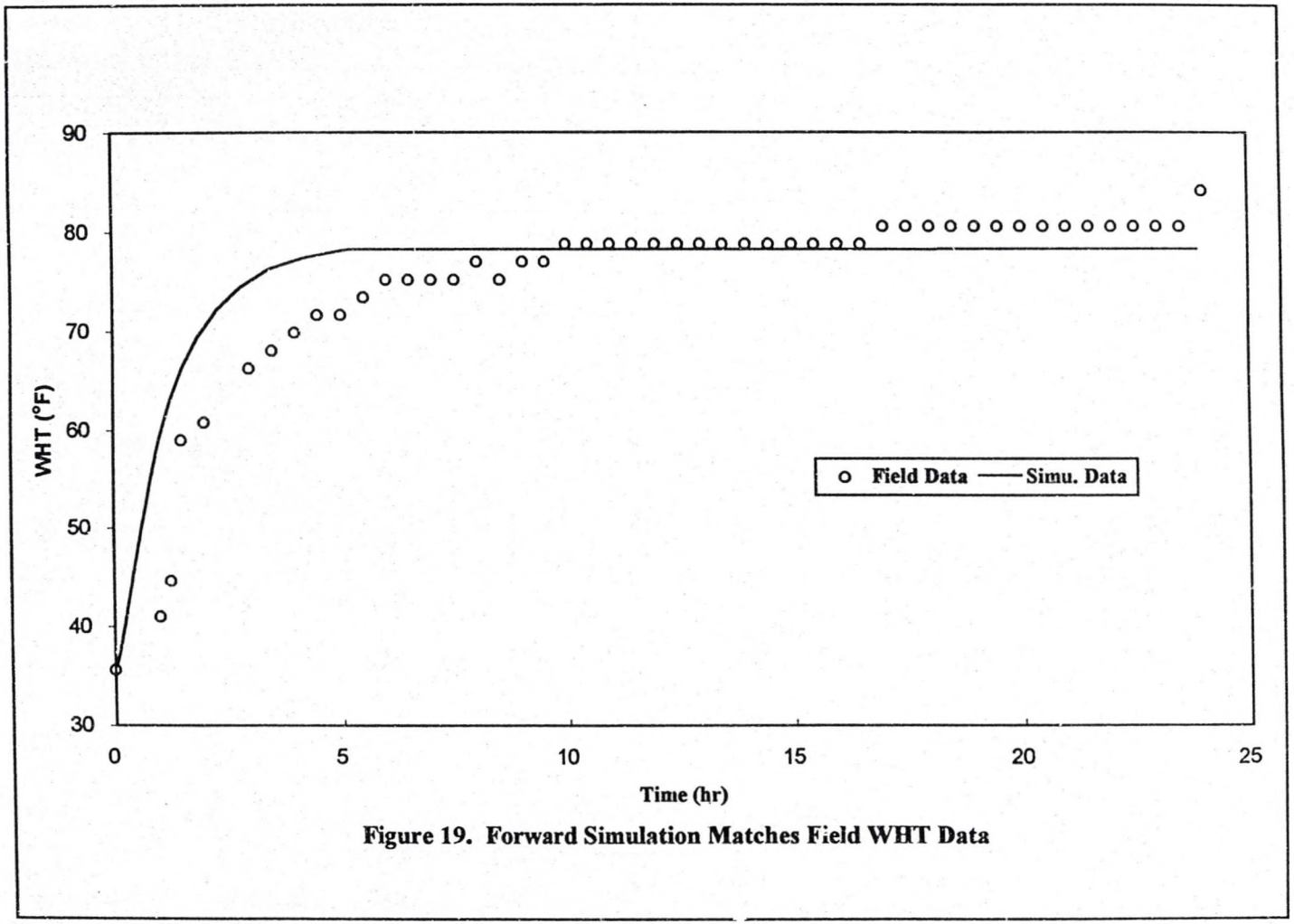

Figure 19. Forward Simulation Matches Field WHT Data

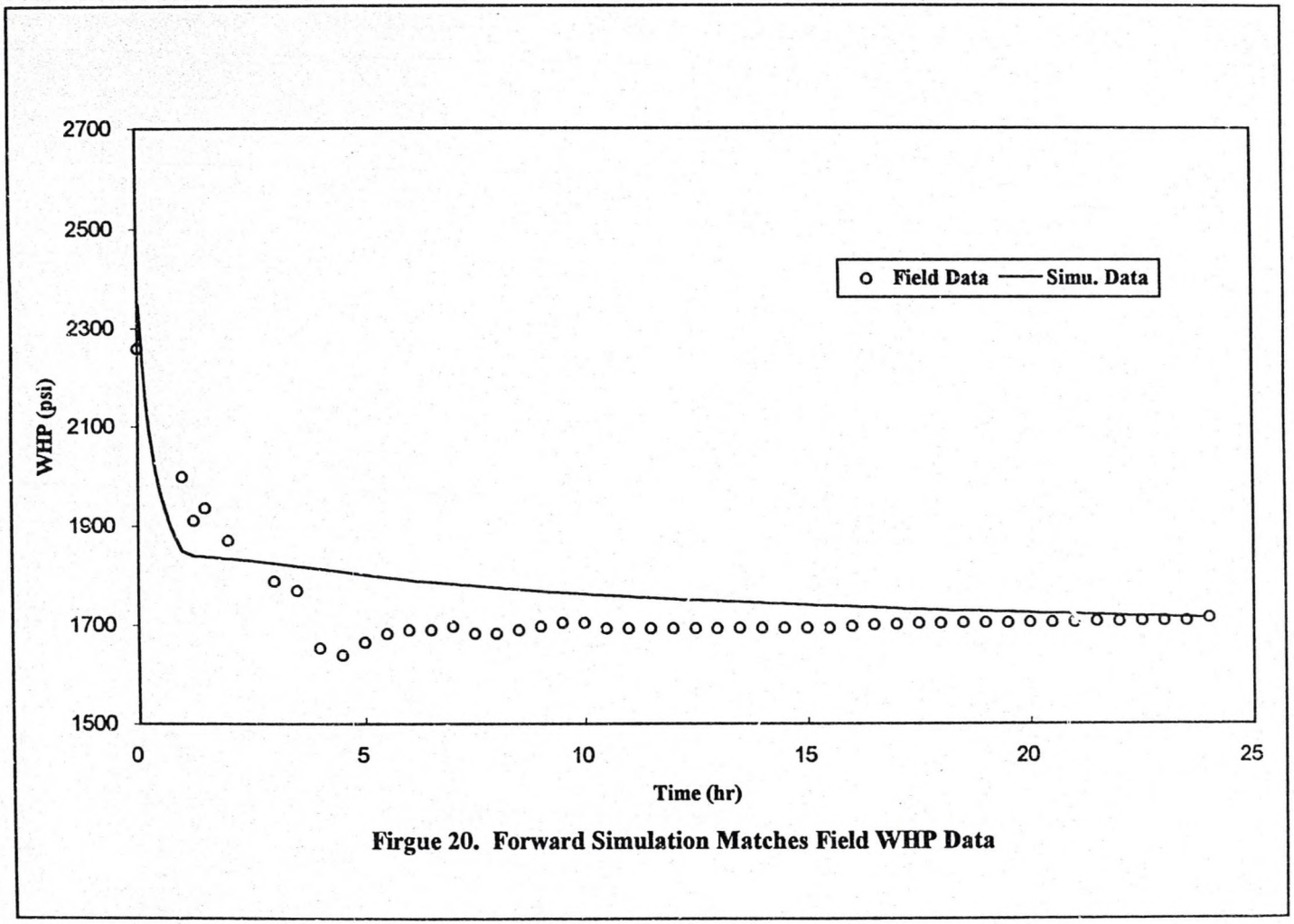

Firgue 20. Forward Simulation Matches Field WHP Data

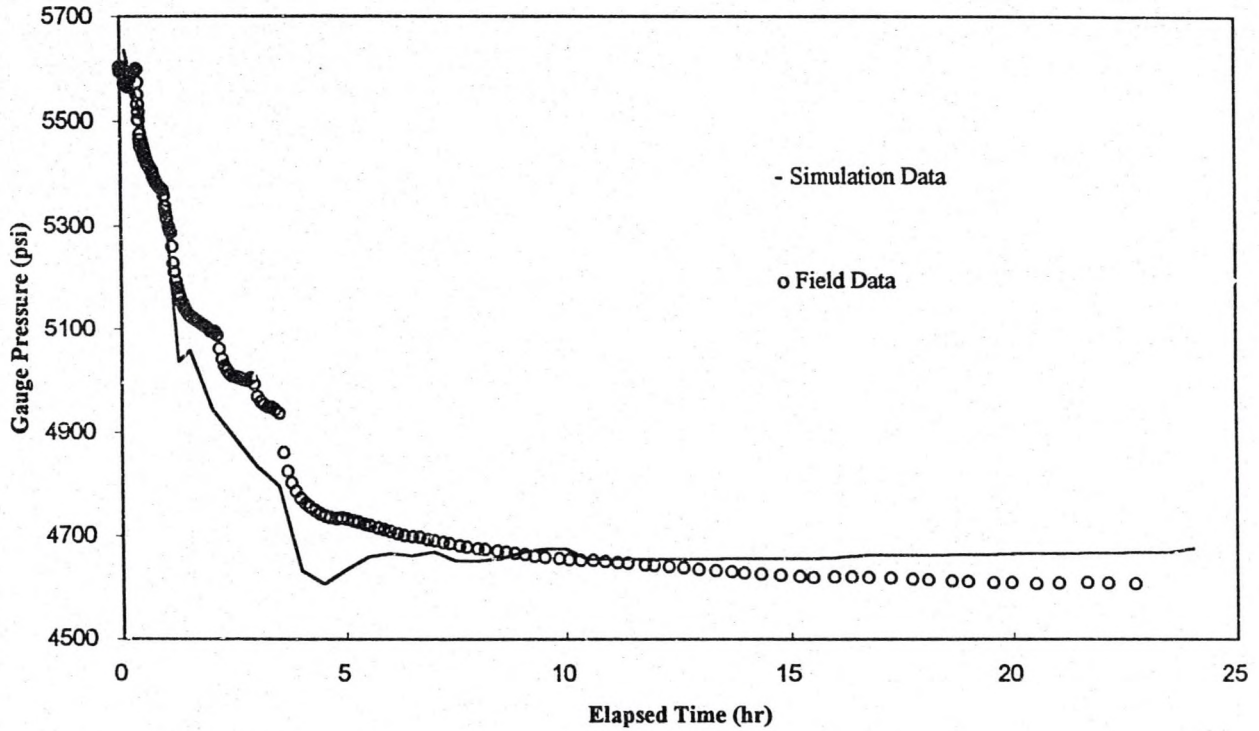

Figure 21. Gauge Pressure Translated by Field WHP and WHT Data

CHAPTER 5

SIMULATION AND SENSITIVITY STUDY

The transient transport model discussed in Chapter 3 has been coded in FORTRAN. We have developed both forward and reverse simulators for gas wells and wells flowing two-phase fluids. These simulations are very helpful in studying the influence of various production and reservoir parameters on wellbore pressure and temperature response. In this chapter, we present sensitivity analysis for wells producing gas, oil, and two-phase fluids.

5.1 Sensitivity Study for Gas Wells

The base case is a well which has a depth of 10,000 ft with a reservoir temperature of 300 °F. Other pertinent data appear in Table 1 (all tables and figures are at the end of this chapter).

Figure 22 shows the typical wellbore fluid temperature and density profiles at different times during the base case drawdown test. Similar results were obtained during the subsequent shut-in. The nonlinear and time-dependent nature of these profiles are worthy of note. These profiles underscore the importance of accounting for thermal effects whenever conversion of wellhead pressure (WHP) to bottomhole pressure (BHP) is desired.

Figure 23 presents the wellhead temperature transients in the drawdown and

buildup simulations. Note the gradual rise in wellhead fluid temperature during the drawdown test and the subsequent gentle decline during the well shut-in period. Also shown in the figure is the profile generated by neglecting the heat absorption or rejection by the wellbore system, that is, tubular, annular fluid, and cement sheaths. Note the sharp increase in wellhead fluid temperature (WHT) at early times during drawdown and a similar sharp decrease during shut-in compared to the base case. The difference between the two WHT signatures is analogous to that observed for either the BHP or WHP when the wellbore fluid storage is included or excluded during a transient test. Because of this analogy, we term this phenomenon associated with the WHT as thermal storage.

To study the effect of production rate on the transient behavior of pressure and temperature, we simulated both drawdown and buildup tests for three flow rates. Figure 24 shows the WHTs corresponding to rates of 2.5, 5.0, and 7.5 million standard cubic feet per day (mmscf/D). Increase in WHT with flow rate is a direct consequence of increased associated fluid enthalpy. Simulations of this nature are prerequisite to designing both subsurface and surface equipment and facilities to handle high WHTs. This point is made clear by evaluating the real case as examined in the previous chapter.

The annular fluid offers significant resistance to heat flow, making its conductivity an important determinant of the wellbore fluid temperature. Figure 25 contrasts the base case wellhead fluid temperature with that for the case when the fluid conductivity is only 0.075 Btu/ft-^{0}F-hr (for the base case k_a = 0.25 Btu/ft-^{0}F-hr). The increased resistance to heat flow in the annulus leads to much higher (about 30%) wellhead temperature. Therefore, the choice of annular fluid, although generally dictated by tubular corrosion

considerations, may be influenced by a desire to lower the WHT.

The transient response of the wellbore fluid may be affected by the exposure of the wellbore section to the cooling effects of seawater and air. To examine the extent of these effects, we simulated both drawdown and buildup tests by submerging the base case well down to a maximum of 500 ft in the seawater (at 60^0F), while keeping 100 ft exposed to air (at 60^0F). Figure 26 shows WHT difference between two cases. After a 6-hour flow period, a temperature loss of only 3.88°F (=143.69^{0}F-139.81^{0}F) occurs compared to the base case. Intermediate seawater depth values yield correspondingly lower temperature differences when compared with the base case. Short residence time of gas in the seawater during high gas rates appears to be the main reason for the minimal heat loss. In all cases, the flowing BHPs remain essentially the same because of the unchanged reservoir conditions.

5.2 Sensitivity Study for Oil Wells

As mentioned early, the two-phase simulation can be used to run single-phase oil well simulations by setting the gas-oil-ratio (GOR) equal to zero. Hence, we explored the effects of certain key parameters upon the transient behavior of pressure and temperature in oil wells. Table 2 presents the wellbore/reservoir data used to generate the base case.

Figure 27 shows the typical wellbore fluid temperature and density profiles for the drawdown case at two different times (0.1 hour and 2.5 hour). Similar results were obtained during the subsequent shut-in. The figure again pointed out the important point, one cannot simply add the hydrostatic head to the WHP to compute the BHP without

properly accounting for fluid temperature and density variations with time and depth.

Figure 28 shows the effects of producing rate on WHP, WHT, and BHP. Increasing WHT with higher rate is a result of increased associated fluid enthalpy. While the BHP shows the expected smooth trend, the early-time WHP is not quite as smooth. This behavior is a consequence of thermal storage, precipitated by storage (during drawdown) or release (during buildup) of thermal energy by tubulars, cement sheaths, and annular fluid.

WHT and WHP are functions of enthalpy, and enthalpy is related to production rate and fluid density. Thus, WHT and WHP not only change with the production rate but also vary with fluid density. Oil density is calculated by

$$\rho_l = \frac{141.5}{131.5 + API^o} \tag{5.1}$$

Figure 29 shows the WHT increases with increasing fluid density (decreasing API gravity). Figure 30 shows decreasing WHP with increasing fluid density.

Questions may arise about the initial formation temperature distribution because fluid circulation during drilling and completion may distort the virgin geothermal gradient in the wellbore vicinity. Our experiences with transient fluid circulation modeling indicate that the fluid temperatures in the annulus and tubing are not very sensitive to the various heat-transfer parameters. Moreover, the entire formation acts essentially as an infinite heat source. Therefore, we believe that the initial formation temperature profile is not distorted to any appreciable extent.

We did however some simulations to address the distorted geothermal gradient issue. Figure 31 shows the transient WHT corresponding to various geothermal gradient values. The idea is to simulate cases assuming fluid circulation before testing caused enough cooling to distort the geothermal gradient itself. As expected, very little difference in WHPs occurs as Figure 32 shows, with no differences in BHPs. Although this simulation approach does not mimic reality, we believe the approach represents the worst possible scenario. Thus, we find the aspect of possible near-wellbore cooling to be unimportant.

High WHT can potentially increase project development cost by raising the metallurgy requirements of tubular, pipelines, and surface facilities. This problem is compounded further when corrosion considerations arise because of sour sulfur-containing crudes. This simulator provides a vehicle for addressing this issue at a project's inception. For example, one can explore consequences of using the water-based mud instead of its oil-based counterpart to establish the anticipated WHT. Figure 33 shows that an oil-based mud, having a low thermal conductivity, is inefficient in losing heat to the surroundings. Consequently, high WHTs are reported.

If high WHT is a concern and an oil-based fluid must be used because of corrosion considerations, a viable option to increase heat loss to the surroundings lies in drilling a deviated well. Figure 34 shows how well deviation increases fluid residence time, thus, leading to a cooler WHTs for wells having the same true vertical depth.

In an offshore producing environment, besides using water-based or higher conductive mud, fluid cooling may be augmented by the presence of seawater. Figure 35

shows that temperature reversal occurs soon after flow initiation when water depth exceeds 2,000 ft. Colder sea water is responsible for this reversal temperature response.

5.3 Sensitivity Study for Two-Phase Wells

The base case chosen for the sensitivity study of two-phase flow is very similar to the base case for the oil well discussed in the last section. In order to obtain a gas phase, we decreased the reservoir pressure from 7000 psi to 5000 psi, increased the gas-oil-ratio (GOR) value to 1000 standard cubic feet per standard barrel, and increased oil gravity to 30 API° . Other pertinent data are the same as those of the oil base case (see Table 2).

We have shown that the typical wellbore gas and oil temperature and density profiles are nonlinear and time dependent. Since the mixture density is a linear combination of the gas-volume fraction, gas density and oil density, one can imagine that the mixture temperature and density profiles during two-phase flow should be also nonlinear. Figures 36 and 37, as expected, show the nonlinear gas-volume fraction, mixture density, and mixture temperature distributions along the wellbore at various times. The nonlinear and time-dependent nature of these profiles confirms that one cannot simply add the hydrostatic head to the WHP to computing the BHP without properly accounting for fluid temperature and density variations with time and depth.

Two important conditions are worthy of note from Figure 37. One is for the initial condition during buildup simulation; the late-time temperature profile in the

drawdown simulation is essentially the same as the early-time temperature profile in the buildup simulation. The other is that the late-time temperature profile during buildup simulation is almost the same as the initial no-flow drawdown condition.

As we pointed out in the oil case, WHT and WHP are functions of the enthalpy, and enthalpy is related to production rate and fluid density. Fluid density is measured as API value. Thus, one may easily figure out that WHT and WHP not only change with the production rates but also vary with the oil density (API value). This should not change when we add a gas phase. Figure 38 shows the effect of producing rate upon WHP, WHT, and BHP. WHT increases with increasing producing rate as a result of increased associated fluid enthalpy. Figure 39 shows WHT increases with fluid density (decreasing API gravity).

As we pointed out earlier, high WHT can potentially increase project development cost by raising the metallurgy requirements of tubular, pipelines, and surface facilities. High WHT will also cause corrosion problems. From the previous gas and oil cases, we know that WHT can be decreased by either providing annular fluid with high conductivity or exposing the wellbore to cooling seawater. Figure 40 shows the WHT changes with different annular fluids. Low conductivity means high resistance to the heat flow, hence, we will see high WHT. This again underscores the importance of the choice of annular fluid. Figure 41 shows the WHT affected by the cooling seawater. This suggested another way to lower the WHT.

Gas-oil-ratio (GOR) is also a key factor in the behavior of WHT and WHP. Higher GOR means more gas in the wellbores. Thus, higher GOR results in lower

mixture density, causing lower pressure drop and consequent higher WHP. Lower mixture density also means less enthalpy (mass) coming from the formation into the wellbore, thus lower WHT can be observed. Figure 42 shows the response of WHT and WHP with three different GOR values.

5.4 Summary

In this Chapter we have shown the development of a rigorous wellbore/reservoir simulator to compute transient pressure and temperature at any point in the wellbore. Large wellbore temperature differences cause severe distortion of transient wellhead pressure response even when single-phase liquid production occurs. Duration of this distortion period is system specific, however. Results of various computations also show that the nonlinear nature of the wellbore density profile makes simple WHP conversion to BHP a difficult proposition, regardless of the nature of the wellbore fluid.

The purposes of these simulators are manifold. For instance, we can design a mud system from a heat-loss standpoint; compute WHTs associated with flow rates so that surface equipment and facilities can be designed properly; assist pipeline design when corrosion considerations are important. We also observed that reservoir fluid cooling in the seawater segment is marginal unless deep-water wells in excess of 2,000 ft are being considered.

Table 1 Well, Reservoir, and Fluid Data For Base Case Gas Well

Reservoir Pressure, psi	5275.0
Well Depth, ft	10,000.0
Tube ID, in	2.548
Tube OD, in	3.5
Casing ID, in	9.0
Casing OD, in	10.75
Pipe Roughness	0.000018
Production Rate, MMscft/D	5.0
Formation Permeability, md	1.0
Formation Thickness, ft	100.0
Formation Porosity	0.1
Formation Fluid Compressibility, /psi	0.00004
Wellbore Skin	0.0
Bottomhole Temperature, ^{0}F	300.0
Geothermal Gradient, ^{0}F/ft	0.024
Formation Thermal Conductivity, Btu/ft-^{0}F-hr	2.5
Formation Density, lb/ft^3	100.0
Formation Heat Capacity, Btu/lb-^{0}F	0.625
Tubing and Casing Material Thermal Conductivity, Btu/lb-^{0}F	30.0
Annulus Fluid Thermal Conductivity, Btu/ft-^{0}F-hr	0.26
Cement Thermal Conductivity, Btu/ft-^{0}F-hr	0.38
Cement Diameter to 500 ft, in	30.0
Cement Diameter from 500 ft to bottomhole, in	24.0

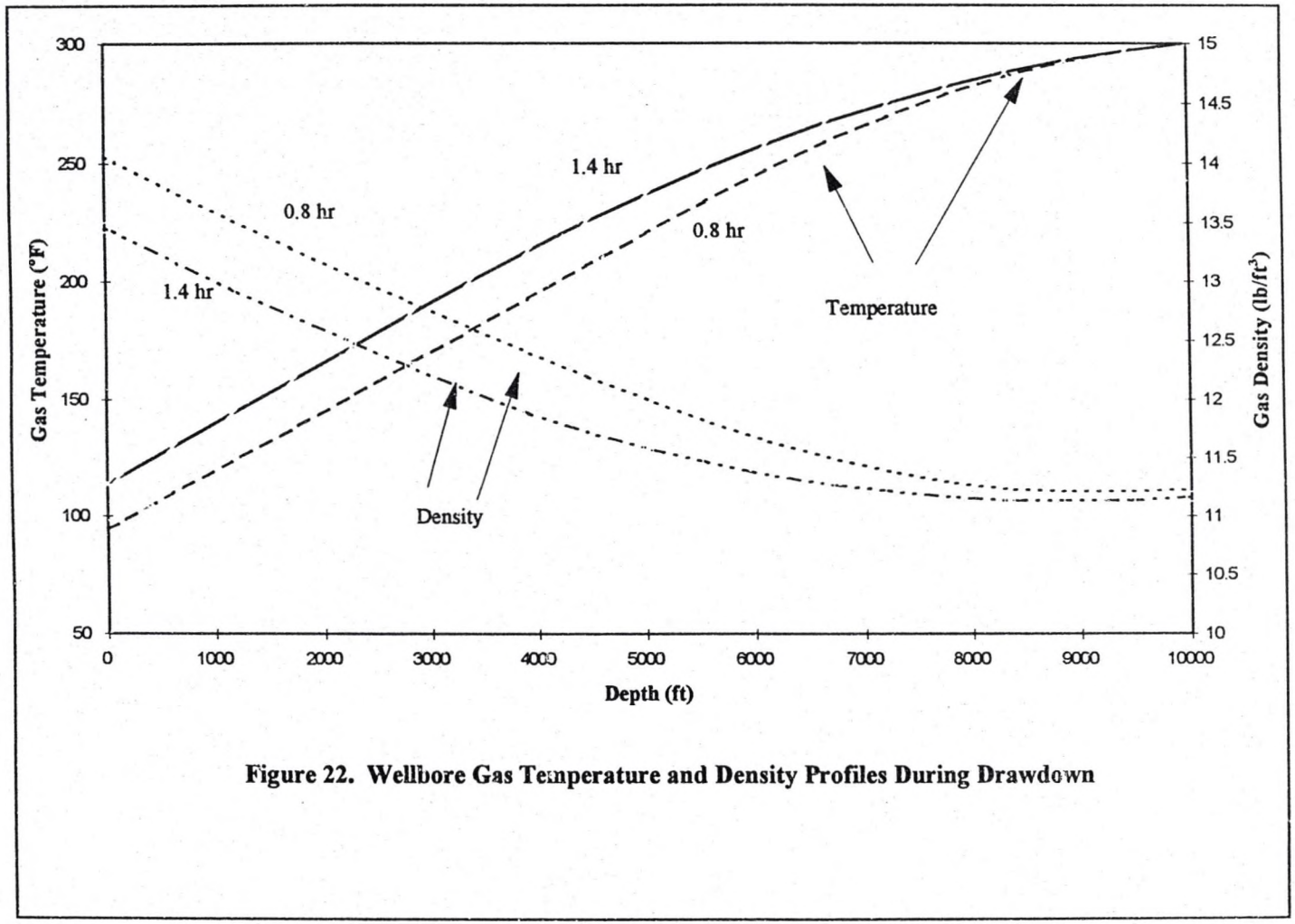

Figure 22. Wellbore Gas Temperature and Density Profiles During Drawdown

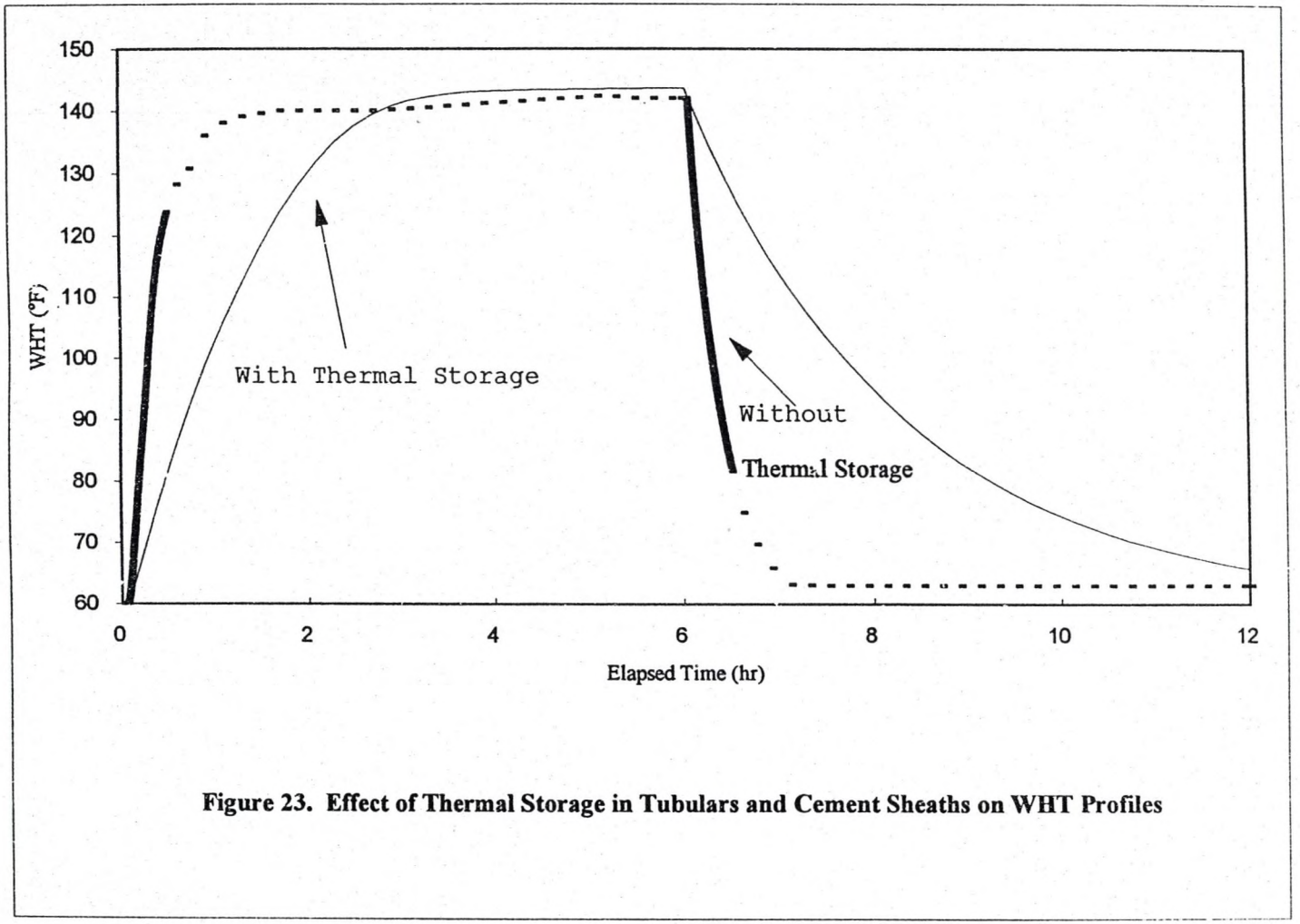

Figure 23. Effect of Thermal Storage in Tubulars and Cement Sheaths on WHT Profiles

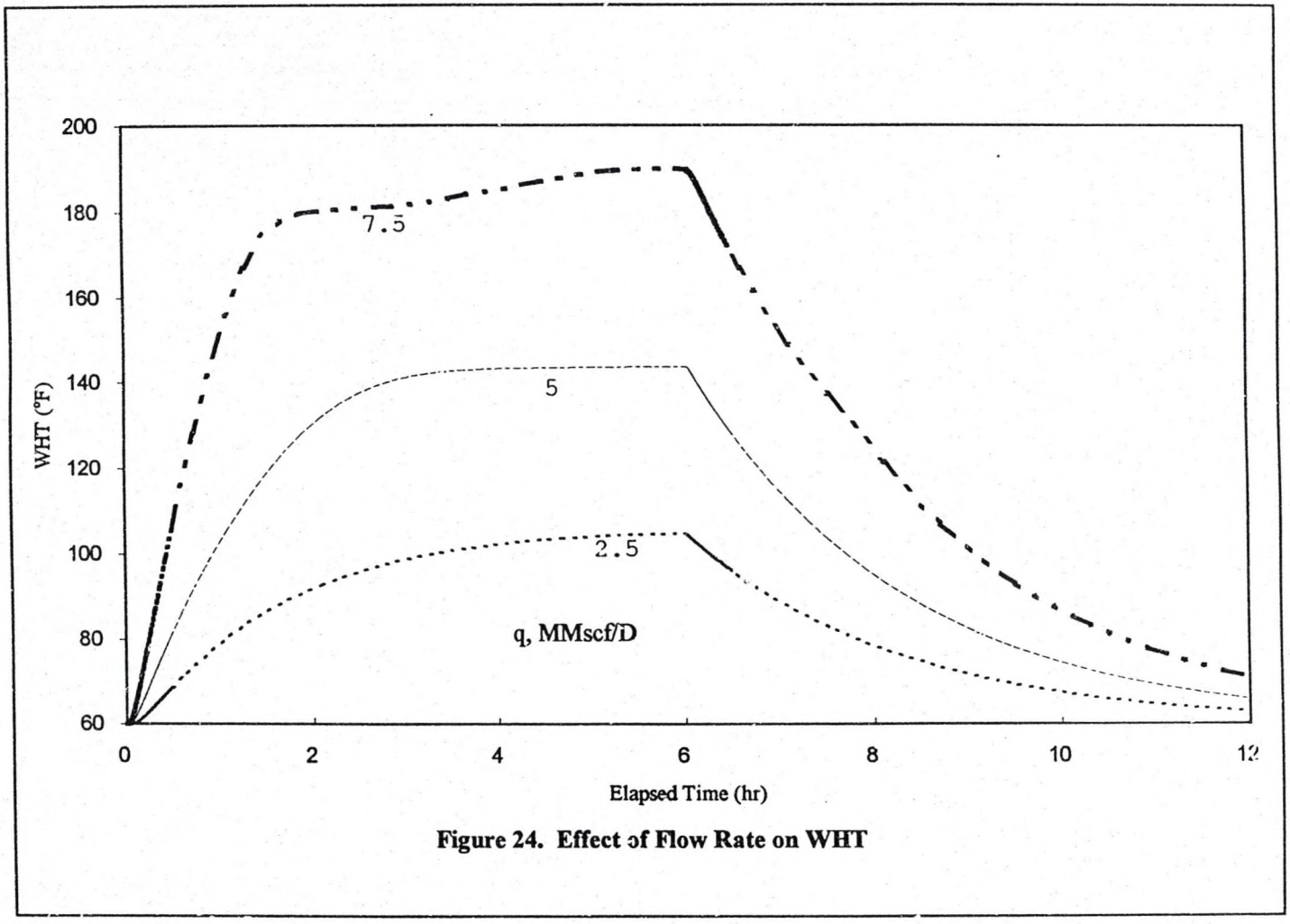

Figure 24. Effect of Flow Rate on WHT

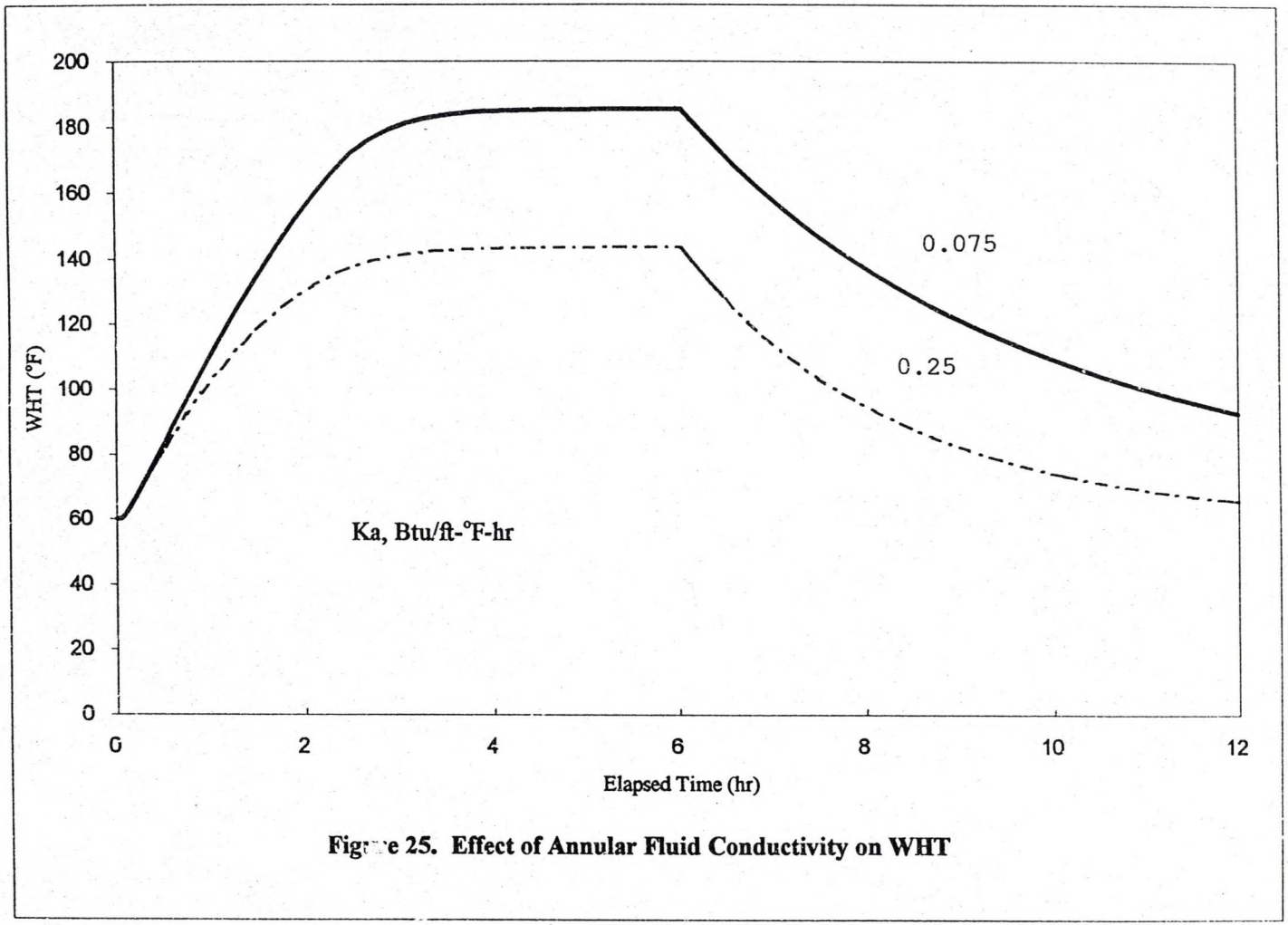

Figure 25. Effect of Annular Fluid Conductivity on WHT

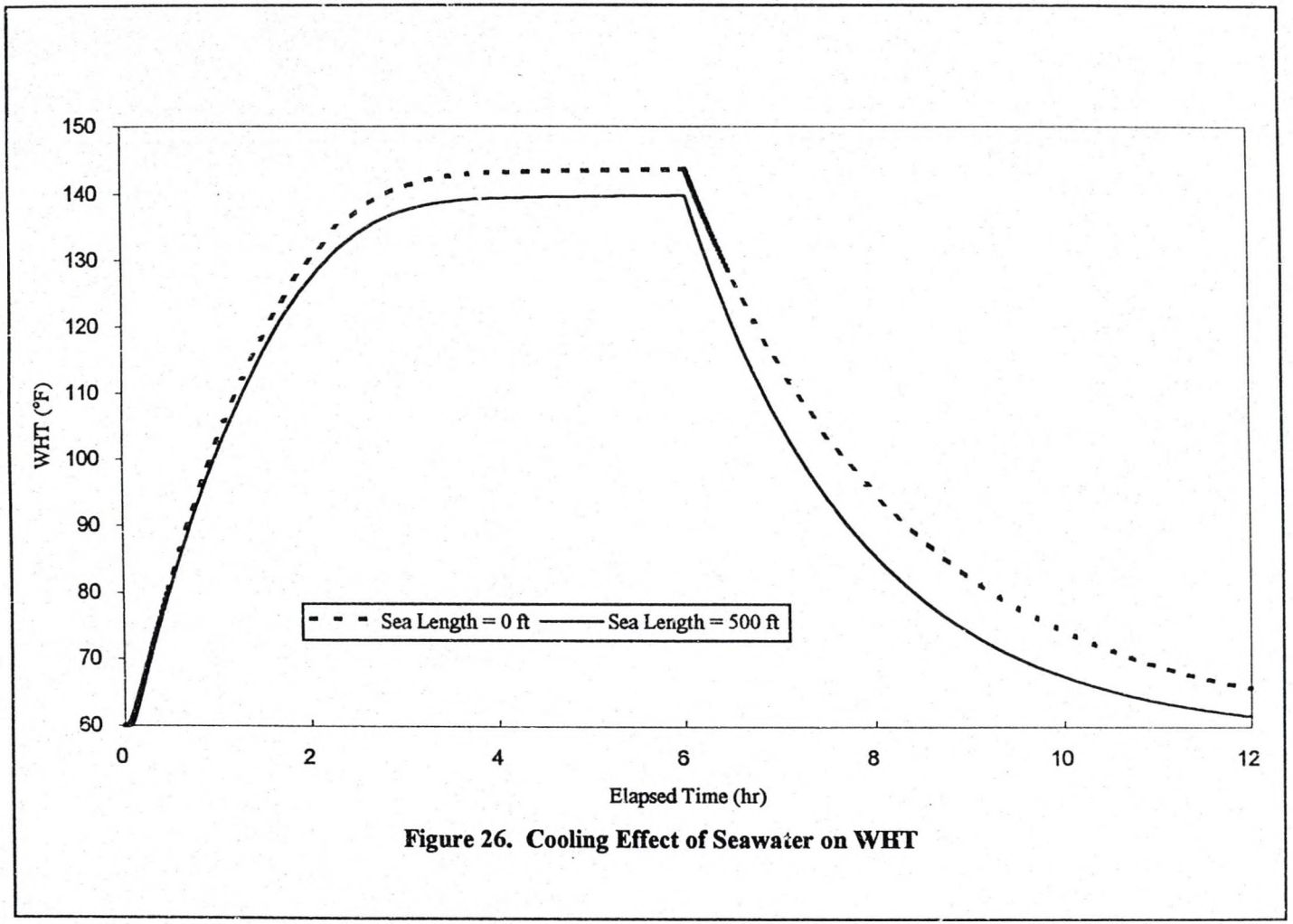

Figure 26. Cooling Effect of Seawater on WHT

Table 2 Well, Reservoir, and Fluid Data For Base Case Oil Well

Reservoir Pressure, psi	7000.0
Well Depth, ft	10,000.0
Tube ID, in	2.75
Tube OD, in	3.5
Casing ID, in	8.9
Casing OD, in	9.375
Pipe Roughness	0.000018
Production Rate, STB/D	2,000
Formation Permeability, md	500.0
Formation Thickness, ft	100.0
Formation Porosity	0.2
Formation Fluid Compressibility, /psi	0.00008
Wellbore Skin	0.0
Bottomhole Temperature, ^{0}F	220.0
Geothermal Gradient, ^{0}F/ft	0.015
Formation Thermal Conductivity, Btu/ft-^{0}F-hr	2.5
Formation Density, lb/ft^{3}	165.0
Formation Heat Capacity, Btu/lb-^{0}F	0.625
Tubing and Casing Material Thermal Conductivity, Btu/lb-^{0}F	30.0
Annulus Fluid Thermal Conductivity, Btu/ft-^{0}F-hr	0.2
Cement Thermal Conductivity, Btu/ft-^{0}F-hr	0.38
Cement Diameter to 500 ft, in	30.0
Cement Diameter from 500 ft to bottomhole, in	20.0
Oil Gravity, ^{0}API	28.0
Gas Gravity (air=1)	0.75

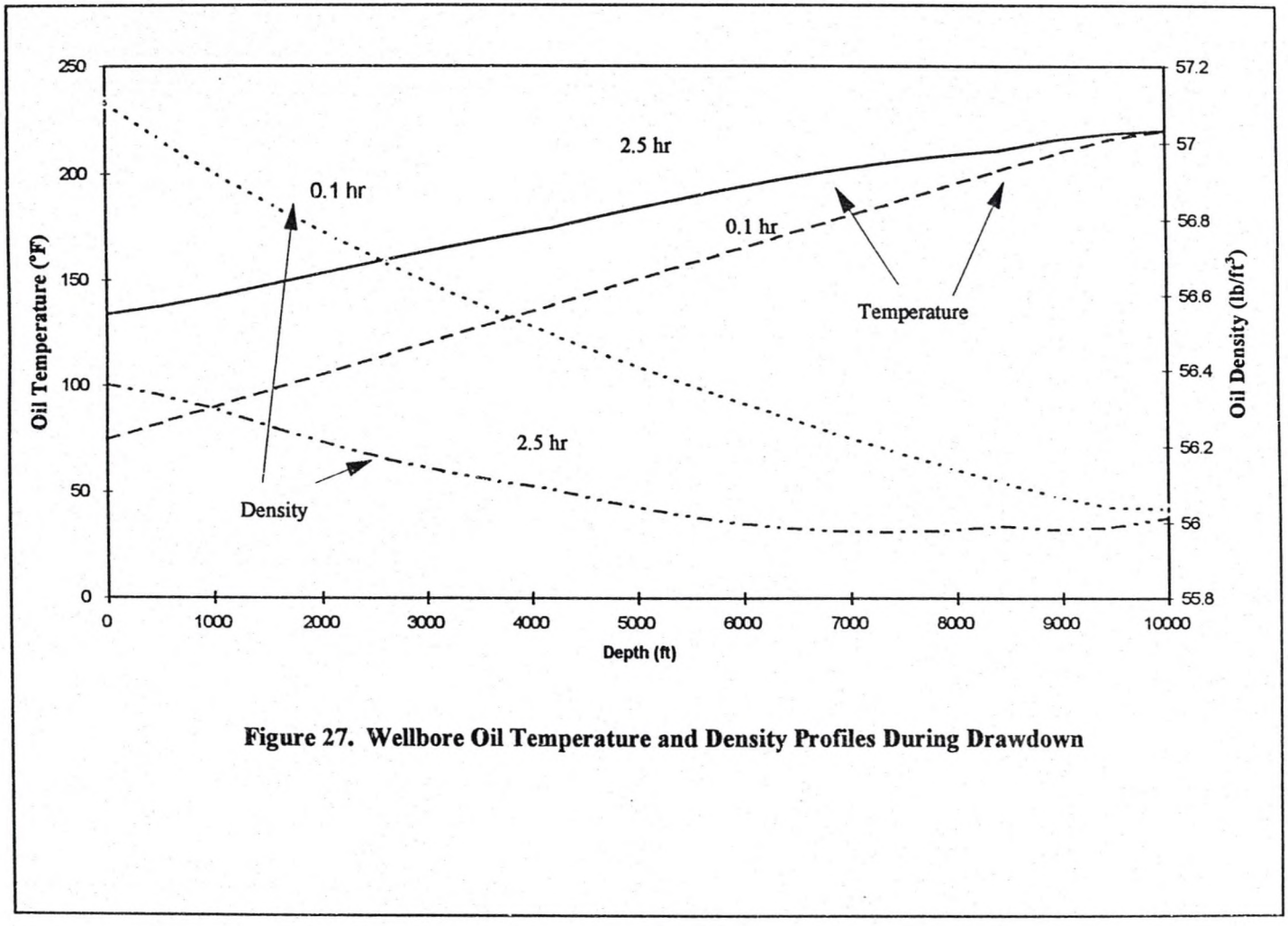

Figure 27. Wellbore Oil Temperature and Density Profiles During Drawdown

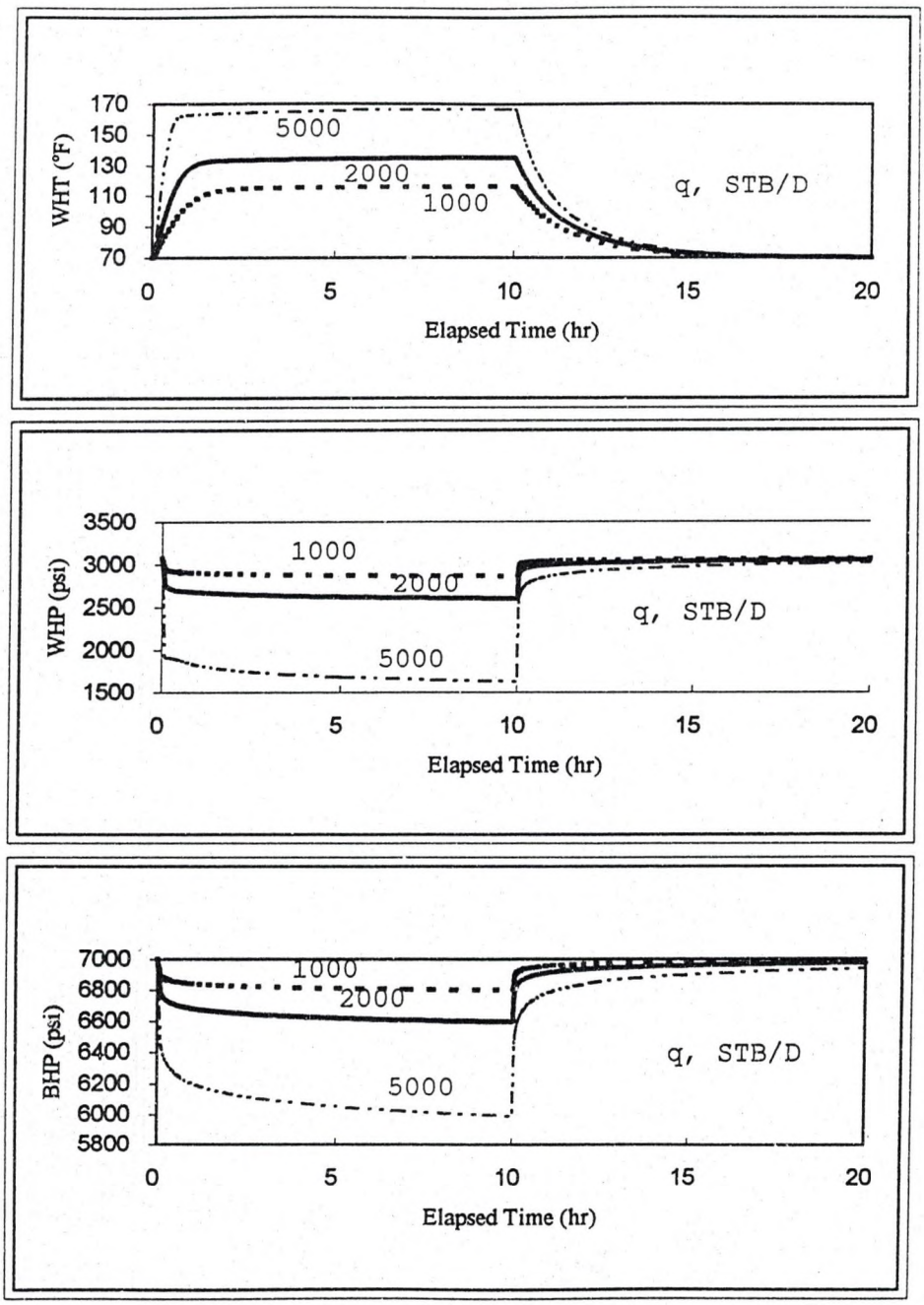

Figure 28. Effect of Production Rate on WHT, WHP, and BHP

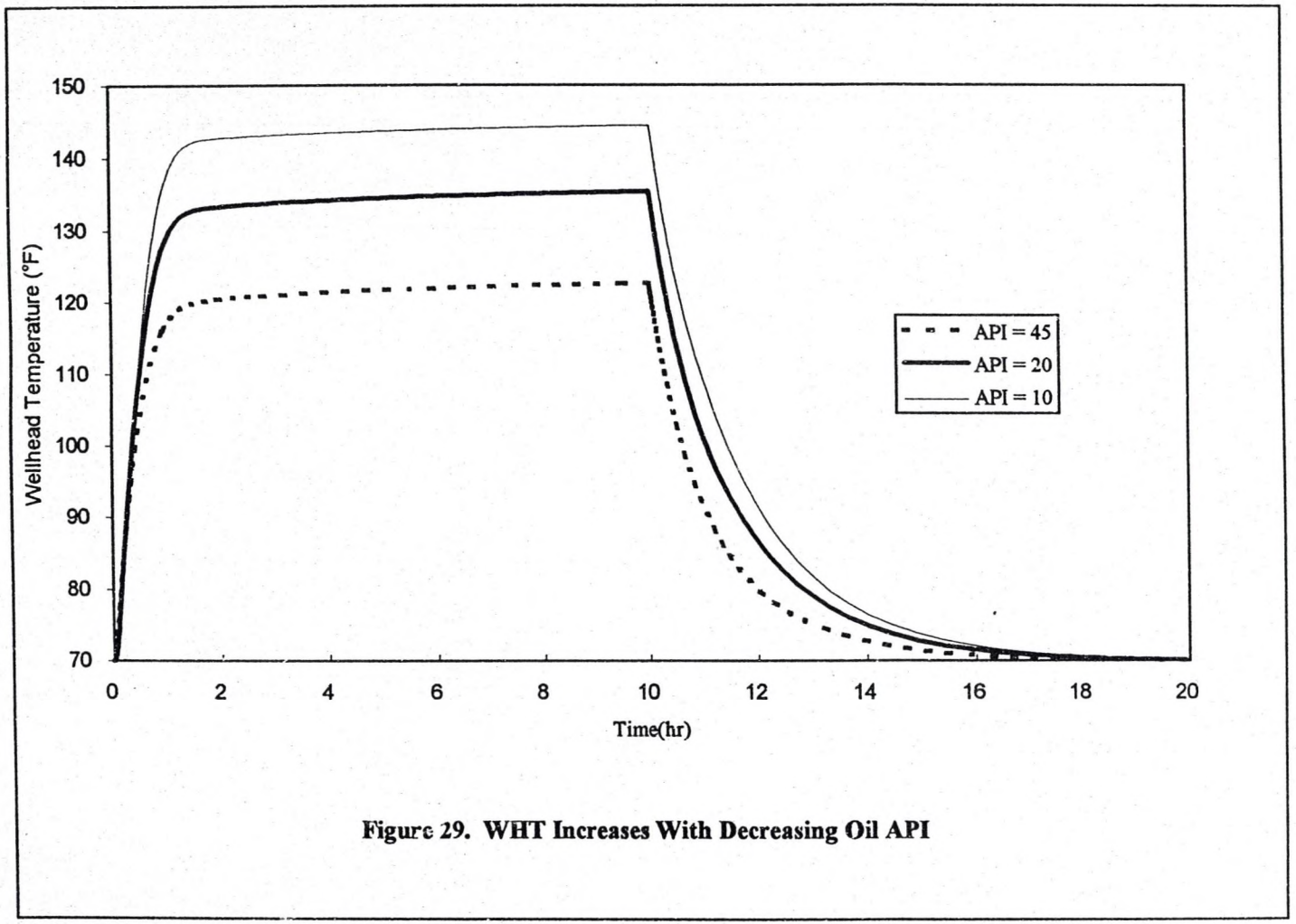

Figure 29. WHT Increases With Decreasing Oil API

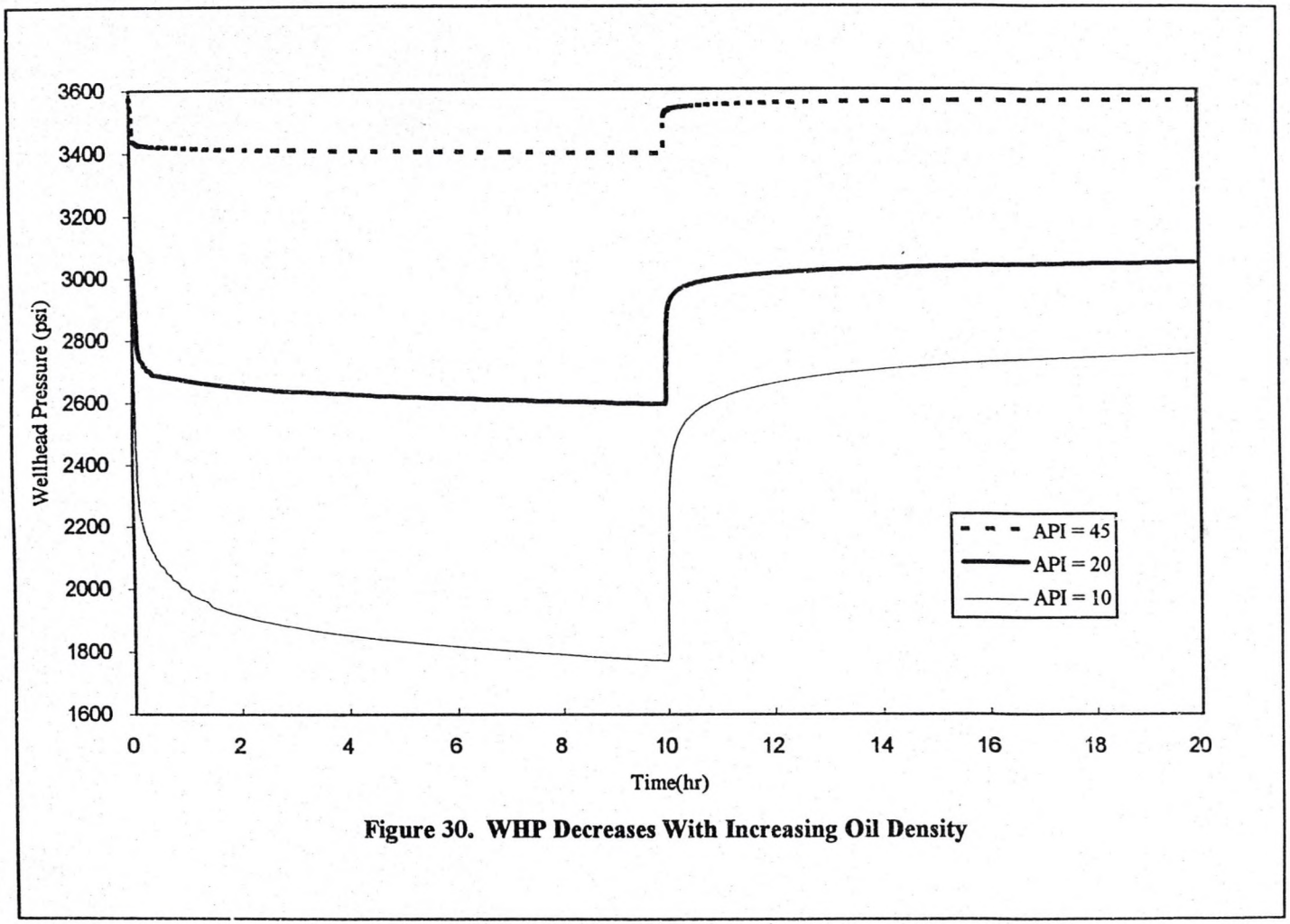

Figure 30. WHP Decreases With Increasing Oil Density

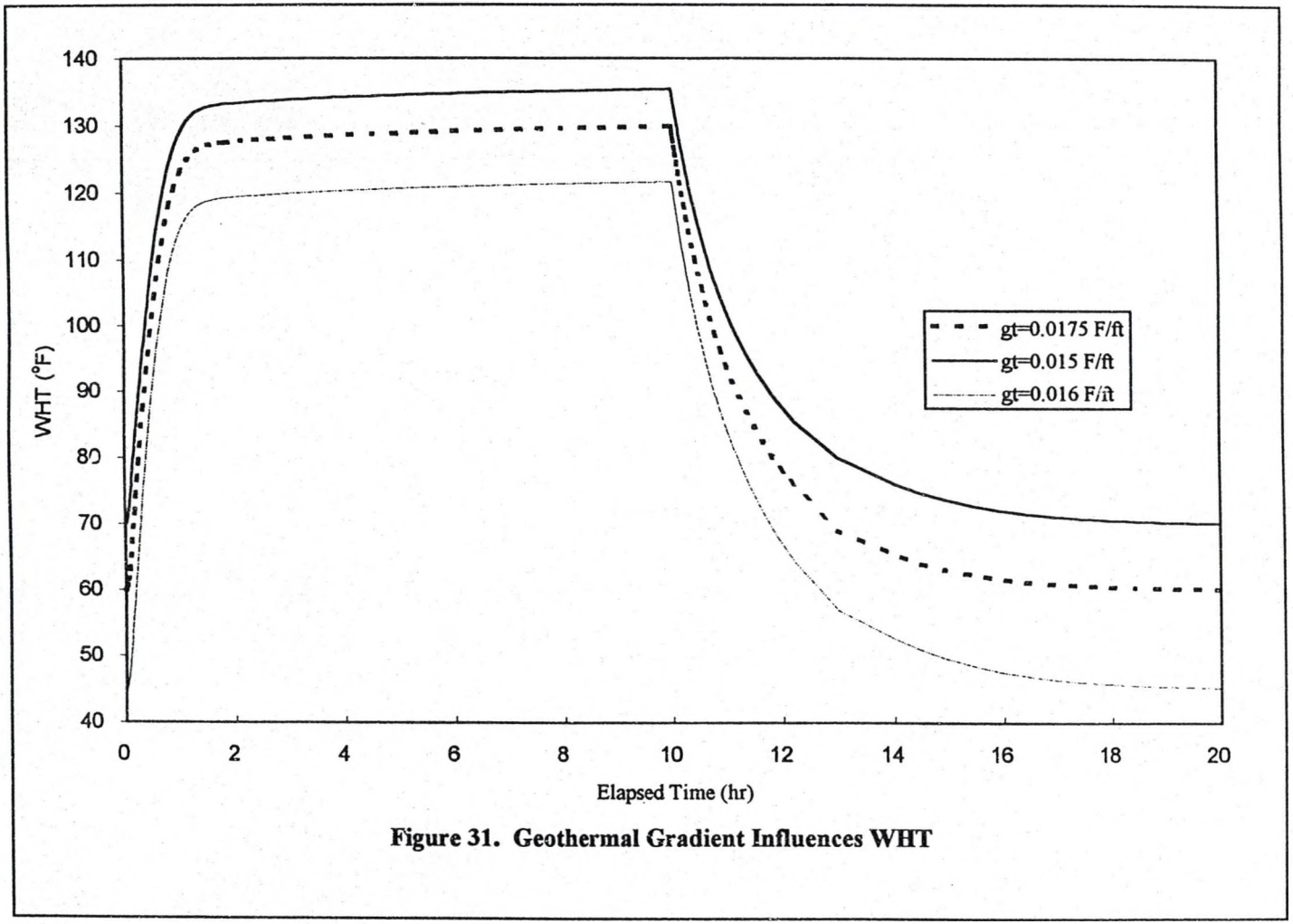

Figure 31. Geothermal Gradient Influences WHT

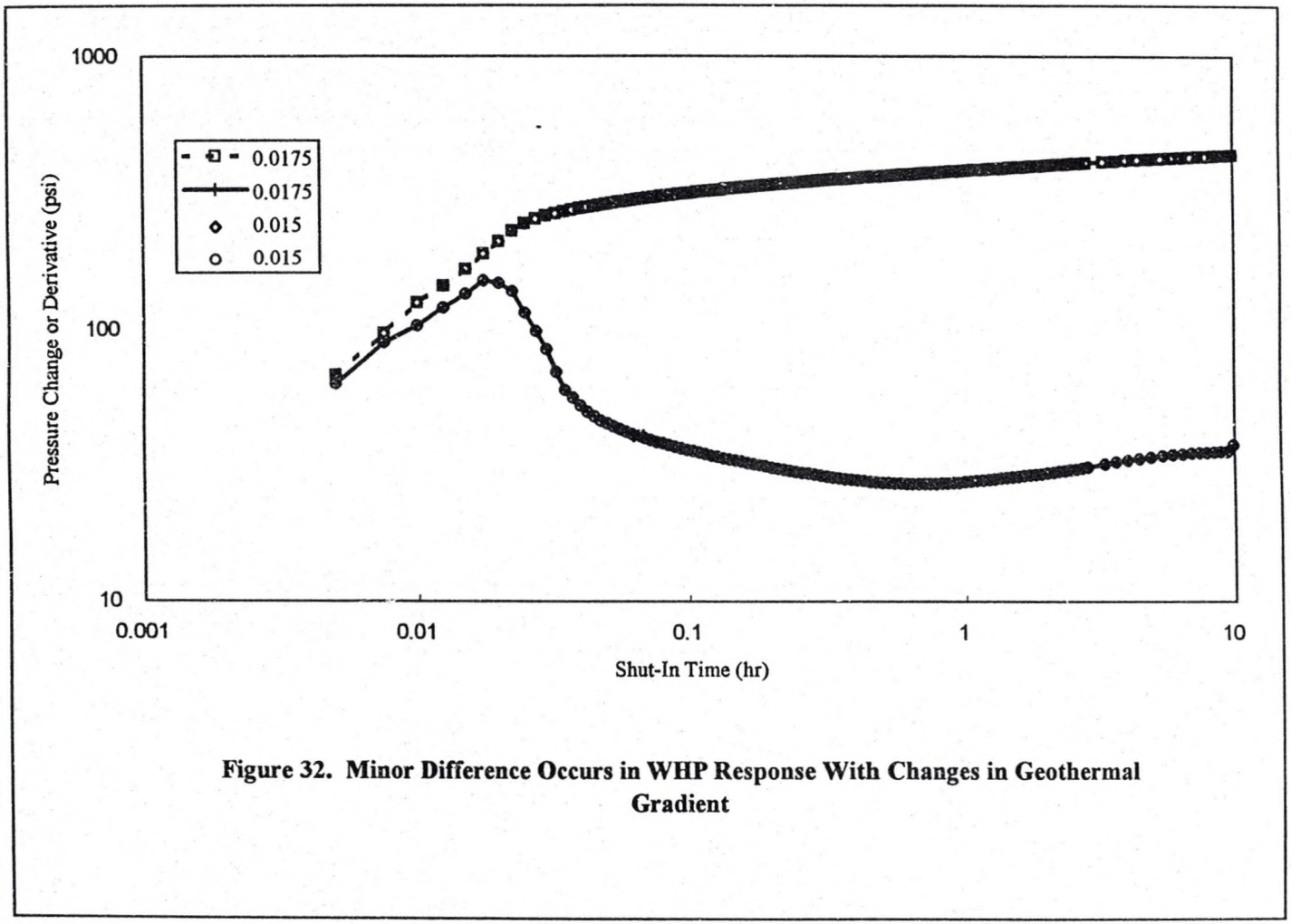

Figure 32. Minor Difference Occurs in WHP Response With Changes in Geothermal Gradient

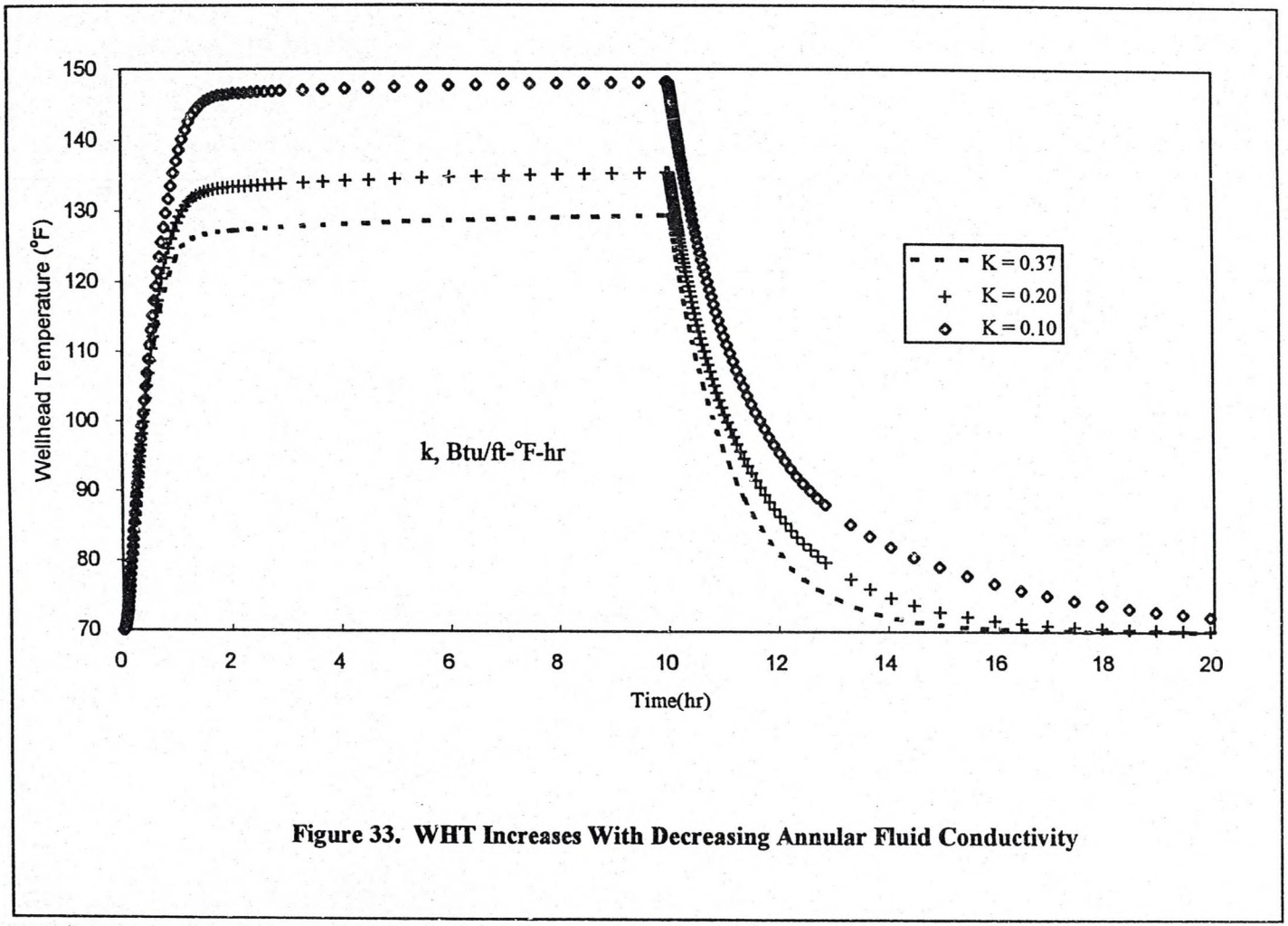

Figure 33. WHT Increases With Decreasing Annular Fluid Conductivity

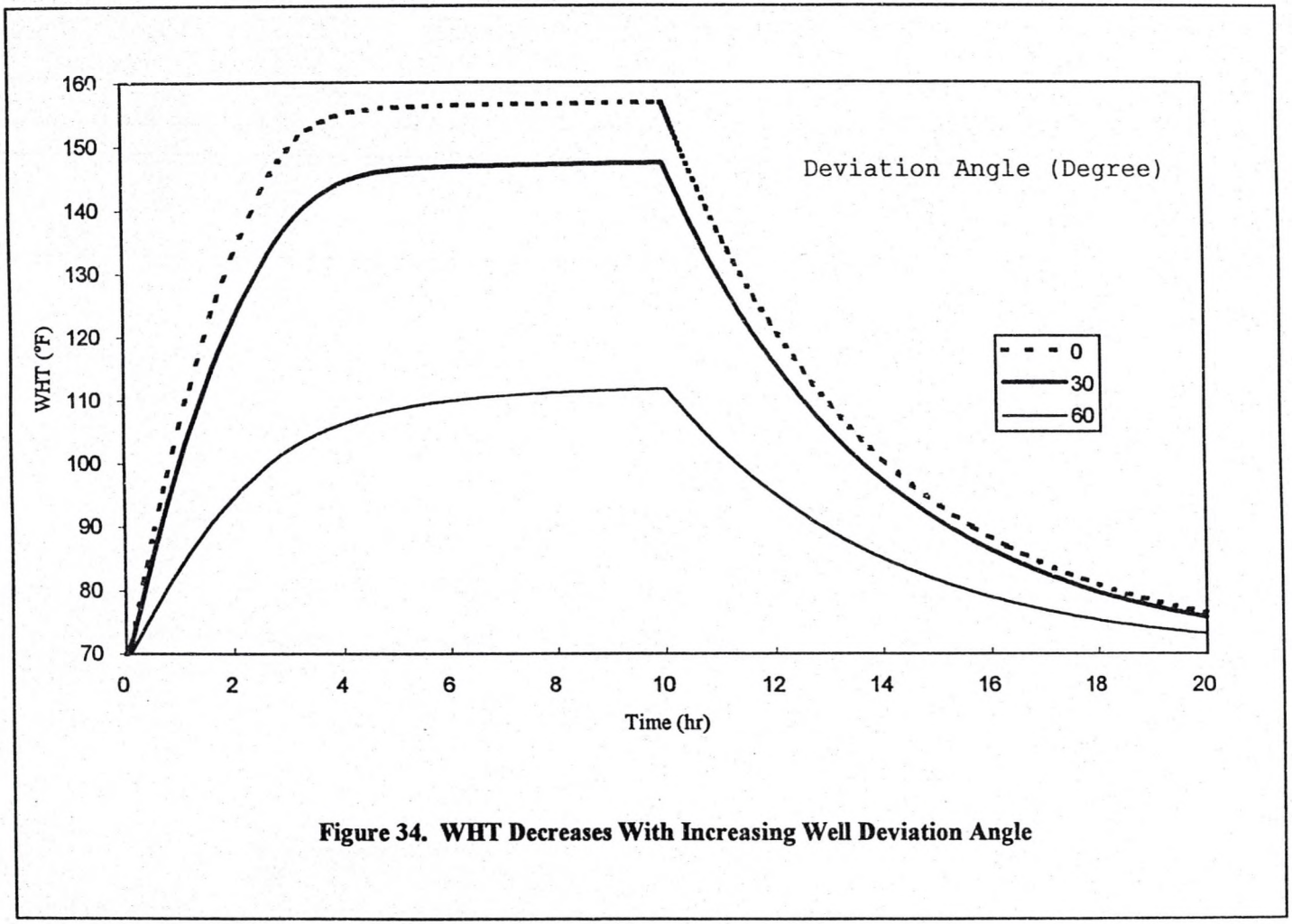

Figure 34. WHT Decreases With Increasing Well Deviation Angle

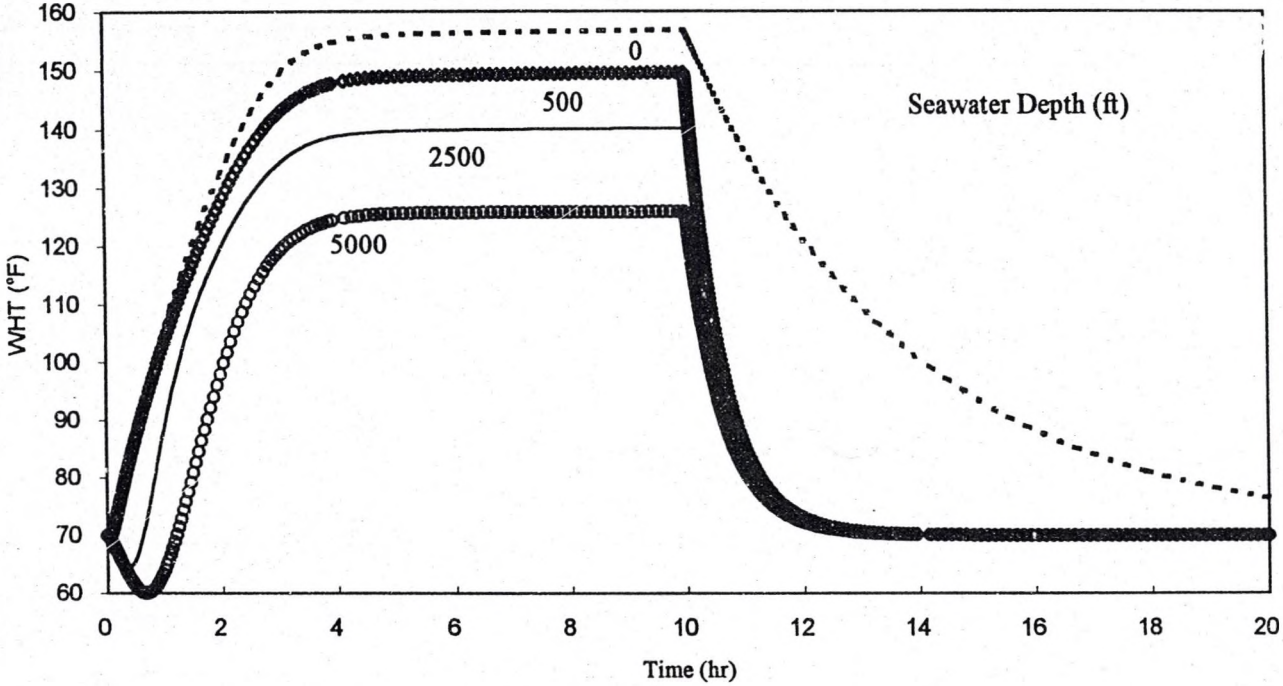

Figure 35. WHT Decreases With Increasing Seawater Depth

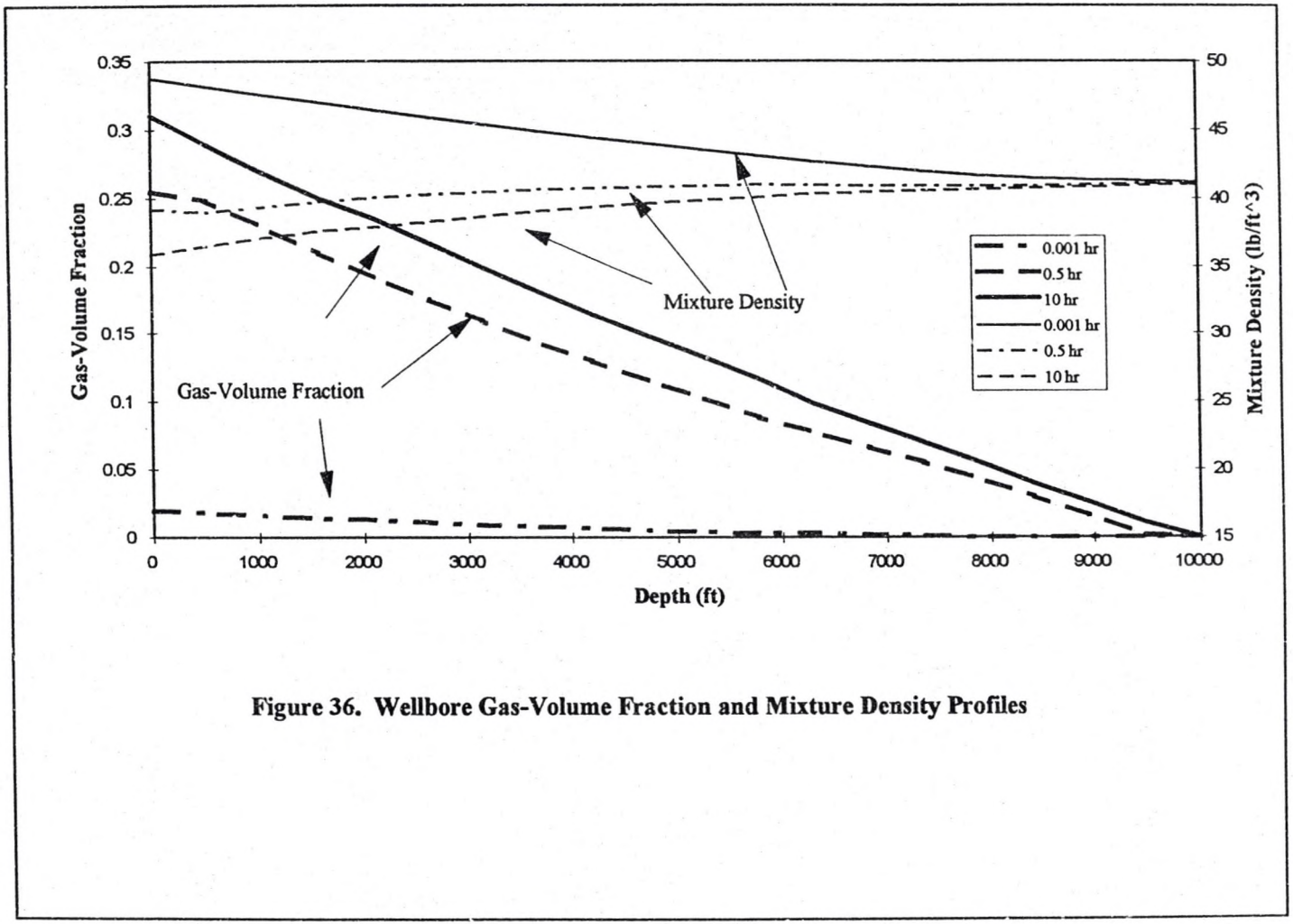

Figure 36. Wellbore Gas-Volume Fraction and Mixture Density Profiles

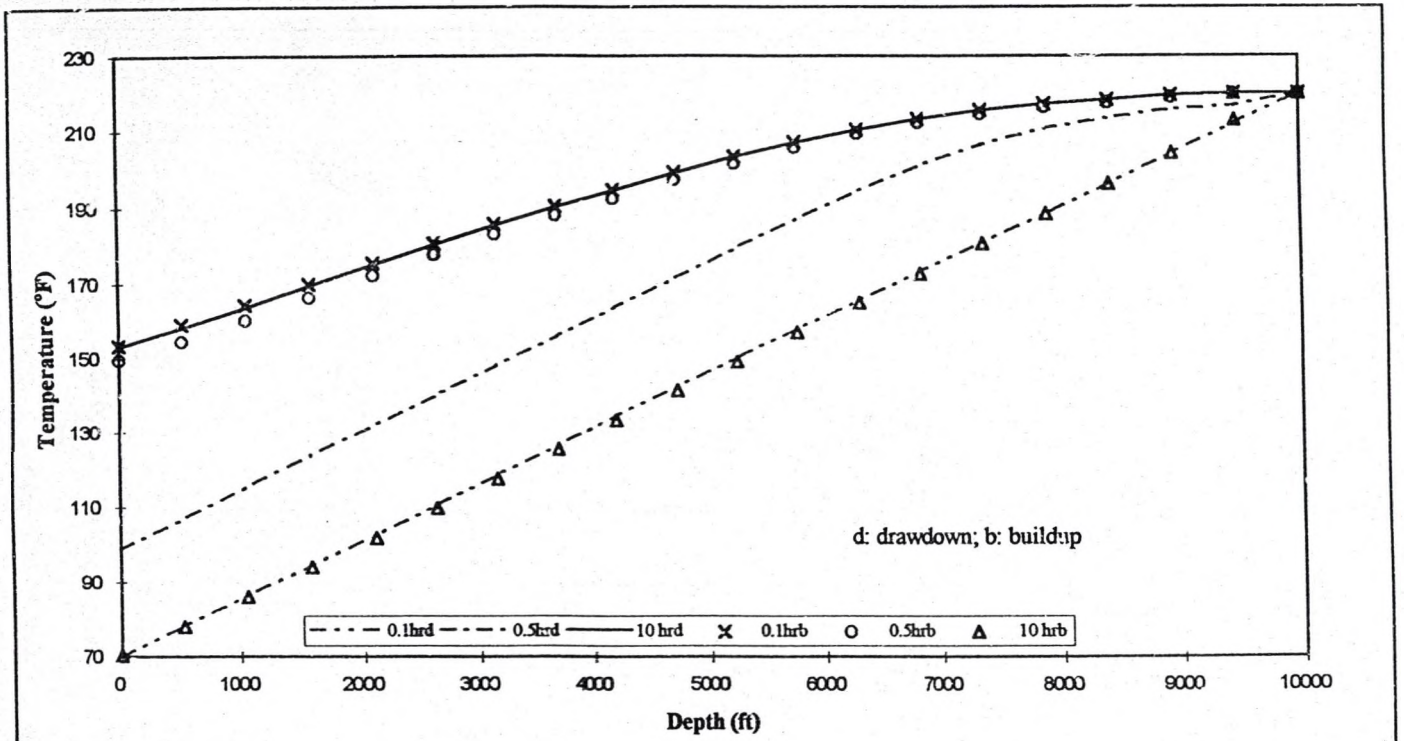

Figure 37. Wellbore Mixture Temperature Profiles

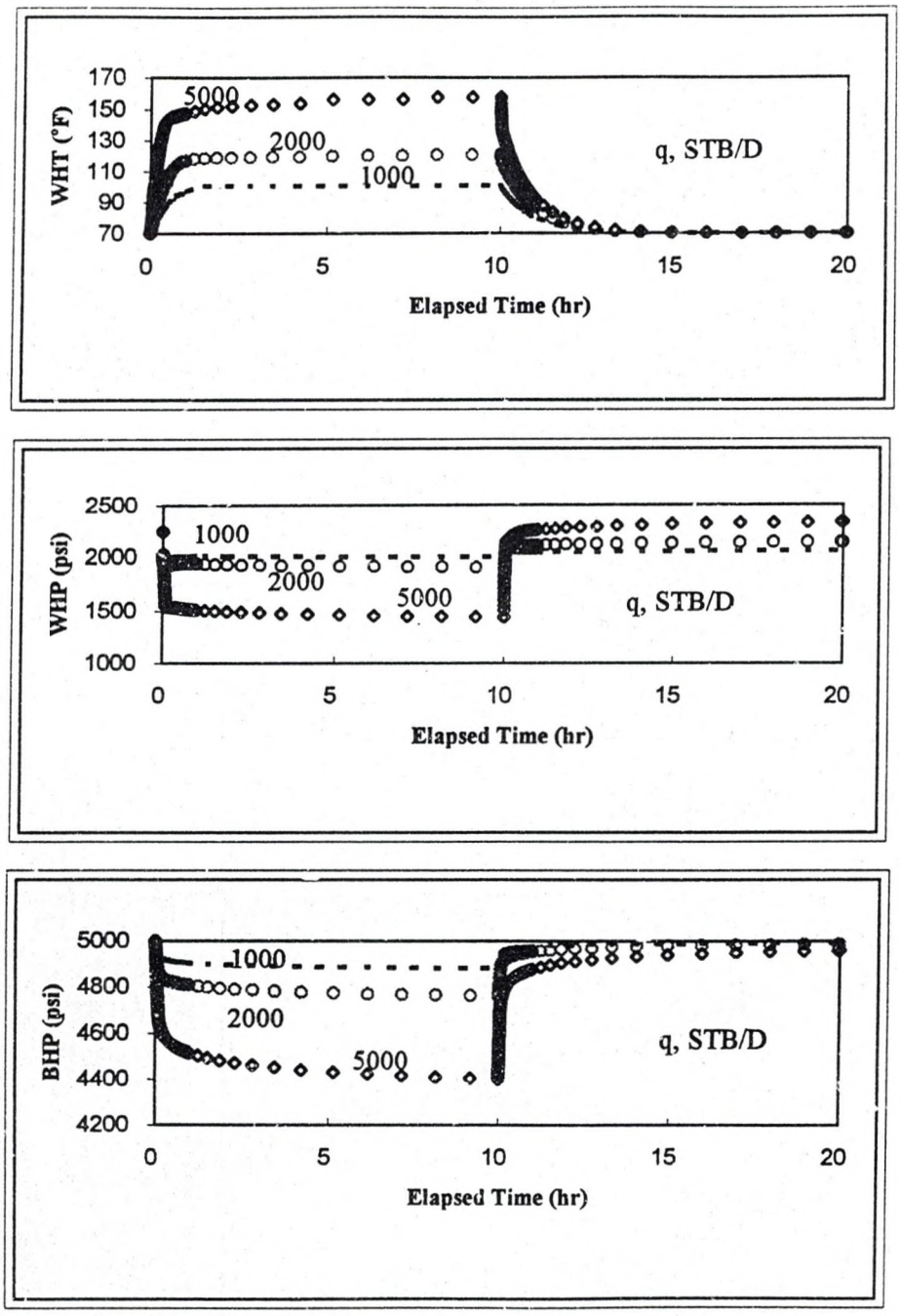

Figure 38. Effect of Producing Rate on Mixture WHT, WHP, and BHP

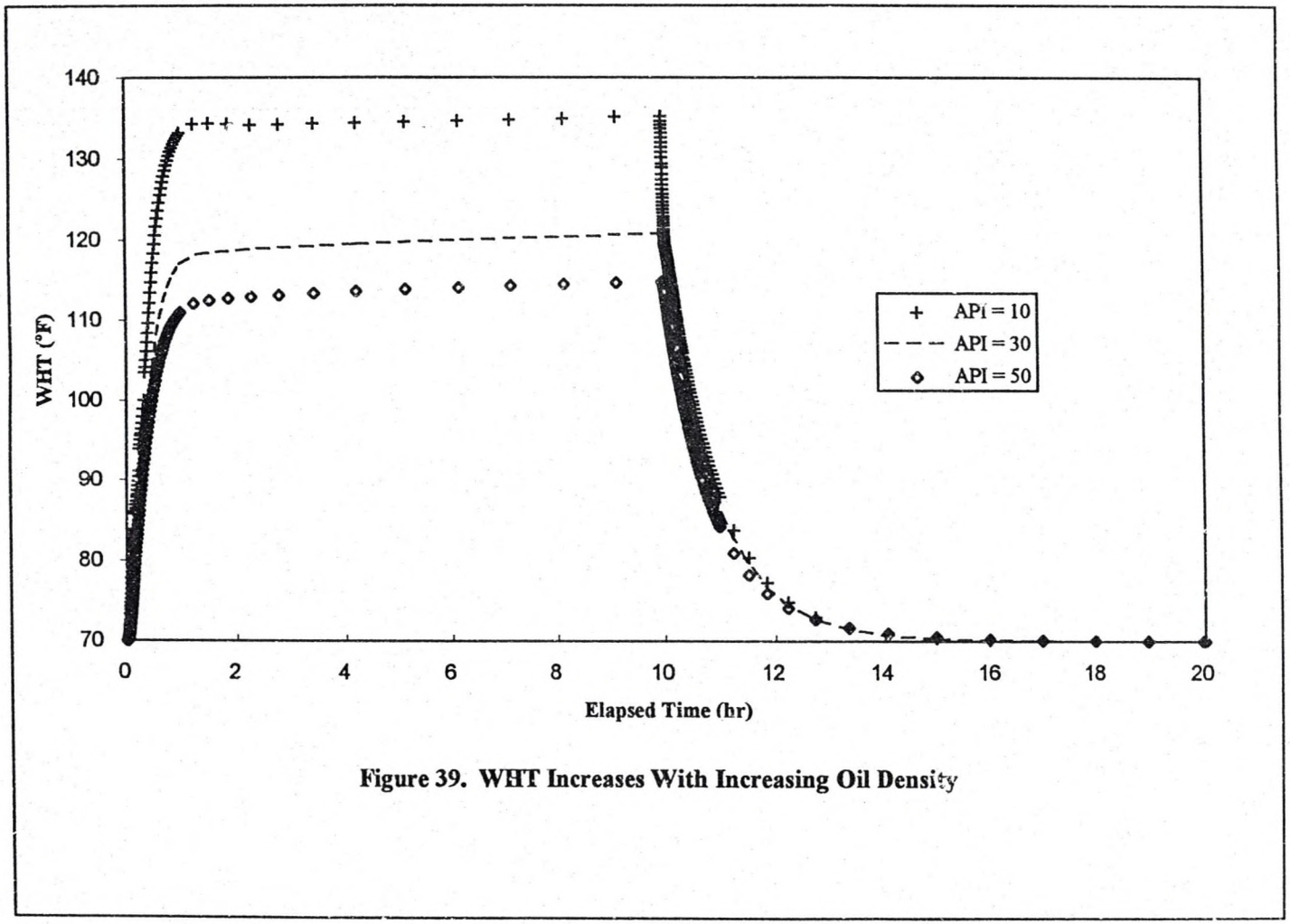

Figure 39. WHT Increases With Increasing Oil Density

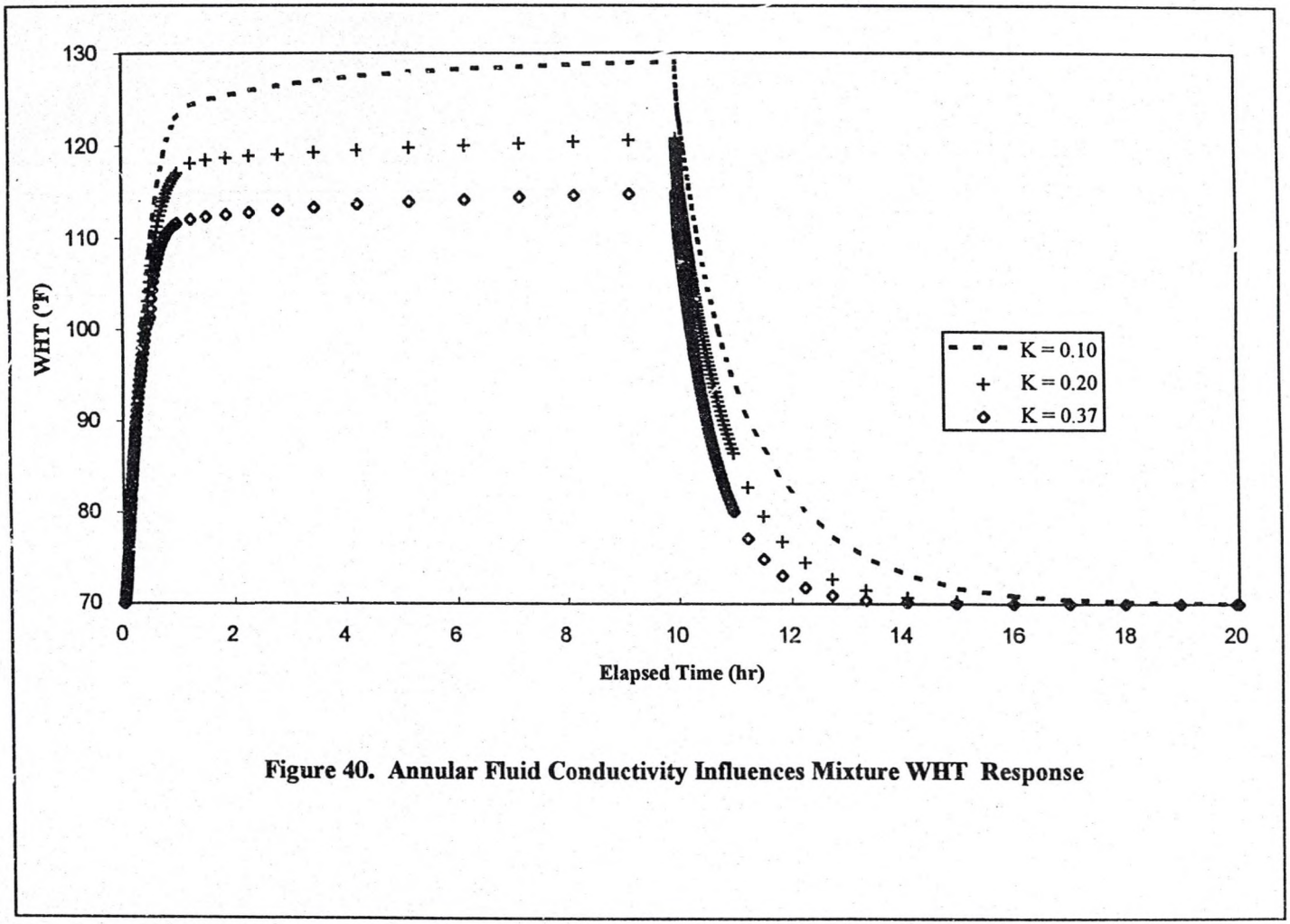

Figure 40. Annular Fluid Conductivity Influences Mixture WHT Response

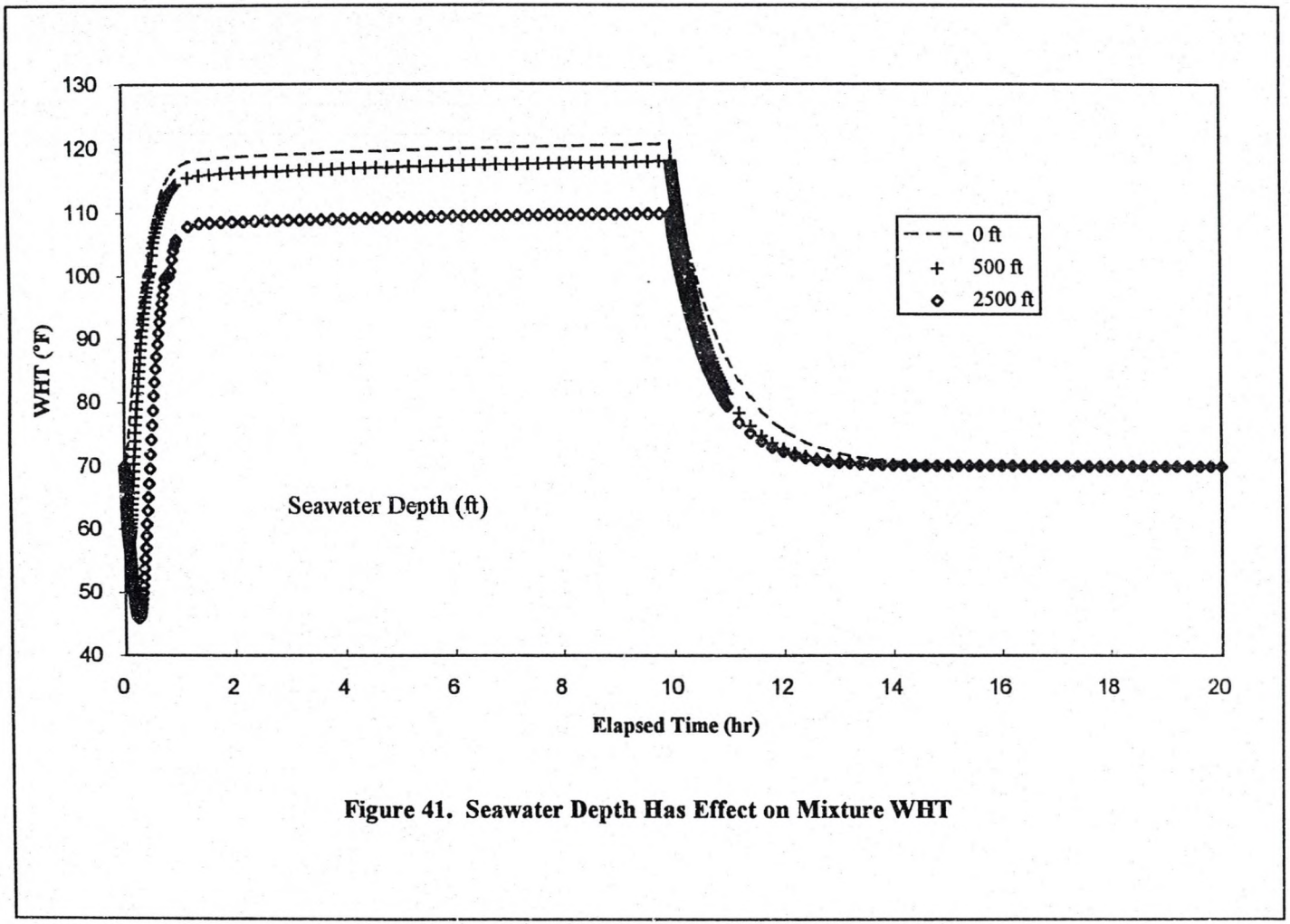

Figure 41. Seawater Depth Has Effect on Mixture WHT

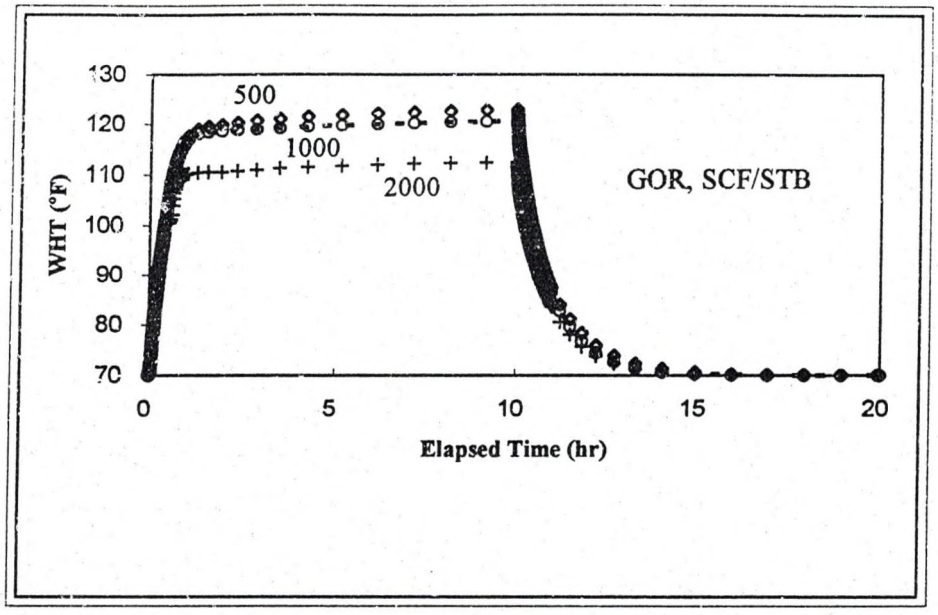

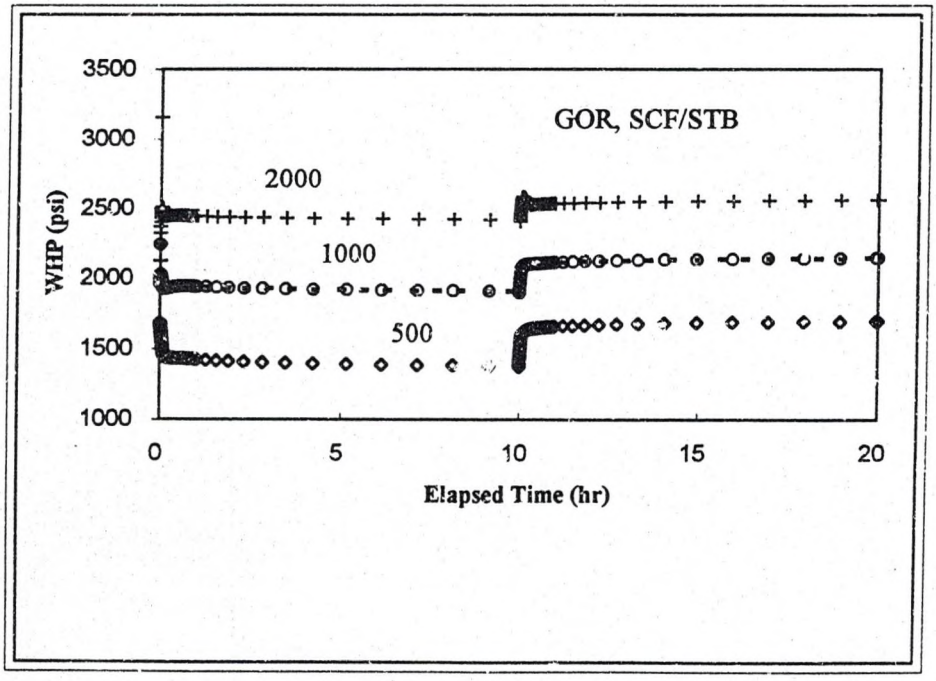

Figure 42. Effect of GOR on WHT and WHP

CHAPTER 6

CONCLUSIONS AND RECOMMENDATIONS

We have developed a rigorous wellbore/reservoir model by simultaneously solving of mass, momentum, and energy balance equations. The associated heat flow is also modeled for the general case of offshore producing systems. The model computes transient pressure and temperature at any point in the wellbore to facilitate design and interpretation of well tests in gas or oil reservoirs. We used the model to study the transient flow behavior in wells producing single-phase gas, single-phase oil, and two-phase fluids. The major conclusions from our study are reported below.

6.1 Conclusions

1. The good agreement between field data and simulations lends strong support to our modeling approach. Forward simulation of BHP, WHP, and WHT has been shown to be quite accurate for engineering purposes. The translating simulator allows us to convert wellhead measurements (WHP and WHT) to bottomhole pressure (BHP) for its subsequent analysis.

2. Our computational approach can be very useful in designing well tests. In addition, the reverse simulation approach can augment many conventional well test analysis. For reservoirs having high temperatures and high pressures, conducting well tests are often very expensive and sometimes impossible. Our approach of gathering wellhead data to conduct

a well test may be very cost-effective in such cases.

3. We have identified the phenomenon of wellbore thermal storage.

4. Our sensitivity study shows that the WHT increases with increasing flow rate, increasing oil density, decreasing annular fluid conductivity, and decreasing geothermal gradient.

5. The simulator provides a vehicle to study a variety of what-if scenarios for wells, mud, equipment, tubular, pipeline, and facilities design during a field development.

6.2 Recommendations

In reverse simulation we used a simplified steady state equation to calculate the fluid temperature profile to initiate computation. This will generate considerable error when the wellbore is exposed to the relatively deeper cooling seawater. In such a situation, we might treat the wellbore as two parts and use our simplified analytical solution separately to improve the accuracy.

APPENDIX A

NOMENCLATURE

A	Flow cross-sectional area, ft^2 (m^2)
B	Fluid formation volume factor, ft^3/Scf
C_D	Wellbore storage coefficient, dimensionless
c_e	Heat capacity of formation, Btu/lb °F (kJ/kg °C)
C_J	Joule-Thompson coefficient, dimensionless
C_o	Flow parameter, dimensionless
c_p	Heat capacity, Btu/lbm °F (kJ/kg °C)
C_{wb}	Fluid compressibility, defined as $(1/\rho)(d\rho/dp)$, $psi^{-1}(pa^{-1})$
d	Pipe inside diameter, ft(m)
E	Internal energy, Btu/lbm (kJ/kg)
E_e	Entrainment of liquid droplets in the gas core in annular flow, dimensionless
E_g	In-situ gas volume fraction or gas void fraction, dimensionless
E_{gc}	Gas void fraction of the core in annular flow, dimensionless
E_{gT}	Gas void fraction for a Taylor bubble, dimensionless
f_f	Film friction factor, dimensionless
f_g	Gas friction factor, dimensionless

f_m	Friction factor, dimensionless
g	Acceleration due to gravity, ft/sec^2 (m/s^2)
g_c	Conversion factor, 32.17 lbm-ft/lbf-sec^2, unity in SI units, dimensionless
g_T	Geothermal temperature gradient, °F/ft (°C/m)
Gr	Grashof number, dimensionless
h	Reservoir pay zone thickness, ft (m)
h_c	Convective heat transfer coefficient for annulus fluid, Btu/hr ft °F (kJ/hr m°C)
h_{sea}	Convective heat transfer coefficient for seawater, Btu/hr ft °F (kJ/hr m°C)
h_t	Convective heat transfer coefficient for the tubing fluid, Btu/hr ft °F (kJ/hr m°C)
H	Enthalpy, Btu/lbm (kJ/kg)
k	Formation permeability, md (mD)
k_{cas}	Conductivity of the casing material, Btu/ft °F (kJ/m°C)
k_{cem}	Conductivity of the cement, Btu/ft °F (kJ/m°C)
k_e	Earth conductivity, Btu/ft °F (kJ/m°C)
k_{ins}	Conductivity of the insulation material, Btu/ft °F (kJ/m°C)
k_t	Tube conductivity, Btu/ft °F (kJ/m°C)
L_R	Relaxation distance, ft^{-1} (m^{-1})
L_{j+1}	The length of the cell j, ft (m)
L_s	Length of a cell in the cellular model of slug flow, ft(m)
L_T	Length of a Taylor bubble in a cell in slug flow, ft(m)
m	Mass of fluid in a control volume, lbm (kg)
m′	Mass per unit length of tubing/casing/cement system, lbm (kg)

m^* Semilog slope (= 162.6 B_g μ/5.615 kh)

p Fluid pressure, psi (kPa)

p_c Critical pressure, psi (Pa)

P_i Reservoir pressure, psi (Pa)

p_r Reduced pressure, dimensionless

Pr Prandtle number, dimensionless

p_{WD} Dimensionless pressure, defined by Eq. (2.47)

q_{sf} Sandface (bottomhole) influx rate, Scf/D (m^3/d)

q_{wh} Wellhead exit rate, Scf/D (m^3/d)

$\bar{Q}$ Heat flow rate from or to the formation, Btu/hr ft (kJ/hr m)

r_{ci} Inside radius of the casing, ft (m)

r_{co} Outside radius of the casing, ft (m)

r_{ins} Outside radius of the insulation, ft (m)

r_{ti} Pipe inside radius, ft (m)

r_{to} Pipe outside radius, ft (m)

r_{wb} Outside radius of the wellbore, ft (m)

R_j Resistance between tubing and annulus fluids, ft °F/Btu (m°C/kJ)

s Steady-state skin factor, dimensionless

t Producing time, hour (s)

t_D Dimensionless time = $\alpha\, t/r_w^2$

T_c Critical temperature, °F (°C)

T_e Earth temperature at time t and distance r, °F (°C)

T_{ei} Static earth temperature at any given depth, °F (°C)

T_{eibh} Static earth temperature at the bottomhole, °F (°C)

T_f Fluid temperature, °F (°C)

T_r Reduced temperature, dimensionless

T_{wb} Wellbore/earth interface temperature, °F (°C)

U_{to} Overall heat transfer coefficient, Btu/hr ft^2 °F

U_{toc} Overall heat transfer coefficient when wellbore is exposed to seawater, Btu/hr ft^2 °F

v_g Gas velocity, ft/hr (m/s)

v_l Oil velocity, ft/hr (m/s)

v_m Mixture velocity, ft/hr (m/s)

v_{sg} Superficial gas velocity, ft/hr (m/s)

v_{sl} Superficial oil velocity, ft/hr (m/s)

v_∞ Terminal rise velocity, ft/hr (m/s)

$v_{\infty T}$ Terminal rise velocity of a Taylor bubble, ft/hr (m/s)

V_{wb} Wellbore volume, ft^3 (m^3)

w Mass flow rate, lbm/hr (kg/h)

x Mass fraction of gas in the mixture, dimensionless

z Variable well length from bottom, ft (m).

Z_c Gas-law deviation factor, dimensionless.

Greek Letters

α	Heat diffusivity of earth, $k_e/C_e\rho_e$, ft^2/hr (m^2/h)
ρ_a	Annulus fluid density in annular flow, lb/ft^3 (kg/m^3)
ρ_c	Core density in annular flow, lb/ft^3 (kg/m^3)
ρ_e	Density of formation, lb/ft^3 (kg/m^3)
ρ_g	Gas density, lb/ft^3 (kg/m^3)
ρ_l	Oil density, lb/ft^3 (kg/m^3)
ρ_m	Mixture density, lb/ft^3 (kg/m^3)
ρ_{sf}	Sandface (bottomhole) fluid density, lb/ft^3 (kg/m^3)
μ_a	Annulus viscosity, cp (mPa.s)
μ_g	Gas viscosity, cp (mPa.s)
μ_l	Oil viscosity, cp (mPa.s)
μ_m	Mixture viscosity, cp (mPa.s)
σ_s	Surface tension, lbm/hr^2 (kg/s^2)
θ	Pipe inclination angle with horizontal, degree

APPENDIX B

Solution Of The Diffusivity Equation

Solution of the diffusivity equation (Eq. 2.22) with the boundary conditions resulting equations (Eqs. 2.23, 2.24 and 2.25) is best carried out using Laplace transform as shown by van Everdingen and Hurst (1949) for a similar set of equations for pressure transients. Laplace Transform of T_e, designated $\bar{T}$, is given by the following definite integral

$$L_{t_D}[T_e] = \int_0^\infty e^{-st_D} T_e \, dt_D = \bar{T} \qquad \text{(B-1)}$$

The definition can be used to arrive at the following transforms for the differentials in Eqs. 2.23-2.25,

$$L_{t_D}\left[\frac{\partial^2 T_e}{\partial r_D^2}\right] = \frac{\partial^2 \bar{T}}{\partial r_D^2} \qquad \text{(B-2)}$$

$$L_{t_D}\left[\frac{\partial T_e}{\partial r_D}\right] = \frac{\partial \bar{T}}{\partial r_D} \qquad \text{(B-3)}$$

$$
\begin{aligned}
L_{t_D}\left[\frac{\partial T_e}{\partial t_D}\right] &= \int_0^\infty e^{-st_D}\,\frac{\partial T_e}{\partial t_D}\,dt_D \\
&= \left[T_e e^{-st_D}\right]_\infty^0 - \int_0^\infty T_e(-s)\,e^{-st_D}\,dt_D \\
&= \overline{T_{ei}} - 0 + \int_0^\infty T_e e^{-st_D}\,dt_D \\
&= \overline{T_{ei}} + s\,\overline{T}
\end{aligned}
\qquad \textbf{(B-4)}
$$

Therefore, in the Laplace domain, Eq. 2.22 and the boundary conditions in dimensionless variables become

$$
\frac{\partial^2 \overline{T}}{\partial r_D^2} + \frac{1}{r_D}\frac{\partial \overline{T}}{\partial r_D} = \overline{T_{ei}} + s\,\overline{T} \qquad \textbf{(B-5)}
$$

$$
\lim_{r_D \to \infty} \frac{\partial \overline{T}}{\partial r_D} = 0 \qquad \textbf{(B-6)}
$$

$$
\frac{\overline{Q}}{s} = -2w\pi k_e \frac{\partial \overline{T}}{\partial r_D} \qquad \textbf{(B-7)}
$$

The general solution of Eq B-5 is

$$
\overline{T} - \overline{T_{ei}} = A I_0(r_D\sqrt{s}) + B K_0(r_D\sqrt{s}) \qquad \textbf{(B-8)}
$$

where the K_0 and K_1 are the zero-order and first-order modified Bessel functions of the second kind respectively. The constants, **A** and **B**, would be determined from the boundary conditions. Thus, in order to satisfy Eq. B-6, **A** must be zero. Therefore,

$$\overline{T} - \overline{T_{ei}} = B K_0(r_D \sqrt{s}) \qquad \textbf{(B-9)}$$

Differentiating the above equation respect to r_D, we obtain

$$\frac{\partial \overline{T}}{\partial r_D}\Big|_{r_D=1} = -\sqrt{s}\, B K_1(\sqrt{s}) \qquad \textbf{(B-10)}$$

Using the second boundary condition, Eq. B-7, we get

$$B = \frac{\overline{Q}}{2w\pi k_e s \sqrt{s}\, k_1(\sqrt{s})} \qquad \textbf{(B-11)}$$

Therefore,

$$\overline{T} - \overline{T_{ei}} = \frac{\overline{Q}\, k_0(r_D\sqrt{s})}{2w\pi k_e\, s\sqrt{s}\, k_1(\sqrt{s})} \qquad \textbf{(B-12)}$$

To obtain the expression for earth temperature T_e, we apply the Mellin Inversion Theorem to obtain

$$T_e - T_{ei} = L^{-1}\left[\frac{\overline{Q} K_0(r_D\sqrt{s})}{2w\pi\, k_e\, s\sqrt{s}\, K_1(\sqrt{s})}\right] \qquad \textbf{(B-13)}$$

$$= \frac{1}{2\pi i}\int_{\gamma-i\infty}^{\gamma+i\infty} \frac{\overline{Q} K_0(r_D\sqrt{s})\, e^{st_D}}{2w\pi\, k_e\, s\sqrt{s}\, K_1(\sqrt{s})}\, ds \qquad \textbf{(B-14)}$$

$$T_e - T_{ei} = \frac{\overline{Q}}{4 w \pi^2 k_e i} \int_{\gamma - i\infty}^{\gamma + i\infty} \frac{K_0(r_D\sqrt{s})\, e^{st_D}}{s\sqrt{s}\, K_1(\sqrt{s})}\, ds \qquad \text{(B-15)}$$

The contour integral of Eq. B - 15 is represented in Fig. 43. Notice that there is a branch point at origin due to the presence of $\sqrt{s}$. By choosing the branch "cut" along the negative real axis, we get a single valued function on each side of the "cut". That is, we get a closed contour A B C D E F G, consisting of a line AB with an infinite length, arcs BC and GA of semi-circle of center at origin with radius r_D ($r_D \approx \infty$), an incomplete circle DEF centered at origin with infinitely small radius ($\epsilon \approx 0$) and two lines CD and GF parallel to and infinitely close to the negative real axis.

Applying Cauchy's theorem to this analytic, single-valued function, we can write,

$$\int_{ABCDEFG} \frac{K_0(r_D\sqrt{s})\, e^{st_D}}{s\sqrt{s}\, K_1(\sqrt{s})}\, ds = 0 \qquad \text{(B-16)}$$

The contour integral in Eq. B - 16 can be expressed as the sum of the integrals along AB, BC, CD, DEF, FG, and GA. Thus, omitting the integrand, Eq. B-16 can be written as

$$\int_{AB} + \int_{BC} + \int_{CD} + \int_{DEF} + \int_{FG} + \int_{GA} = 0 \qquad \text{(B-17)}$$

Use of theorems on limiting contours allows us to set the integrals $\int_{BC}$ and $\int_{GA}$ equal to zero. In addition, Van Everdingen and Hurst indicated that $\int_{DEF}$ also vanishes. Hence sum of the integrations along CD and FG equals the integration along AB. The

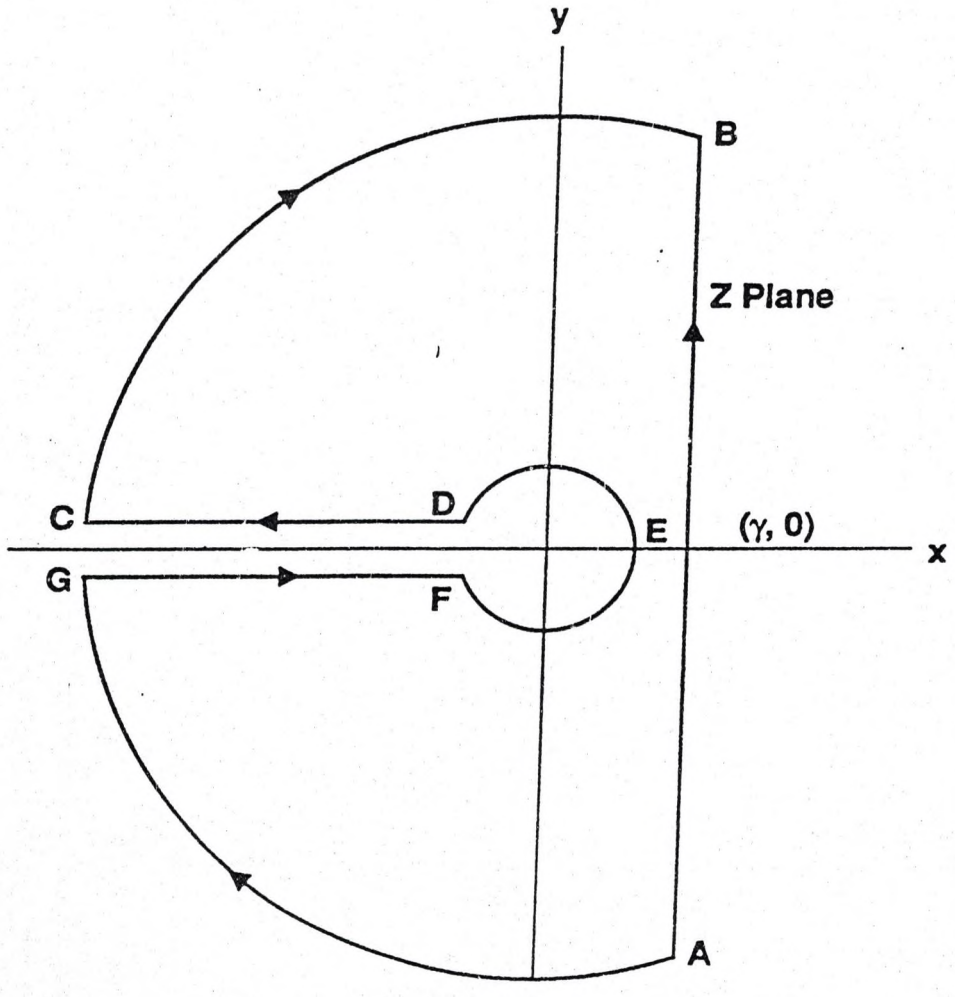

Figure 43. Contour Integration in Establishing the Constant Terminal Rate Case for Infinite Extent

integration on the upper portion of the "cut" can be obtained by letting $s = u^2 e^{i\pi}$, which yields

$$\int_{CD} = \frac{1}{2\pi i} \int_0^\infty \frac{K_0(r_D\sqrt{s})\, e^{st_D}}{s^{3/2}\, K_1(\sqrt{s})}\, ds$$

$$= \frac{1}{\pi i} \int_0^\infty \frac{K_0(u e^{i\pi/2} r_D)\, e^{u^2 t_D e^{i\pi}}}{u^2\, e^{\pi i/2}\, K_1(u e^{i\pi/2})}\, du \qquad \textbf{(B-18)}$$

ting that $e^{\pi i} = -1$ and $e^{\pi i/2} = I$, we rewrite Eq. B-18 as,

$$\int_{CD} = -\frac{1}{\pi} \int_0^\infty \frac{K_0(u e^{i\pi/2} r_D)\, e^{-t_D u^2}}{u^2\, K_1(u e^{i\pi/2})}\, du \qquad \textbf{(B-19)}$$

The modified Bessel functions of the first and second kind of arguments $ue^{\pi/2}$ can be expressed as regular Bessel functions of zero and first order and first and second kind, J_0, J_1, Y_0 and Y_1. Thus,

$$K_0(u e^{i\pi/2}) = \frac{\pi i}{2}\left[-J_0(u r_D) + i Y_0(u r_D)\right] \qquad \textbf{(B-20)}$$

$$K_1(u e^{i\pi/2}) = -\frac{\pi}{2}\left[J_1(u) - i Y_1(u)\right] \qquad \textbf{(B-21)}$$

Then,

$$\int_{CD} = \frac{1}{\pi} \int_0^\infty \frac{e^{-u^2 t_D}}{u^2} \frac{-i J_0(u r_D) - Y_0(u r_D)}{J_1(u) - i Y_1(u)}\, du \qquad \textbf{(B-22)}$$

In a similar manner, integration along the lower portion of the "cut", i.e. along EG, can be obtained by letting $s = u^2 e^{-i\pi}$ and noting that $e^{-i\pi} = -1$, giving

$$\int_{EG} = \frac{1}{\pi} \int_0^\infty \frac{e^{-u^2 t_D}}{u^2} \frac{i\, J_0(ur_D) - Y_0(ur_D)}{J_1(u) + i\, Y_1(u)}\, du \qquad \text{(B-23)}$$

Combining the line integrals of CD and EG, we obtain,

$$\int_{CD} + \int_{EG} = \frac{2}{\pi} \int_0^\infty \frac{e^{-u^2 t_D}}{u^2} \frac{Y_1(u)\, J_0(ur_D) - J_1(u)\, Y_0(ur_D)}{J_1^2(u) + Y_1^2(u)}\, du \qquad \text{(B-24)}$$

Hence the integral along AB becomes

$$\begin{aligned} \int_{AB} &= -\int_{CD} - \int_{EG} \\ &= -\frac{2}{\pi} \int_0^\infty \frac{e^{-u^2 t_D}}{u^2} \frac{Y_1(u)\, J_0(ur_D) - J_1(u)\, Y_0(ur_D)}{J_1^2(u) + Y_1^2(u)}\, du \end{aligned} \qquad \text{(B-25)}$$

Eq. B - 15 can now be used to obtain the following expression, presented in main text as Eq. 2.26, for earth temperature, T_{ei}, as a function of dimensionless time t_D and radial distance from the wellbore, r_D,

$$T(r_D, t_D) = T_{ei} + \frac{\overline{Q}}{\pi^2\, w\, k_e} I' \qquad \text{(B-26)}$$

APPENDIX C

REFERENCES

Almehaideb, R.A., Aziz, K., and Pedrosa, O.A.: "A Reservoir/Wellbore Model for Multiphase Injection and Pressure Transient Analysis," paper SPE 17941 presented at the 1989 SPE Middle East Oil Show, Manama, Bahrain, March 11-14.

Alves, I. N., Alhanati, F. J. S., Shoham, O.: "A Unified Model for Predicting Flowing Temperature Distribution in Wellbores and Pipelines," *SPEPE* (Nov. 1992) 363.

Baker, A.C. and Price, M.: "Modeling the Performance of High-Pressure High-Temperature Wells," paper SPE 20903 presented at the Europec Meeting, The Hague, The Netherlands, October 22-24, 1990.

Ansari, A. M., et al: "A Comprehensive Mechanistic Model for Upward Two-phase Flow in Wellbores," SPEPE (May 1994) 143.

Bird, J.M.: "Interpretation of Temperature Logs in Water-and Gas-Injection Wells and Gas-Producing Wells," *Drill. and Prod. Prac.*, API (1954) 187.

Carslaw, H.S. and Jaeger, J.C.: *Conduction of Heat in Solids*, Oxford U. Press, Amen House, London (1950).

Curtis, M.R., and Witterholt, E.J.: "Use of the Temperature Log for Determining Flow Rates in Producing Wells," paper SPE 4637 presented at the 1973 SPE Annual Fall Meeting, Las Vegas, Oct. 1-3.

Davidson, A.R., Prise, G., and French, C.: "Successful High-Temperature/High-Pressure Well Testing From a Semisubmersible Drilling Rig," *SPE Drilling and Completion* (March 1993) 7-13.

Dowdle, W.L. and Cobb, W.M.: "Static Formation Temperature from Well Logs-An Empirical Method," *JPT* (Nov. 1975) 1326.

Dropkin, D. and Sommerscales, E.: "Heat Transfer by Natural Convection in Liquids Confined by Two Parallel Plates Inclined at Various Angles With Respect to the Horizontal," *J. Heat Transfer; Trans.*, ASME, Series C (Feb. 1965)87, 77-78.

Edwardson, M.J. *et al.*: "Calculation of Formation Temperature Disturbances Caused by Mud Circulation," *JPT* (April 1962) 416; *Trans.*, AIME, 225.

Griston, S. and Willhite, G.P.: "Numerical Model for Concentric Steam Injection Wells,"

paper SPE 16337 presented at the SPE California Regional Meeting, Ventura, CA, April 8-10, 1987.

Gopal, V.N.: "Gas Z-Factor Equations Developed for Computer," *Oil & Gas J.* (Aug. 8, 1977) 58-60.

Hamby, T.W., Broussard, L.P., and Taylor, D.B.: "Producing Mississippi's Deep, High-Pressure Sour Gas," *JPT* (June 1976) 629-38.

Hamby, T.W.: "Development of High-Pressure Sour Gas Technology," *JPT* (May 1981) 792-98.

Hasan, A.R.: "Void Fraction in Bubbly, Slug, and Churn Flow in Vertical Two-Phase Up-Flow," Chem. Eng. Comm. (April 1988) 101.

Hasan, A.R. and Kabir, C.S.: "A Study of Multiphase Flow Behavior in Vertical Wells," SPEPE (May 1988) 263.

Hasan, A.R. and Kabir, C.S.: "Aspects of Heat Transfer During Two-Phase Flow in Wellbores," *SPEPE* (Aug. 1994) 279.

Hasan, A.R., Wang, Xiaowei, and Kabir, C.S.: "A Transient Wellbore/Reservoir Model for

Testing Gas Wells in High-Temperature Reservoirs, Part I. Model Development," paper SPE 28402 presented at the 1994 Annual Technical Conference and Exhibition, New Orleans, LA, September 25-28.

Hasan, A.R. and Kabir, C.S.: "Modeling Changing Storage During a Shut-in Test," *SPEPE* (Dec. 1994).

Hasan, A.R., Kabir, C.S., and Wang, Xiaowei: "Development and Application of a Wellbore/Reservoir Simulator for Testing Oil Wells," paper SPE 29892 presented at the 1995 SPE Middle East Oil Show, Manama, Bahrain, March 11-14.

Hasan, A.R., C.S. Kabir, M.M. Ameen, and Wang, Xiaowei: "A Mechanistic Model for Circulating Fluid Temperature," SPE Journal (June 1996 Volume 1 Number 2) 133-144.

Hasan, A.R., Wang, Xiaowei, and Kabir, C.S.: "Development and Application of a Wellbore/Reservoir Simulator for Managing Water Injection Projects," paper to be presented at the 1996 Annual Technical Conference and Exhibition, Denver, Colorado, USA, October 6-9.

Hasan, A.R., Gene Kouba and Wang, Xiaowei: "Pressure Transient Analysis to Locate and Characterize Flowline Restrictions in Gas Wells," paper to be presented at the 1996 Annual Technical Conference and Exhibition, Denver, Colorado, USA, October 6-9.

Herrera, J.O., Birdwell, B.F., and Hanzlik, E.J.: "Wellbore Heat Losses in Deep Steam Injection Wells, S1-B Zone, Cat Canyon Field," SPE 7117, presented at the SPE California Regional Meeting, San Francisco, April 12-14, 1978.

Hong, K.C. and Griston, S.: "New Methods for Controlled Injection of Steam into Multiple Sands," SPE 15472 presented at the Annual SPE Technical Conference, New Orleans, LA, Oct. 5-8, 1986.

Huntoon, G.G.: "Completion Practices in Deep Sour Tuscaloosa Wells," *JPT* (January 1984) 79-88.

J.F. Stanislav/C.S.Kabir:"Pressure Transient Analysis," Prentice-Hall, Inc. (1990).

Kabir, C.S., Hasan, A.R., Jordan, D.L., and Wang, Xiaowei: "A Transient Wellbore/Reservoir Model for Testing Gas Wells in High-Temperature Reservoirs, Part II. Field Application," paper SPE 28403 presented at the 1994 Annual Technical Conference and Exhibition, New Orleans, LA, September 25-28.

Kirkpatrick, C.V.: "Advances in Gas-Lift Technology," *Drill. & Prod. Prac., API* (March 1959) 24.

Krus, H. and Prieur, J.M.: "High-Pressure Well Design," *SPE Drilling Engineering*

(December 1991) 24-44.

Lesem, I.B., Greytok, F., Marotta, F. and McKetta, J.J.: "A method of Calculating the Distribution of Temperature in Flowing Gas Wells," *Trans.*, AIME (1957) 210, 169.

Low, E. and Seymour, K.P.: "The Drilling and Testing of High-Pressure Gas Condensate Wells in the North Sea," paper IADC/SPE 17224 presented at the 1988 IADC/SPE Drilling Conference, Dallas, TX, Feb. 28 - March 2, 1993.

MacAndrew, R. *et al.*: "Drilling and Testing Hot, High-Pressure Wells," *Oilfield Review* (April-July, 1993) 15-32.

Michael J. Economides, A. Daniel Hill and Christine Ehlig-Economides:"Petroleum Production Systems," PTR Prentice Hall (1994).

Miller, C.W.: "Wellbore Storage Effect in Geothermal Wells," *SPEJ* (December 1980) 555.

Mitchell, R.F. and Wedelich, H.F.: "Prediction of Downhole Temperatures Can be Key for Optimal Wellbore Design," paper SPE 18900 presented at the 1989 SPE Production Operations Symposium, Oklahoma City, OK, March 13-14.

Moss, J.T. and White, P.D.: "How to Calculate Temperature Profiles in a Water-Injection

Well," *Oil & Gas J.* (March 9, 1959) 57, No. 11, 174.

Nowak, T.J.: "The Estimation of Water Injection Profiles from Temperature Surveys," *JPT* (Aug. 1953) 203; *Trans.*, AIME, 198.

Pacheco, E.F. and Farouq Ali, S.M.: "Wellbore Heat Losses and Pressure Drop in Steam Injection," *JPT* (Feb. 1972) 139.

Ramey, H.J. Jr.: "Wellbore Heat Transmission," *JPT* (April 1962) 427; *Trans.*, AIME, 225.

Roux, B., Sanyal, S.K., and Brown, S.L.: "An Improved Approach to Estimating True Reservoir Temperature from Transient Temperature Data," paper SPE 8888 presented at the SPE Calif. Regional Meeting, Los Angeles, April 9-11, 1980.

Sagar, R.K, Dotty, D.R., and Schmidt, Z.: "Predicting Temperature Profiles in a Flowing Well," SPE Annual Tech. Mtg., San Antonio, TX Oct. 8-11, 1989.

Schlumberger, M., Doll, H. G., and Perebinossoff, A. A.: "Temperature Measurements in Oil Wells," *J. Inst. Pet. Technologists* (Jan. 1937) 23, 159.

Schlutz, R.R., Stehle, D.E., and Murali, J.: "Completion of a Deep, Hot, and Corrosive

East Texas Gas Well," paper SPE 14983 presented at the SPE Deep Drilling and Production Symposium, Amarillo, TX, April 6-8, 1986.

Seyer, W., and Langden, I.: "Estimation of Bottomhole Temperature from Surface Condition in Cyclic Steam Injection," paper CIM/SPE 90-110, CIM/SPE Int. Tech. Mtg., Calgary, June 10-13, 1990.

Shiu, K.C. and Beggs, H.D.: "Predicting Temperatures in Flowing Oil Wells," *J. Energy Resources Tech.* (March 1980); *Trans.*, ASME.

Shoham, O.: "Flow Pattern Transition and Characterization in Gas-liquid Two-phase Flow in Inclined Pipes," Ph.D. Thesis, Univ. Of Tel Aviv (1982).

Standing, M.P. and Katz, D.L.: "Density of Natural Gases," Trans., *AIME* (1942) **146**, 140-149.

Stone, T.W., Edmonds, N.R., and Kristoff, B.J.: "A Comprehensive Wellbore/Reservoir Simulator," paper SPE 18419 presented at the 1989 SPE Reservoir Simulation Symposium, Houston, TX, February 6-8.

Van Everdingen, A.F. and Hurst, W.: "The Application of the Laplace Transformation to Flow Problems in Reservoirs," *Trans., AIME* (1949) 186, 305.

Vidick, B. and Acock, A.: "Minimizing Risks in High Temperature/ High Pressure Cementing: The Quality Assurance/Quality Control Approach," paper SPE 23074 presented at the Offshore Europe Conference, Aberdeen, Scotland, September 3-6, 1991.

Willhite, G.P.: "Over-all Heat Transfer Coefficients in Steam and Hot Water Injection Wells," *JPT* (May 1967) 607.

Winterfeld, P.H.: "Simulation of Pressure Buildup in a Multiphase Wellbore/Reservoir System," *SPEFE* (June 1989) 247.